REPORT DOCUMENTATION PAGE

AFRL-SR-BL-TR-99-

0305

1. AGENCY USE ONLY *(Leave blank)*	2. REPORT DATE	3. REPORT TYPE AND DATES COVERED
	19 Nov 1999	Final Technical Report 01 Aug 97 to 31 Jul 99

4. TITLE AND SUBTITLE
Stress/Failure Analysis Software for Multi-Material Interfaces

5. FUNDING NUMBERS
F49620-97-C-0045

STTR/TS

6. AUTHOR(S)
Dr. Ricardo Actis

7. PERFORMING ORGANIZATION NAME(S) AND ADDRESS(ES)
Engineering Software Research & Development, Inc.
10845 Olive Blvd, Ste 170
St. Louis, MO 63141-7760

8. PERFORMING ORGANIZATION REPORT NUMBER

9. SPONSORING/MONITORING AGENCY NAME(S) AND ADDRESS(ES)
AFOSR/NM
801 N. Randolph Street, Rm 732
Arlington, VA 22203-1977

10. SPONSORING/MONITORING AGENCY REPORT NUMBER
F49620-97-C-0045

11. SUPPLEMENTARY NOTES

12a. DISTRIBUTION AVAILABILITY STATEMENT
Approved for Public Release; Distribution Unlimited.

12b. DISTRIBUTION CODE

13. ABSTRACT *(Maximum 200 words)*

The main objective of this project was the development of an innovative computer program with advanced capabilities for providing means for establishing reliable quantitative failure initiation criteria for laminated composites and adhesively bonded joints. The existing software product Stress Check, which is based on the p- and hp-version of the finite element method and has a-posteriori error estimation capabilities, provided the framework for this development.

19991230 025

14. SUBJECT TERMS	15. NUMBER OF PAGES
	68
	16. PRICE CODE

17. SECURITY CLASSIFICATION OF REPORT	18. SECURITY CLASSIFICATION OF THIS PAGE	19. SECURITY CLASSIFICATION OF ABSTRACT	20. LIMITATION OF ABSTRACT
Unclassified	Unclassified	Unclassified	UL

Engineering Software Research and Development, Inc.
10845 Olive Boulevard, Suite 170
St. Louis, MO 63141-7760

Stress/Failure Analysis Software for Multi-Material Interfaces

Final Technical Report

Ricardo L. Actis, Principal Investigator

Contract #F49620-97-C-0045
Project No. FQ8671-9701107 STTR/TS

October 25, 1999

1 Introduction

The main objective of this project was the development of an innovative computer program with advanced capabilities for providing means for establishing reliable quantitative failure initiation criteria for laminated composites and adhesively bonded joints. The existing software product Stress Check, which is based on the p- and hp-version of the finite element method and has a-posteriori error estimation capabilities, provided the framework for this development.

The evaluation of strength was based on recent technological advances which made it possible to determine the natural straining modes and their intensities at singular points associated with multi-material interfaces by numerical methods. The project was concerned with proof of concept and implementation in a fully three-dimensional setting, in conjuction with the hp-version of the finite element method. During the Phase II project, a set of failure criteria for composite-laminated bonded structures based on stress averaging and material nonlinear analysis were identified as important failure prediction methods of interest to the Air Force, Navy and their contractors. Therefore a change in the original technical objectives of Phase II was incorporated during the last 6 months of the project.

The project utilized an existing finite element software product called Stress Check which was developed by the small business concern (ESRD) over the past ten years. The research institution (Washington University) provided specialized expertise needed for effecting transfer of the new technology to professional practice. The new technological capability developed under this project makes it possible to improve the design from the point of view of durability. It will also make it possible to properly interpret experimental observations concerning failure initiation events in composite materials and bonded joints and thereby advance the use of composite materials technology in both civilian and military applications.

2 Technical objectives

During the Phase II project, the following tasks were completed:

Task 1: Development, implementation, testing and documentation of an algorithm for the computation of *eigenpairs* that characterize the temperature distribution in the vicinity of singular edges in multi-material interface for steady state heat transfer problems.

Task 2: Development, implementation, testing and documentation of an algorithm for the computation of the *generalized flux intensity factors* (GFIFs) for edge singularities in the case of steady state heat transfer problems.

Task 3: Testing and documentation of the procedures described in tasks 1 and 2. These procedures were implemented in the finite element analysis software product Stress Check and a posteriori error estimation capability in terms of the flux intensity factors is provided.

Task 4: Development, implementation, testing and documentation of an algorithm for the computation of *eigenpairs* that characterize the strain distribution in the vicinity of singular edges in multi-material interface elasto-static problems.

Task 5: Development, implementation, testing and documentation of an algorithm for the computation of the *generalized stress intensity factors* (GSIFs) for edge singularities when an elastic body is subjected to mechanical and thermal loads.

Task 6: Testing and documentation of the procedures described in tasks 4 and 5. These procedures were implemented in the finite element analysis software product Stress Check and a posteriori error estimation capability in terms of the stress intensity factors is provided.

Task 7: Development, implementation, testing and documentation of a capability for the computation of average stress/strain along element edges, element faces or arbitrary curves for two- and three-dimensional elasticity problems. The average is understood in the integral sense over a characteristic length/area.

Task 8: Development, implementation, testing and documentation of an automatic nonlinear solution procedure for the evaluation of composite bonded joints. The procedure involves a material nonlinear analysis of the joint for the design load followed by the determination of the failure load based on several predefined criteria. This automatic procedure is accessible from within the handbook framework of Stress Check.

Task 9: Development, implementation, testing and documentation of a capability to input orthotropic material properties for individual plies and for sub-laminate properties for 2D plane-strain analyses. The procedure allows entering the 3D material coefficients in the material axes of the composite and performs the necessary transformations to compute the equivalent 2D

properties in the Stress Check XY work plane. When a set of plies need to be combined in a single layer (sub-laminate), the properties of the sub-laminate are determined by homogenization of the material properties.

Task 10: Delivery of one copy of Stress Check software executable on a Windows NT workstation and pertinent documentation to the Air Force Rome Laboratory. Rome Laboratory shall have the same rights to Stress Check as a "paid-up" licensee.

The details of these activities are described in the following sections.

3 Technical background

There is a growing demand for efficient and reliable means for predicting and eventually preventing failure initiation and propagation in multi-chip modules (MCM), electronic packages and composite materials subjected to mechanical and thermal loads. Thermal, elastic and thermo-elastic problems associated with large scale integrated circuits, electronic packaging, and composites increase in complexity and importance. These components are assemblages of dissimilar materials with different thermal and mechanical properties. The mismatch of the physical properties cause flux and stress intensification at the corners of interfaces and can lead to mechanical failures.

The traditional finite element analysis of stresses is inadequate to handle these types of problems[1]: "*Since the stress and displacement fields near a bonding edge show singularity behavior, the adhesive strength evaluation method, using maximum stresses calculated by a numerical stress analysis, such as the finite element method, is generally not valid*".

These material interfaces, as well as crack tips, are called singular points because the temperature flux is infinity in the linear theory of steady-state heat conduction and so are the stresses in the linear theory of elasticity. Typical singular points where failures initiate and propagate in an electronic device are shown in Figure 1.

New approaches to predicting the initiation and extension of delamination in plastic encapsulated LSI (Large Scale Integrated Circuit) devices, for example, are based on the computation of certain functionals, called the generalized flux/stress intensity factors (GFIFs/GSIFs), the strength of the stress singularity, and in thermo-elastic problems the thermal stress intensity factors (TSIFs). Since the stress and strain components are generally not bounded, it is not possible to construct failure initiation events with them. A key requirement for formulating failure laws is a software-tool which computes *reliably* the GFIFs/GSIFs and the strength of the singularity. The reliability and accuracy of numerical results is an essential requirement for proper evaluation and formulation of failure theories through experimental observation of failure initiation events.

1. T. Hattori, S. Sakata and G. Murakami, "A stress singularity parameter approach for evaluating the interfacial reliability of plastic encapsulated LSI devices", Jour. Electronic Packaging, **111**, (1989), pp. 243-248.

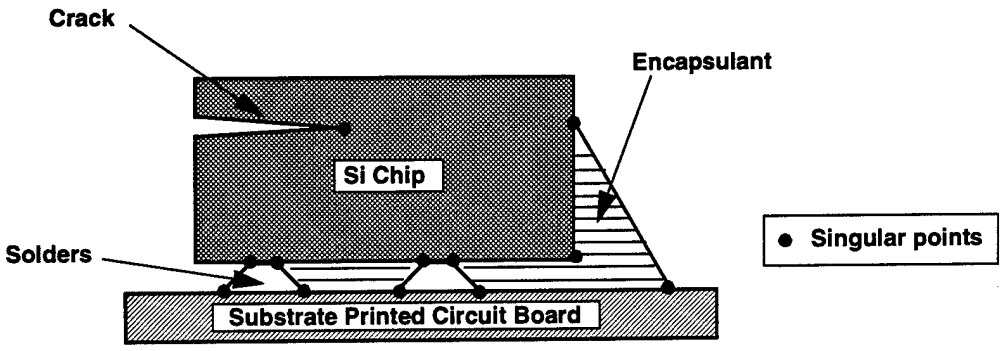

FIGURE 1. Typical sites of failure initiation in an electronic device.

3.1 Introduction and Notation

In the neighborhood of singular points the exact solution of two-dimensional elastostatic problems for example, can be expanded in the form:

$$\{u\} = \sum_{i=1}^{\infty} A_i r^{\alpha_i} \{\Phi_i(\theta)\} \tag{1}$$

where $\{u\}$ is the displacement vector with components $u_x(x,y)$, $u_y(x,y)$, r and θ are polar coordinates centered on the singular point; α_i are called eigenvalues and $\phi_i(\theta)$ are called eigenfunctions.These *eigenpairs* (α_i, ϕ_i) depend on the material properties, the geometry and the boundary conditions [$\phi_i(\theta)$ are smooth vector functions]. The A_i are coefficients which depend on the loading. Because of their close analogy to stress intensity factors in linear elastic fracture mechanics, A_i are called *generalized stress intensity factors (GSIFs).* In the case of heat transfer problems they are called *generalized flux intensity factors (GFIFs).*

The stresses in the same neighborhood can be computed from the displacements given by Eq. (1) and the material properties as:

$$\{\sigma\} = \sum_{i=1}^{\infty} A_i r^{\alpha_i - 1} \{\psi_i(\theta)\} \tag{2}$$

where $\psi_i(\theta)$ depend on the eigenfunctions $\phi_i(\theta)$ in Eq. (1) and the material coefficients. It is clear from Eq. (2) that when $\alpha_i < 1$, the stresses become singular for $r=0$. For additional details see Ref. [2]-[5].

Three-dimensional singularities are considerably more difficult to analyze than two-dimensional ones, where only one type of singularity exists. In 3D in a neighborhood of the edges and the vertices the singular behavior is different.

Edge Singularities: If a coordinate system (x,y,z) is located at an edge, with the y-axis along the edge, then there are three edge GSIFs which are y-dependent: $A_I(y)$, $A_{II}(y)$ *and* $A_{III}(y)$. These edge GSIFs are analytic along the edge, however they become themselves singular when this edge intersects with a free plane, at a vertex. In the neighborhood of an edge-vertex type geometry the GSIFs can be represented once again by vertex and vertex-edge stress intensity factors. For example, $A_I(y) = \sum_j S_{I,j}\, y^{\tilde{\eta}_{I,j}} +$ *smoother terms.*

Vertex Singularities: In the neighborhood of a vertex, and away from edge-vertex geometry, the displacement field can be represented by only one vertex intensity factor and the corresponding eigenpairs. Investigating the mathematical behavior of the singularities in 3-D is an active field of research in the mathematical community, and the decomposition of the displacement field into singular and regular terms is documented in some recent papers.

3.2 Formulation

The solution of second order elliptic boundary value problems (BVP) in three-dimensions in the vicinity of any singular point, can be decomposed into three different forms, depending whether the singular point is in the neighborhood of an edge, a vertex or an intersection of the edge and the vertex. Mathematical details of the decomposition can be found e.g. in Ref. [8]-[11] and the references therein. A representative three-dimensional domain denoted by Ω, which contains typical 3D singular points is shown in Figure 2. Vertex singularities arise in the neighborhood of the vertices A_i, and the edge singularities arise in the neighborhood of the edges singularities Λ_{ij}. Close to the vertex/edge intersection, vertex-edge singularities arise.

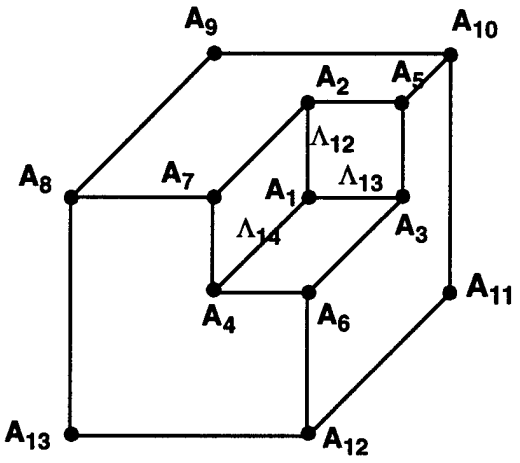

FIGURE 2. Typical 3D singularities.

Consider the simplest elliptic BVP, the Laplace equation:

$$\nabla^2 u = 0 \qquad \text{in } \Omega \tag{3}$$

$$u = 0 \quad \text{on } \Gamma_D \subset \partial\Omega, \quad \frac{\partial u}{\partial n} = 0 \quad \text{on } \Gamma_N \subset \partial\Omega \tag{4}$$

where $u(x_1, x_2, x_3)$ denotes the temperature field (in the following x_1, x_2 and x_3 will be either Cartesian, cylindrical or spherical coordinates), and $\Gamma_D \cup \Gamma_N = \partial\Omega$. It shall be assumed that curved edges that intersect at vertices do not exist, at that crack faces, if any, lie in a plane.

Edge Singularities: We first examine the edges denoted by Λ_{ij} which connect the vertices A_i and A_j. Moving away from the vertex a distance $\delta/2$, and creating a cylindrical subdomain of radius $r = R$ with the edge Λ_{ij} as its axis, we define a subdomain in the vicinity of the edge denoted by $\varepsilon_{\delta,R}(\Lambda_{ij})$. Figure 3 shows the edge singularity subdomain $\varepsilon_{\delta,R}(\Lambda_{12})$. We restrict our attention to domains having straight edges.

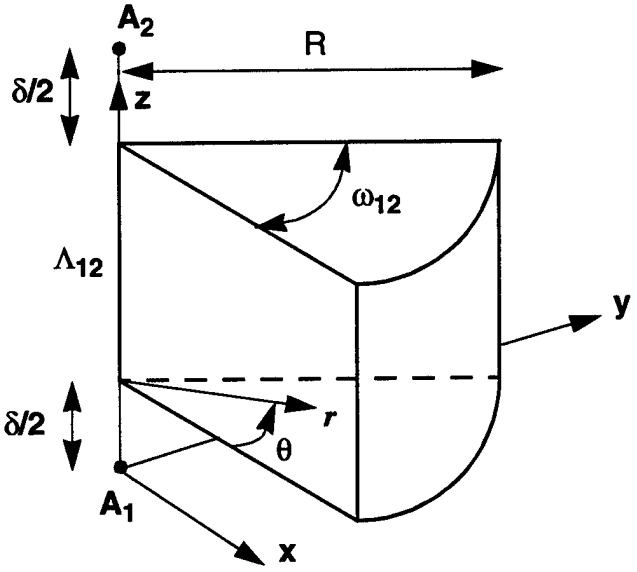

FIGURE 3. The edge neighborhood $\varepsilon_{\delta,\varepsilon}(\Lambda_{12})$.

The solution in $\varepsilon_{\delta,R}$ can be decomposed as follows:

$$u(r,\theta,z) = \sum_{k=1}^{K}\sum_{s=0}^{S} a_{ks}(z)\; r^{\alpha_k}(\ln r)^s f_{ks}(\theta) \;+\; v(r,\theta,z) \tag{5}$$

where $S \geq 0$ is an integer which is zero unless a_k is an integer, $\alpha_{k+1} \geq \alpha_k$ are called edge eigenvalues; $a_{ks}(z)$ are called the edge flux intensity functions (EFIFs), are analytic in z but can become very large as they approach one of the vertices; and $f_{ks}(\theta)$, called eigenfunctions, are analytic in θ. The function $v(r,\theta,z)$ belongs to $H^q(\varepsilon)$, the Sobolev space, where q can be as large as required and depends on K. We shall assume that α_k for $k \leq K$ is not an integer, therefore Eq. (5) becomes:

$$u(r,\theta,z) = \sum_{k=1}^{K} a_k(z)\ r^{\alpha_k}\ f_k(\theta) + v(r,\theta,z) \tag{6}$$

Vertex Singularities: A sphere of radius $\rho = \delta$, centered in the vertex A_1 for example, is constructed and intersected by the domain Ω. Then, a cone having an opening angle $\phi = \sigma$ is constructed along every edge intersecting at A_1, and removed from the previously constructed subdomain, as shown in Figure 4.

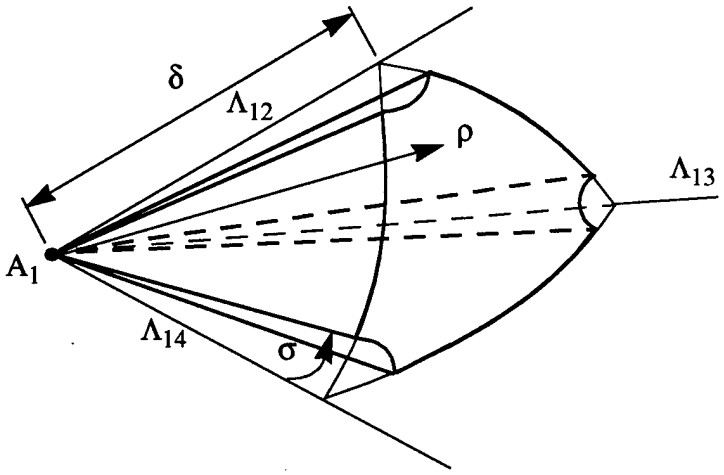

FIGURE 4. The vertex neighborhood $V_\delta(A_1)$.

The resulting vertex subdomain is denoted by $V_\delta(A_1)$, and the solution u can be decomposed in $V_\delta(A_1)$ using a spherical coordinate system by:

$$u(\rho,\phi,\theta) = \sum_{l=1}^{L}\sum_{q=0}^{Q} b_{lq}\ \rho^{\gamma_l}(\ln\rho)^q h_{lq}(\phi,\theta) + v(\rho,\phi,\theta) \tag{7}$$

where $Q \geq 0$ is an integer which is zero unless γ_l is an integer, $\gamma_{l+1} \geq \gamma_l$ are called vertex eigenvalues, and $h_{lq}(\phi,\theta)$, called the eigenfunctions, are analytic in ϕ and θ. The b_{lq} are called vertex flux intensity factors (VFIFs). The function $v(r,\theta,z)$ belongs to $H^q(V)$, where q depends on L. We shall assume that γ_l for $l \leq L$ is not an integer, therefore, Eq. (7) becomes:

$$u(\rho,\phi,\theta) = \sum_{l=1}^{L} b_l\ \rho^{\gamma_l}\ h_l(\phi,\theta) + v(\rho,\phi,\theta) \tag{8}$$

Vertex-Edge Singularities: The most complicated decomposition of the solution arises in case of vertex-edge intersections. For example, let us consider the neighborhood where the edge Λ_{12} approaches the vertex A_1. A spherical coordinate system is located in the vertex A_1, and a cone having an opening angle $\phi = \sigma$ with its vertex coinciding with A_1 is constructed with Λ_{12} being its center axis. This cone is terminated by a ball-shaped basis having a radius $\rho = \delta$, as shown in Figure 5.

The resulting vertex-edge subdomain is denoted by $V\varepsilon_{\delta,\varepsilon}(A_1, \Lambda_{12})$, and the solution u can be decomposed in $V\varepsilon_{\delta,\varepsilon}(A_1, \Lambda_{12})$:

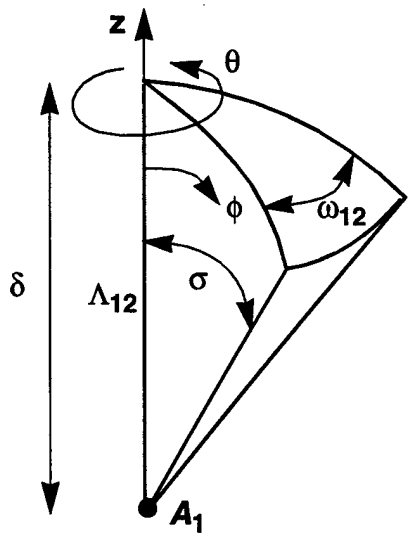

FIGURE 5. The vertex-edge neighborhood $V\varepsilon_{\delta,\varepsilon}(A_1, \Lambda_{12})$.

$$u(\rho,\phi,\theta) = \sum_{k=1}^{K}\sum_{s=0}^{S}\left(\sum_{l=1}^{L} a_{ksl}\ \rho^{\gamma_l} + m_{ks}(\rho)\right)(\sin\phi)^{\alpha_k}[\ln(\sin\Phi)]^s g_{ks}(\theta) + \sum_{l=1}^{L}\sum_{q=0}^{Q} c_{lq}\rho^{\gamma_l}(\ln\rho)^q h_{lq}(\phi,\theta) + v(\rho,\phi,\theta) \quad (9)$$

where $m_{ks}(\rho)$ is analytic in ρ; $g_{ks}(\theta)$ is analytic in θ, and $h_{lq}(\phi,\theta)$ is analytic in ϕ and θ. The function $v(r,\theta,z)$ belongs to $H^q(V\varepsilon)$ where q can be as large as required depending on L and K. Again we shall assume that γ_l for $l \le L$ is not an integer, and α_k for $k \le K$ is not an integer, therefore, Eq. (9) becomes:

$$u(\rho,\phi,\theta) = \sum_{k=1}^{K}\left(\sum_{l=1}^{L} a_{kl}\ \rho^{\gamma_l} + m_k(\rho)\right)(\sin\phi)^{\alpha_k} g_k(\theta) + \sum_{l=1}^{L} c_l\ \rho^{\gamma_l}\ h_l(\phi,\theta) + v(\rho,\phi,\theta) \quad (10)$$

The eigenvalues and the eigenfunctions are associated pairs (eigenpairs) which depend on the material properties, the geometry, and the boundary conditions in the vicinity of the singular point/edge only. Similarly, the solution for problems in linear elasticity, in the neighborhood of singular points/edges is analogous to Eq. (5)-Eq. (10), the differences are that the equations are in vector form and the eigenpairs may be complex. For general singular points the exact solution u_{EX} is generally not known explicitly, i.e., neither the exact eigenpairs nor the exact EFIFs, VFIFs are known, therefore numerical approximations must be found.

4 Implementation and results

4.1 Task 1: Eigenpairs for edge singularities in heat transfer problems

Separation of variables was utilized for the Laplace equation in the neighborhood of the edge singularity as shown in Eq. (6). Each eigenpair $r^{\alpha k} f_k(\theta)$ is independent of z and satisfies the Laplace equation over the plane (r,θ) which is perpendicular to the edge. This is exactly a two-dimensional problem and therefore the computation of eigenpairs was performed using the modified Steklov method described in Ref. [3] and summarized below.

The algorithm developed for two-dimensional heat-transfer problems was extended to three-dimension by considering a slice contained in the plane normal to the edge singularity. The region denoted by Ω^*_R in Figure 6, represents a cross section along the edge singularity. The edge is assumed to be

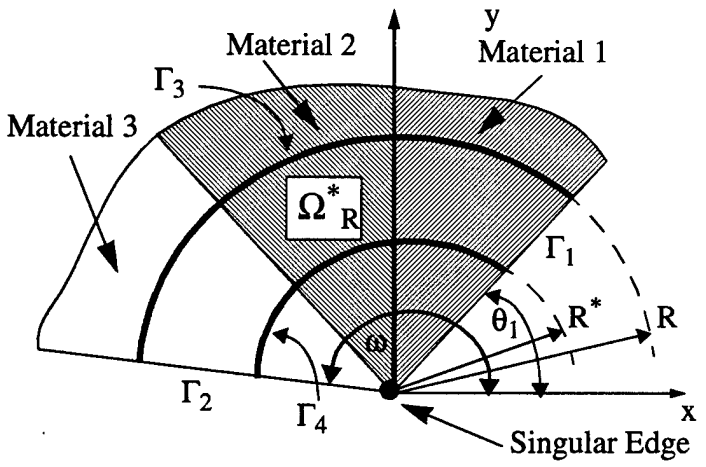

FIGURE 6. Cross section of an edge singularity for the modified Steklov formulation.

along the local z axis, and (r, θ) are the coordinates of a cylindrical system located at the intersection of the normal plane and the singular edge. The area around the singularity is internally divided into sub-domains.

This '2D-internal mesh' is arranged in a circular ring around the singularity in such a way that the element boundaries coincide with the material interfaces as shown in Figure 7.

The number of elements of the internal mesh is controlled by the number of material interfaces around the singularity. The largest solid angle for a single element is limited to 120°. Therefore, if the partition of a single material is larger than 120°, the element is divided in two or more partitions. For each element of the 'internal mesh' the corresponding stiffness and trace matrices are computed, and after assembly, the following eigenvalue problem is obtained:

$$[K_S]\{u_R\} = \alpha[M]\{u_R\} \tag{11}$$

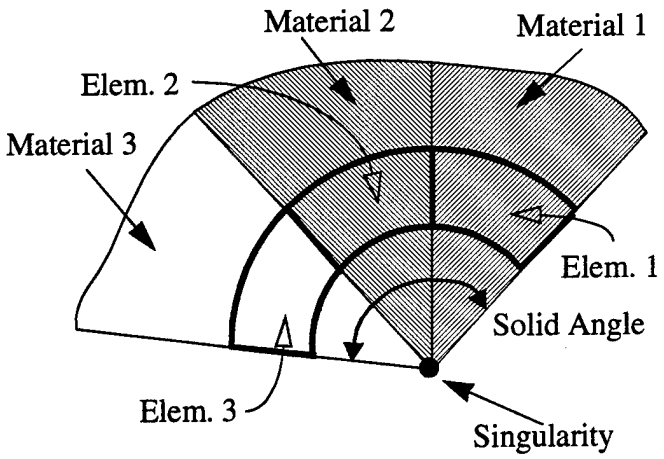

FIGURE 7. Typical 'internal mesh' around the singularity.

where $[K_S]$ is the condensed stiffness matrix, $[M]$ is the trace matrix computed by integration on the circular boundary segments on Ω^*_R, and $\{u_R\}$ is the vector of coefficients that correspond to the degrees of freedom associated with the circular boundaries of the 'internal mesh'. The solution of the eigen-problem given by the above equation yields approximation for the eigenvalues α_i and the corresponding eigenvectors. The steps and fundamentals for obtaining the system described by Eq. (11) are described in the following.

By formulating the weak form over Ω^*_R, the singularity is excluded from the domain of interest such that the accuracy of the finite element solution does not deteriorate in its vicinity. On the boundaries Γ_1 and Γ_2 consider either zero temperature or zero flux boundary conditions:

$$u = 0 \quad \text{or} \quad \frac{\partial u}{\partial n} = 0 \qquad \text{on } \Gamma_i,\ i = 1, 2. \tag{12}$$

In Ω^*_R, the temperature field u can be represented as follows:

$$u = r^{\alpha} f(\theta) \tag{13}$$

Differentiating Eq. (13), and considering the boundary Γ_3 we can write:

$$\frac{\partial u}{\partial r} = (\alpha/R)u \tag{14}$$

and a similar condition on Γ_4.

Multiplying the Laplace equation by a test function v in $H^1(\Omega^*_R)$, integrating over the domain Ω^*_R and using Green's theorem, the modified Steklov weak form is obtained:

$$\textbf{Seek} \qquad \alpha \in \Re, \qquad 0 \neq u \in H^1(\Omega_R)$$

$$B(u,v) - (N_R(u,v) + N_{R^*}(u,v)) = \alpha(M_R(u,v) + M_{R^*}(u,v)), \qquad \forall\ v \in H^1(\Omega_R^*) \tag{15}$$

where

$$B(u,v) = \int_{\Omega_R^*}\int ([D]v)^T[E]([D]u)d\Omega, \tag{16}$$

$$M_R(u,v) = \int_{\theta}[v[Q]^T[E][Q]u]_{r=R}\ d\theta, \tag{17}$$

$$N_R(u,v) = \int_{\theta}[v[Q]^T[E]([D^{(\theta)}]u)]_{r=R}\ d\theta, \tag{18}$$

and $[D]$, $[D^{(\theta)}]$, $[Q]$ and $[R]$ are given as follows:

$$[D] = \begin{bmatrix} \dfrac{\partial}{\partial x} \\ \dfrac{\partial}{\partial y} \end{bmatrix}, \qquad [Q] = \begin{bmatrix} \cos\theta \\ \sin\theta \end{bmatrix}, \qquad [D^{(\theta)}] = \begin{bmatrix} (-\sin\theta)\dfrac{\partial}{\partial\theta} \\ \cos\theta\dfrac{\partial}{\partial\theta} \end{bmatrix} \tag{19}$$

[E] is the 2D material matrix reduced from the 3D material matrix.

Remark 1. The domain Ω^*_R does not include singular edge, hence no special refinement of the finite element mesh is required.

Remark 2. The formulation of the weak form was not based on the assumption that the material is isotropic, and in fact can be applied to multi-material anisotropic interface.

The domain Ω^*_R is divided into finite elements through a meshing process, as described before. The polynomial basis and trial functions, $\{\Psi_j\}$, are defined on a standard element in the ξ, η space such that $-1 < \xi < 1$, $-1 < \eta < 1$. The temperature field is then expanded in terms of the known polynomial shape functions multiplied by a set of unknown coefficients $\{u_{tot}\}$:

$$u = \lfloor u_{tot} \rfloor \{\Psi\} \tag{20}$$

The entries of the unconstrained stiffness matrix corresponding to $B(u,v)$ are given by (see Ref. [3]):

$$K_{ij} = \int_{\Omega_R^*}\int ([D]\{\Psi_i\})^T[E][D]\{\Psi_j\}d\Omega \tag{21}$$

Similar expressions are obtained for the matrices $[N_R]$, $[N_{R*}]$ and $[M_R]$, $[M_{R*}]$ associated with the bilinear forms $N_R(u,v)$ and $M_R(u,v)$.

Denoting the set of all unknown coefficients by $\{u_{tot}\}$, and the set of coefficients associated with Γ_3 and Γ_4 by $\{u_R\}$, the following eigen-problem is obtained:

$$([K]-[N_R]-[N_{R^*}])\{u_{tot}\} = \alpha([M_R]+[M_{R^*}])\{u_R\} = \alpha[M]\{u_R\} \tag{22}$$

The vector which represents the total number of nodal values in Ω^*_R can be divided into two vectors such that one contains the coefficients $\{u_R\}$, the other contains the remaining coefficients: $\{u_{tot}\}^T = \{\{u_R\}^T, \{u_{in}\}^T\}$. By eliminating $\{u_{in}\}$, the reduced eigen-problem is obtained:

$$[K_S]\{u_R\} = \alpha[M]\{u_R\} \tag{23}$$

The solution of the eigen-problem given by Eq. (23) yields approximations for eigenpairs with high accuracy, efficiency and robustness.

The procedure implemented in Stress Check for the computation of the eigenpairs requires the user only to click with the mouse cursor along the singular edge. The program then determines a cutting plane normal to the singular edge at the pick point and creates the partitions indicated in Figure 7 based on the material properties of the elements intersecting the cutting plane. Once these partitions are identified, the elemental matrices are computed and the system of equations is assembled and solved.

4.2 Task 2: Generalized flux intensity factors for edge singularities in heat transfer problems

The algorithm for the computation of the GFIFs is based on L^2 projection of the finite element solution into the space of functions characterized by the asymptotic expansion in terms of the eigenpairs. The algorithm can be summarized as follows:

Consider the domain around a singular edge for a heat transfer problem shown in Figure 8. The temperature field can be expanded around the singular edge in terms of the eigenpairs and the generalized flux intensity factors:

$$u(r,\theta) = \sum_{i=1}^{N} A_i r^{\alpha_i} f_i(\theta) = \lfloor \phi \rfloor \{A\} \tag{24}$$

where A_i are the GFIFs, α_i are the eigenvalues and $f_i(\theta)$ are the corresponding eigenfunctions, with $\phi_i = r^{\alpha i} f_i(\theta)$.

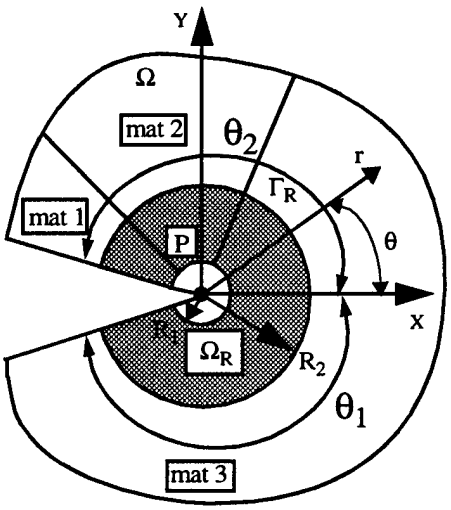

FIGURE 8. Typical cross-section of an edge singularity through point P.

Let $u_{FE}(r,\theta)$ be the finite element solution of the temperature distribution around the singular edge. Then the L^2 projection of u_{FE} into the domain Ω_R is characterized by the following:

$$\int_{\Omega_R}(u-u_{FE})v dA = 0, \qquad for\ all\ v \in S \tag{25}$$

where S is the space of eigenfunctions, and $v(r,\theta)$ is a test function given by:

$$v(r,\theta) = \sum_{i=1}^{N} B_i r^{\alpha_i} f_i(\theta) = \lfloor B \rfloor \{\phi\} \tag{26}$$

Substituting Eq. (24) and Eq. (26) into Eq. (25) and rearranging we have:

$$\lfloor B \rfloor \int_{\Omega_R} \{\phi\}\lfloor\phi\rfloor dA\{A\} = \lfloor B \rfloor \int_{\Omega_R} \{\phi\} u_{FE} dA \tag{27}$$

Eliminating B_i from Eq. (27) and noting that $dA=rdrd\theta$, the following system is obtained:

$$\int_{R_1}^{R_2}\int_{\theta_1}^{\theta_2} \{\phi\}\lfloor\phi\rfloor r dr d\theta \{A\} = \int_{R_1}^{R_2}\int_{\theta_1}^{\theta_2} \{\phi\} u_{FE} r dr d\theta \tag{28}$$

From the definition of $\{\phi\}$ in Eq. (24) and integrating in the radial direction, the system of equation reduces to:

$$K_{ij}A_j = R_j$$

$$K_{ij} = \frac{R_2^{(\alpha_i+\alpha_j+2)} - R_1^{(\alpha_i+\alpha_j+2)}}{2+\alpha_i+\alpha_j}\int_{\theta_1}^{\theta_2} f_i(\theta) f_j(\theta) d\theta \tag{29}$$

$$R_j = \int_{R_1}^{R_2}\int_{\theta_1}^{\theta_2} r^{(\alpha_j+1)} f_j(\theta) u_{FE} dr d\theta$$

Solving the system of equations represented by Eq. (29) over the domain Ω_R gives the values of A_i (the GFIFs). The L^2 projection provides excellent approximation when the generalized intensity fac-

tor along the singular edge is either constant or linear, but the approximation deteriorates for cases in which the variation is of higher order. Nevertheless the current implementation provides a very robust algorithm for a large class of practical problems.

The procedure implemented in Stress Check for the computation of the generalized flux intensity factors requires the user to first solve the heat transfer problem given the topology, material properties and boundary conditions. After the finite element solution is available, the post-processing operation requires only to click with the mouse cursor along the singular edge. The program then determines a cutting plane normal to the singular edge at the pick point and computes the eigenvalues and corresponding eigenvectors as explained in the previous section. With the eigenpairs and the temperature distribution obtained from the finite element solution the program constructs the system given by Eq. (29), the solution of which provides the GFIFs as shown in the next section.

4.3 Task 3: Model problems - Eigenpairs and generalized flux intensity factors

The procedures described in the previous sections for the computation of the eigenpairs and the corresponding generalized flux intensity factors for edge singularities in steady state heat transfer (scalar) problems, are illustrated in the following.

Scalar problem 1: Clamped-free crack in isotropic material. Circular domain of unit radius with a crack along the positive x-axis. One face of the crack (Γ_1) has zero temperature boundary condition and the other face (Γ_2) is flux free. The outside boundary (Γ_R) has an imposed flux (Figure 9). The finite element mesh consisting on 16 solid elements is also shown in Figure 9.

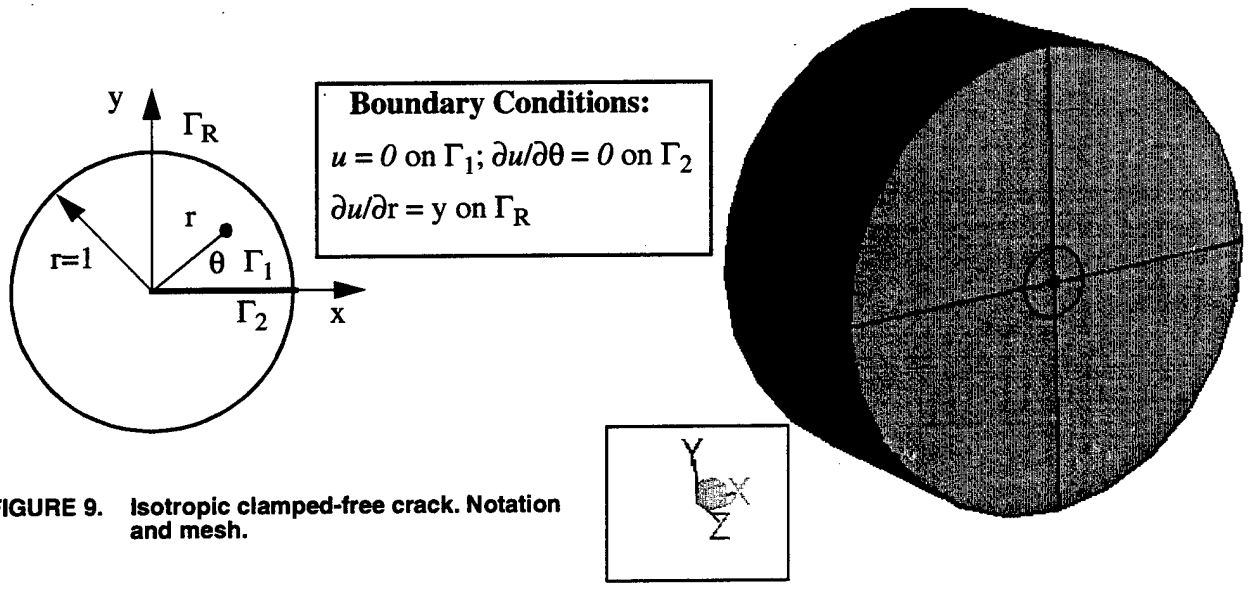

FIGURE 9. Isotropic clamped-free crack. Notation and mesh.

The elements are graded towards the singular edge in geometric projection with a common factor of 0.15.

The exact solution for this problem is given by (Ref. [1]):

$$u(r,\theta) = -1.35812r^{1/4}\sin(\theta/4) + 0.970087r^{3/4}\sin(3\theta/4) + \ldots \quad (30)$$

The exact values of the first two eigenvalues for this problem are: α_1=1/4 and α_2=3/4, and the corresponding generalized flux intensity factors are: A_1=1.358097, A_2=0.970087.

The finite element solution was obtained for polynomial orders ranging from 1 to 8. The estimated relative error in energy norm for the sequence of finite element solutions is shown in Figure 10.

(1) Solution = SOL, runs #1 to #8

Run #	DOF	Total Potential Energy	Convergence Rate	% Error
1	32	-2.032896794902e+000	0.00	31.85
2	112	-2.228519967775e+000	0.76	12.24
3	200	-2.248067253504e+000	0.74	7.96
4	352	-2.252250724991e+000	0.31	6.70
5	572	-2.254400378353e+000	0.25	5.95
6	876	-2.255778943319e+000	0.22	5.41
7	1280	-2.256771999437e+000	0.21	4.99
8	1800	-2.257536919443e+000	0.21	4.64
Estimated Limit		-2.262400478095123e+000		

FIGURE 10. Estimated relative error in energy norm for scalar problem 1.

The first and second eigenvalues computed in Stress Check and the corresponding values of the GFIFs are shown in Figure 11. The tabular data shows the convergence of the A_1 and A_2 as a function of the number of degrees of freedom (DOF) corresponding to eight finite element solutions obtained for polynomial orders ranging from 1 to 8.As can be seen, the numerically computed eigenvalues are practically identical to the theoretical values. The generalized flux intensity factor are also very close to the theoretical values. The estimated limits shown in the table are computed by a projection to infinite number of degrees of freedom of the three values with the highest DOF. The value in brackets

represents the percent deviation between the estimated limit and the value corresponding to run #8.

```
Number of E-pairs: 2, Solid angle: 3.600000e+002
Global coord. of point along edge: X=0.0, Y=0.0, Z=0.0
No. 1, Eval = 2.500000e-001
No. 2, Eval = 7.500000e-001

                        GFIFs
                Isotropic clamped-free crack
 (0) Solution = SOL, runs 1 to 8 (nodes=16-16,angle=360.0),
    Generalized Flux Intensity Factors, Int. Radius = 0.5
-------------------------------------------------------------
  Run       DOF       Radius          A1              A2
-------------------------------------------------------------
    1        32  5.00000e-001  -1.12165e+000  8.40991e-001
    2       112  5.00000e-001  -1.28522e+000  9.60927e-001
    3       200  5.00000e-001  -1.32626e+000  9.70949e-001
    4       352  5.00000e-001  -1.33414e+000  9.70400e-001
    5       572  5.00000e-001  -1.33718e+000  9.70066e-001
    6       876  5.00000e-001  -1.34012e+000  9.70035e-001
    7      1280  5.00000e-001  -1.34257e+000  9.70081e-001
    8      1800  5.00000e-001  -1.34437e+000  9.70092e-001
-------------------------------------------------------------
Est.Limit A1=-1.353007e+000 ( 0.64%)
Est.Limit A2=9.700747e-001 ( 0.00%)
```

FIGURE 11. Eigenvalues and Generalized Flux Intensity Factors for scalar problem 1.

Finally, Figure 12 shows the numerically computed eigenfunctions associated with the first and second eigenvalues.

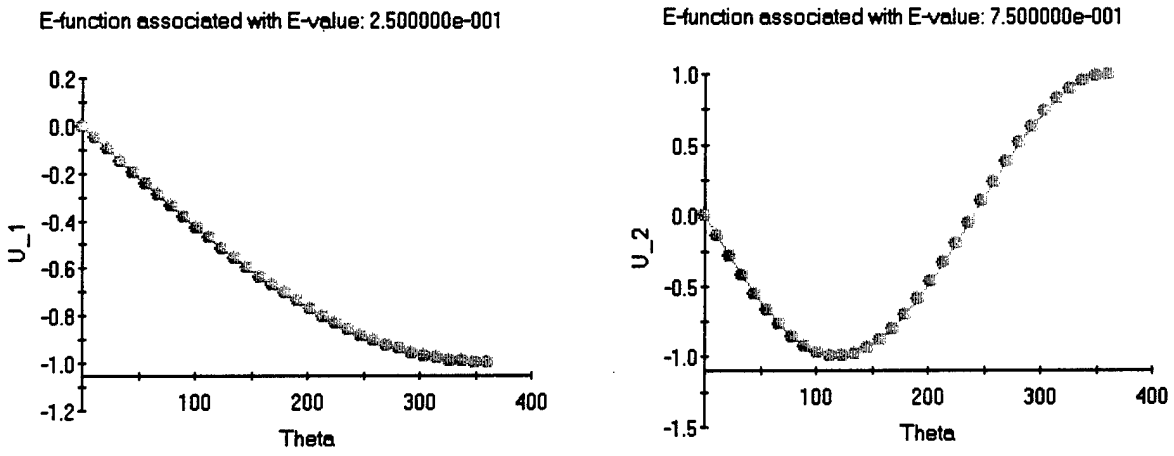

FIGURE 12. Eigenfunctions associated with the first and second eigenvalues for scalar problem 1.

Scalar problem 2: Anisotropic reentrant corner. This is a heat transfer problem in an anisotropic material whose boundary consists of a 90° reentrant corner generated by two flux-free faces Γ_1 and Γ_2, which meet along an edge as shown in Figure 13. The cylindrical boundary of the domain (Γ_R) is loaded by flux boundary condition which corresponds to the first symmetric eigenfunction of the asymptotic expansion of $u(x,y,z)$ about the reentrant edge as given in Ref. [6]. The finite element mesh created in Stress Check consisting of three solid elements is also shown in the figure.

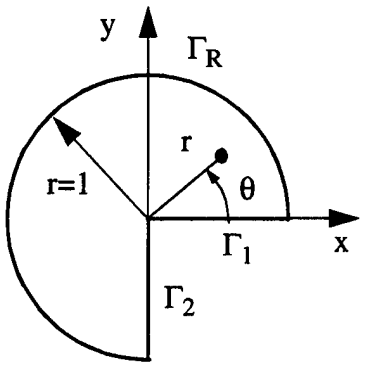

Material properties:
kxx=4.0
kyy=kzz=1.0

Boundary Conditions:
$u(0,0,0) = 0.0$
$\partial u/\partial\theta = 0$ on Γ_1, Γ_2

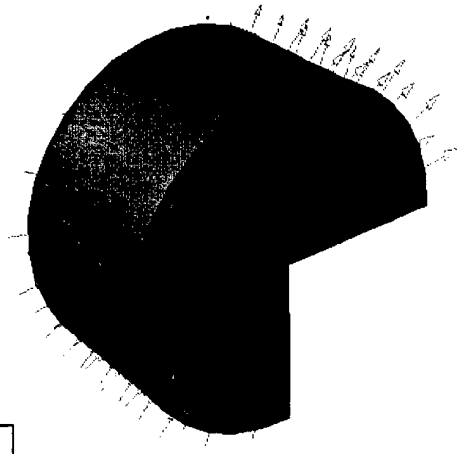

FIGURE 13. Anisotropic reentrant corner. Notation and mesh.

The exact values of the first and second eigenvalues and the corresponding GFIFs are α_1=2/3, A_1=1.0 and α_2=4/3, A_2=0.0, respectively. The finite element solution was obtained for polynomial orders ranging from 1 to 8. The estimated relative error in energy norm for the sequence of solutions is shown in Figure 14. The estimated error is around 3% for the solution with 433 degrees of freedom (DOF).

Error Estimate
Anisotropic reentrant corner
(0) Solution = SOL, runs #1 to #8

Run #	DOF	Total Potential Energy	Convergence Rate	% Error
1	9	-8.823659296528e-001	0.00	29.06
2	28	-9.425922961277e-001	0.59	14.81
3	53	-9.540787151703e-001	0.61	10.01
4	91	-9.584817509602e-001	0.56	7.38
5	145	-9.605587799983e-001	0.54	5.74
6	218	-9.616691556281e-001	0.53	4.63
7	313	-9.623188417919e-001	0.52	3.83
8	433	-9.627258673192e-001	0.52	3.24
Estimated Limit		-9.637358320546628e-001		

FIGURE 14. Estimated realtive error in energy norm for scalar problem 2.

The first and second eigenvalues computed in Stress Check and the corresponding eigenvectors are shown in Figure 15, while the values of the GFIFs are shown in Figure 16. The tabular data shows the

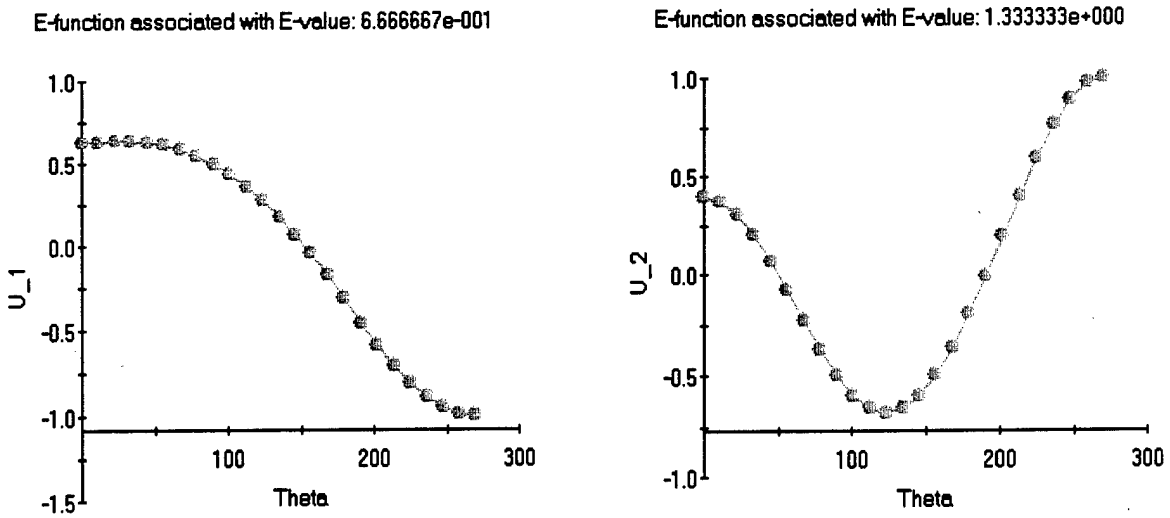

FIGURE 15. Eigenfunctions associated with the first and second eigenvalues for scalar problem 2.

convergence of the A_1 and A_2 as a function of the number of degrees of freedom (DOF) corresponding to eight finite element solutions obtained for polynomial orders ranging from 1 to 8. As can be

```
Number of E-pairs: 2, Solid angle: 2.700000e+002
Global coord. of point along edge: X=0.0, Y=0.0, Z=-0.147912
No. 1, Eval = 6.666667e-001
No. 2, Eval = 1.333333e+000

                Fracture Extraction
            Anisotropic reentrant corner
(0) Solution = SOL, runs 1 to 8 (nodes=1-1,angle=270.0),
  Generalized Flux Intensity Factors, Int. Radius = 0.9
-------------------------------------------------------
  Run      DOF      Radius          A1          A2
-------------------------------------------------------
    1        9   9.000e-001  -8.850e-001  -5.038e-002
    2       28   9.000e-001  -9.879e-001  -2.443e-003
    3       53   9.000e-001  -9.837e-001  -4.930e-004
    4       91   9.000e-001  -9.951e-001   8.555e-004
    5      145   9.000e-001  -9.962e-001   2.111e-004
    6      218   9.000e-001  -9.970e-001   4.884e-005
    7      313   9.000e-001  -9.987e-001   2.482e-004
    8      433   9.000e-001  -9.984e-001   7.792e-006
-------------------------------------------------------
Est.Limit A1=-9.979279e-001
Est.Limit A2=1.103098e-004
```

FIGURE 16. Eigenvalues and Generalized Flux Intensity Factors for scalar problem 2.

seen, the numerically computed eigenvalues are practically identical to the theoretical values. The generalized flux intensity factor are also very close to the theoretical values.

Scalar problem 3: Two material interface. Two materials perfectly bonded along a common edge satisfying the following equation:

$$k_i \nabla^2 u = 0 \qquad in\ \Omega_i \tag{31}$$

with the following flux conditions along the external boundary (Figure 17):

$$\frac{\partial u}{\partial r} = k_i[\alpha_1 r^{\alpha_1 - 1} h_1(\theta) + \alpha_2 r^{\alpha_2 - 1} h_2(\theta)] \qquad on\ \Gamma_i = \partial\Omega_i \qquad i = 1,2 \tag{32}$$

The material coefficients are: k_1=10, k_2=1; the eigenvalues are: α_1=0.731691779, α_2=1.268308221, and:

$$h_1(\theta) = \begin{cases} \cos[(1-a)\theta] + c_1 \sin[(1-a)\theta] \rightarrow on\ \Gamma_1 \\ c_1 \cos[(1-a)\theta] + c_2 c_3 \sin[(1-a)\theta] \rightarrow on\ \Gamma_2 \end{cases} \tag{33}$$

$$h_2(\theta) = \begin{cases} \cos[(1+a)\theta] - c_3 \sin[(1+a)\theta] \rightarrow on\ \Gamma_1 \\ c_1 \cos[(1+a)\theta] - c_2 c_3 \sin[(1+a)\theta] \rightarrow on\ \Gamma_2 \end{cases} \tag{34}$$

where c_1=6.318181818182, c_2=-2.681818181818, c_3=0.64757612580273, and a=0.26830822130025. The exact solution for this problem is (Ref. [7]):

$$u(r,\theta) = A_1 r^{\alpha_1} h_1(\theta) + A_2 r^{\alpha_2} h_2(\theta) \tag{35}$$

where $A_1 = A_2 = 1$.

A sequence of finite element solutions was obtained for the mesh shown in Figure 17 consisting of 6 solid elements graded in geometric progression towards the singular edge with a common factor of 0.15. The estimated relative error in energy norm for this problem is shown in Figure 18. As can be seen from the results, the global error of the solution is well under 1% for p=8 (716 DOF).

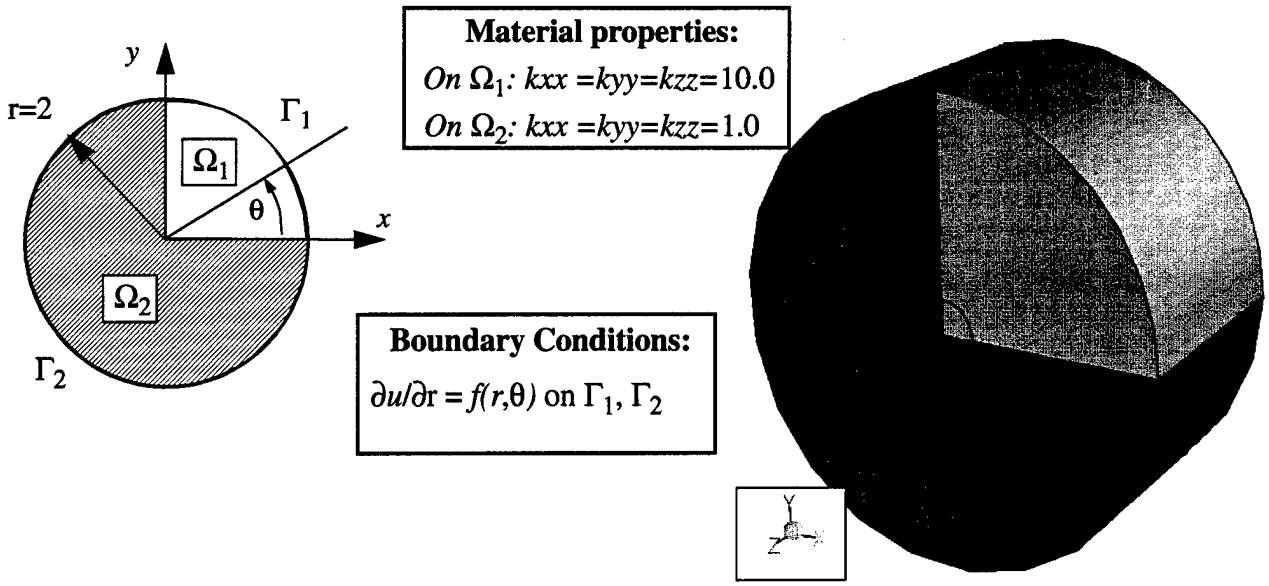

FIGURE 17. Two material interface. Notation and mesh.

Error Estimate
Two material Interface
(0) Solution = SOL, runs #1 to #8

Run #	DOF	Total Potential Energy	Convergence Rate	% Error
1	13	-5.135011591076e+001	0.00	73.67
2	44	-1.110656827166e+002	1.60	10.51
3	81	-1.115029819039e+002	0.36	8.46
4	142	-1.122893439218e+002	3.39	1.26
5	230	-1.123012918676e+002	1.14	0.73
6	351	-1.123044837205e+002	0.90	0.50
7	511	-1.123054822500e+002	0.59	0.40
8	716	-1.123060704408e+002	0.59	0.33

Estimated Limit -1.123072750529331e+002

FIGURE 18. Estimated relative error in energy norm for scalar problem 3.

The first and second eigenpairs are shown in Figure 19. Note that the maximum of these functions are located at 225 degrees for the first eigenfunction and at 154 degrees for the second eigenfunction. In

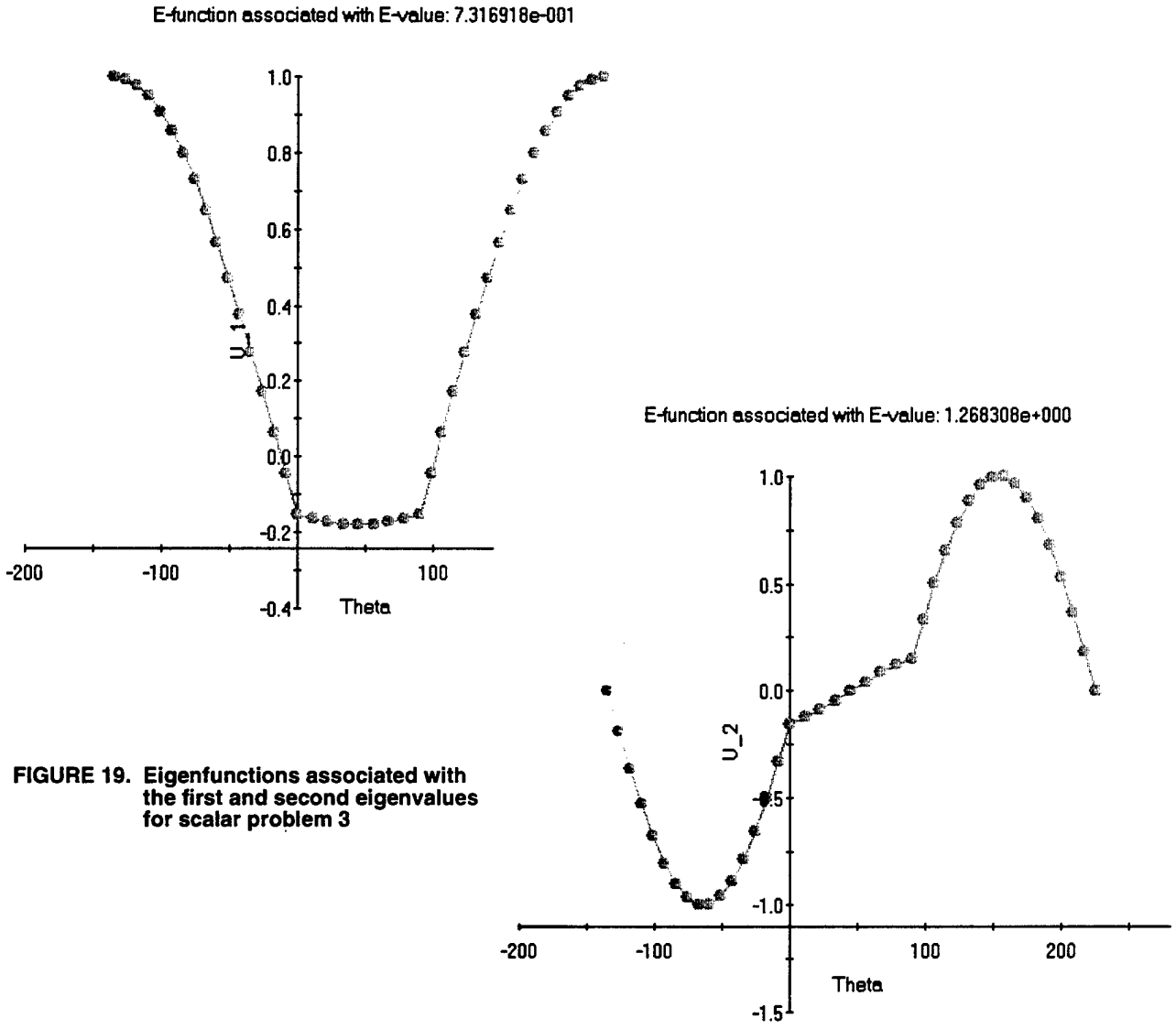

FIGURE 19. Eigenfunctions associated with the first and second eigenvalues for scalar problem 3

both cases the maximum is unity. For the exact eigenvectors given in Eq. (33) for the first eigenvalue and in Eq. (34) for the second eigenvalue, the maximum occur at the same angular positions (225 and 154 degrees respectively) but their magnitude is different (6.5525 for λ_1 and λ_2).

The first and second eigenvalues and the corresponding flux intensity factors computed numerically are shown in Figure 20. As before, the approximation of the eigenvalues is very good, and the values of A_1 and A_2 are also close when considering the difference in the amplitude of the eigenvectors mentioned above. Referring to Eq. (35), it is apparent that the approximate and exact solutions give the

same temperature field in the neighborhood of the singular edge. That is because the product of the GSIFs and the eigenvectors is the same.

```
Number of E-pairs: 2, Solid angle: 3.600000e+002
Global coord. of point along edge: X=0.0, Y=0.0, Z=-5.04279e-002
No. 1, Eval = 7.316918e-001
No. 2, Eval = 1.268308e+000

                Fracture Extraction
              Two material Interface
(0) Solution = SOL, runs 1 to 8 (nodes=17-17,angle=360.0),
  Generalized Flux Intensity Factors, Int. Radius = 0.5
-------------------------------------------------------
   Run      DOF      Radius         A1           A2
-------------------------------------------------------
     1       13   5.000e-001   5.379e+000   8.777e-001
     2       44   5.000e-001   6.408e+000   6.875e+000
     3       81   5.000e-001   6.536e+000   6.883e+000
     4      142   5.000e-001   6.545e+000   6.586e+000
     5      230   5.000e-001   6.544e+000   6.549e+000
     6      351   5.000e-001   6.546e+000   6.551e+000
     7      511   5.000e-001   6.547e+000   6.552e+000
     8      716   5.000e-001   6.548e+000   6.552e+000
-------------------------------------------------------
Est.Limit A1=6.549912e+000 ( 0.03%)
Est.Limit A2=6.552459e+000 ( 0.00%)
```

FIGURE 20. Eigenvalues and Generalized Flux Intensity Factors for scalar problem 3.

Finally, Figure 21 shows the convergence graph of A_1 and A_2 as a function of the number of degrees

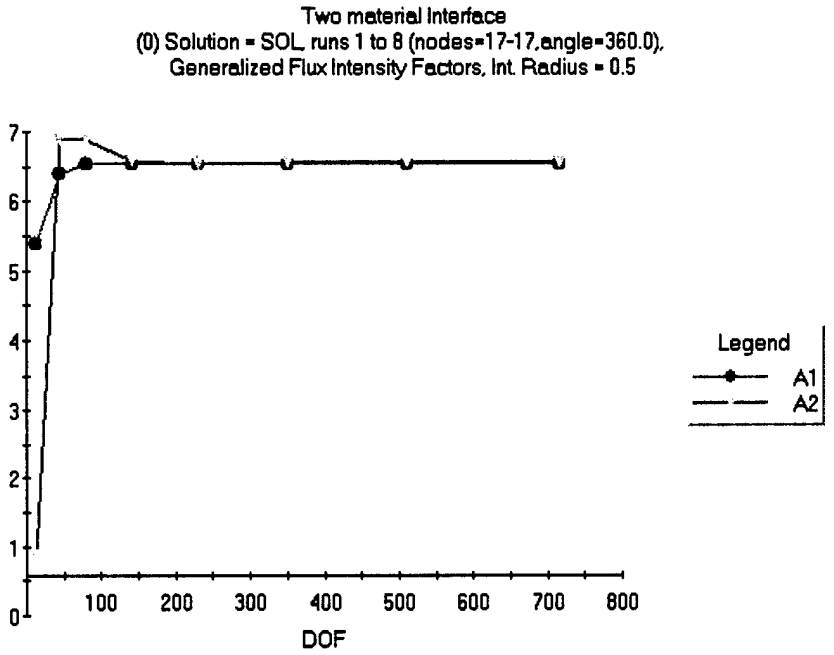

FIGURE 21. Convergence of A1 and A2 for scalar problem 3.

of freedom (DOF). It is apparent from the results, that the generalized flux intensity factors are practically independent of the discretization.

Scalar problem 4: Isotropic reentrant corner. To illustrate the quality of approximation when the generalized flux intensity factor varies along the singular edge, consider the reentrant corner shown in Figure 22.

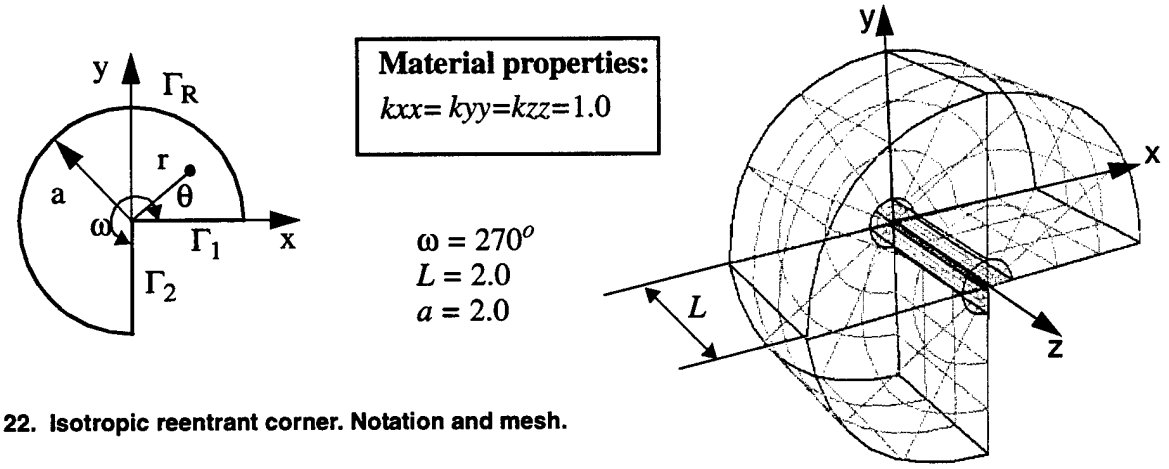

FIGURE 22. Isotropic reentrant corner. Notation and mesh.

This is a heat transfer problem of an isotropic material whose boundary consists of a 90^o reentrant corner generated by two flux-free faces Γ_1 and Γ_2, which meet along an edge. The cylindrical boundary of the domain (Γ_R) and the front (z=L) and back (z=0) faces have Diritchlet boundary conditions, that is the temperature distribution $u(r,\theta,z)$ is imposed using the expansion:

$$u(r,\theta,z) = A_1(z)r^{\alpha_1}\cos(\alpha_1\theta) + A_2(z)r^{\alpha_2}\cos(\alpha_2\theta)$$

$$A_1(z) = a_{11} + a_{12}z, \qquad A_2(z) = a_{21} + a_{22}z$$

where α_i=$i\pi/\omega$ are the exact eigenvalues and the variation of the GFIFs A_1 and A_2 along the singular edge is linear. Selecting $a_{11} = a_{21} = 1.0$ and $a_{12} = a_{22} = 0.5$, the exact values of the GFIFs along the singular edge are:

$$A_1(z) = A_2(z) = A_{EX} = 1.0 + 0.5z$$

A sequence of finite element solutions was obtained for the mesh shown in Figure 22 consisting of 9 solid elements graded in geometric progression towards the singular edge with a common factor of 0.15. The estimated relative error in energy norm is shown in Figure 23. With this mesh, the error at

Error Estimate
Isotropic reentrant corner
(0) Solution = SOL, runs #1 to #8

Run #	DOF	Total Potential Energy	Convergence Rate	% Error
2	9	1.102985683990e+001	0.00	11.12
3	18	1.107409522030e+001	0.28	9.16
4	45	1.108501491406e+001	0.07	8.61
5	93	1.110944485218e+001	0.24	7.23
6	171	1.115382367217e+001	1.17	3.54
7	288	1.116486612363e+001	1.49	1.63
8	453	1.116705996903e+001	1.49	0.83
Estimated Limit		1.116782792307470e+001		

FIGURE 23. Estimated realtive error in energy norm for scalar problem 4.

p=8 (453 DOF) is less than 1%. The corresponding GFIF values obtained using the L^2 projection algorithm implemented in Stress Check are shown in Table 1 at various positions along the singular edge. As can be seen, the numerical results are practically identical to the exact values.

TABLE 1. Numerical and exact values of GFIFs along singular edge

z	$A_1(z)$	$A_2(z)$	A_{EX}
0.053	1.026	1.026	1.0265
0.664	1.332	1.332	1.3320
1.333	1.667	1.667	1.6665
1.967	1.983	1.983	1.9835

4.4 Task 4: Eigenpairs for edge singularities in elasticity problems

The elastostatic displacement field in three-dimensions in the vicinity of an edge singularity can be decomposed in terms of the eigenpairs and the corresponding stress intensity functions. Mathematical details on the decomposition are found in Ref. [8], [10] and the references therein. Elastic edge singularities associated with anisotropic materials and multi-material interfaces have been less investigated, however. Analytical methods as in Ref. [12], [13] provide procedures for the computation of eigenpairs, but require very involved mathematical operations.

In the following, a description of the numerical procedure implemented in Stress Check for the computation of eigenpairs for edge singularities in elasticity is addressed. In the neighborhood of a typical edge singularity the displacement fields can be written as:

$$\vec{u}(r,\theta,z) = \sum_{k=1}^{K}\sum_{s=0}^{S} a_{ks}(z)\; r^{\alpha_k}(\ln r)^s \vec{f}_{ks}(\theta) \;+\; \vec{w}(r,\theta,z) \tag{36}$$

where $S \geq 0$ is an integer which is zero for most practical problems, and $a_{ks}(z)$ are analytic in z and are called the generalized stress intensity functions. The vector function $\boldsymbol{w}(r,\theta,z)$ belongs to $[H^q(\varepsilon_{\delta,R})]^3$, where q depends on K. Considering the case $S = 0$, Eq. (36) becomes:

$$\vec{u}(r,\theta,z) = \sum_{k=1}^{K} a_k(z)\; r^{\alpha_k}\; \vec{f}_k(\theta) \;+\; \vec{w}(r,\theta,z) \tag{37}$$

The tractions on the boundaries are denoted by $\vec{T} = (T_x\ T_y\ T_z)^T$, and the Cartesian stress tensor by $\vec{\sigma} = \sigma_x\ \sigma_y\ \sigma_z\ \tau_{xy}\ \tau_{yz}\ \tau_{zx}$. Body forces are not considered in the vicinity of the singular edge.

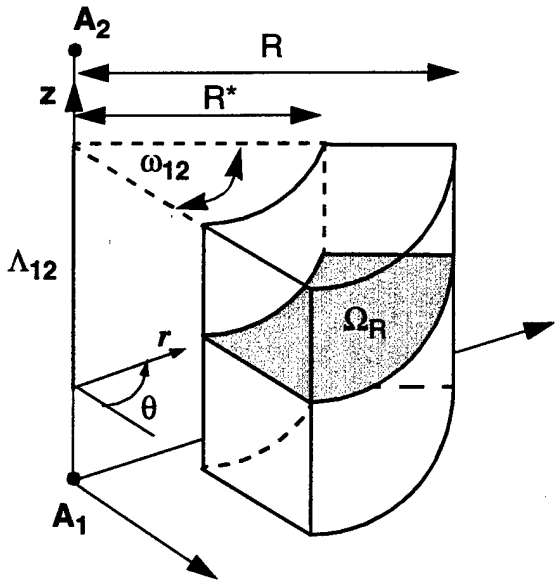

FIGURE 24. The modified Steklov domain Ω_R.

For computing the eigenpairs, a two-dimensional sub-domain Ω_R is constructed in a plane perpendicular to the edge bounded by $r=R$ and $r=R^*$ as shown in Figure 24. On the boundary $\theta=0$ and $\theta=\omega_{12}$ of the sub-domain Ω_R homogenous tractions, homogeneous displacement constraints or a combinations of these are prescribed.

In view of Eq. (37) the displacement vector in Ω_R has the following functional representation:

$$u = a(z)r^{\lambda}\begin{bmatrix} f_x(\theta) \\ f_y(\theta) \\ f_z(\theta) \end{bmatrix} = a(z)r^{\lambda}\underset{\sim}{f}(\theta) \tag{38}$$

and the in-plane variation of the displacements is written as:

$$\underset{\sim}{\hat{u}}(r,\theta) = \frac{\underset{\sim}{\hat{u}}}{a(z)} \tag{39}$$

Following the steps presented in detail in Ref. [14], an eigenvalue problem is cast in a weak form over a two dimensional domain involving all three displacement components:

$$\text{Seek } \alpha \in C, \qquad 0 \neq \underset{\sim}{\hat{u}} \in [H^1(\Omega_R)]^3, \quad \text{such that,} \quad \forall \underset{\sim}{\hat{v}} \in [H^1(\Omega_R)]^3$$

$$B(\underset{\sim}{\hat{u}}, \underset{\sim}{\hat{v}}) - [N_R(\underset{\sim}{\hat{u}}, \underset{\sim}{\hat{v}}) - N_{R^*}(\underset{\sim}{\hat{u}}, \underset{\sim}{\hat{v}})] = \lambda[M_R(\underset{\sim}{\hat{u}}, \underset{\sim}{\hat{v}}) - M_{R^*}(\underset{\sim}{\hat{u}}, \underset{\sim}{\hat{v}})] \tag{40}$$

with

$$B(\underset{\sim}{\hat{u}}, \underset{\sim}{\hat{v}}) = \int_{R^*}^{R}\int_{0}^{\omega_{12}} \left\{\left([A_r]\partial_r + [A_\theta]\frac{\partial_\theta}{r}\right)\underset{\sim}{\hat{v}}\right\}^T [E]\left\{\left([A_r]\partial_r + [A_\theta]\frac{\partial_\theta}{r}\right)\underset{\sim}{\hat{u}}\right\} r dr d\theta$$

$$N_R(\underset{\sim}{\hat{u}}, \underset{\sim}{\hat{v}}) = \int_0^{\omega_{12}} (\underset{\sim}{\hat{v}})^T [A_r]^T [E][A_\theta]\partial_\theta \underset{\sim}{\hat{u}}\Big|_{r=R} d\theta$$

$$M_R(\underset{\sim}{\hat{u}}, \underset{\sim}{\hat{v}}) = \int_0^{\omega_{12}} (\underset{\sim}{\hat{v}})^T [A_r]^T [E][A_r]\underset{\sim}{\hat{u}}\Big|_{r=R} d\theta \tag{41}$$

where [E] is a 6x6 material matrix with up to 21 independent coefficient for a completely anisotropic material; $\partial_r = \partial/\partial r$, $\partial_\theta = \partial/\partial\theta$; and

$$[A_r] = \begin{bmatrix} \cos\theta & 0 & 0 \\ 0 & \sin\theta & 0 \\ 0 & 0 & 0 \\ \sin\theta & \cos\theta & 0 \\ 0 & 0 & \sin\theta \\ 0 & 0 & \cos\theta \end{bmatrix} \qquad [A_\theta] = \begin{bmatrix} -\sin\theta & 0 & 0 \\ 0 & \cos\theta & 0 \\ 0 & 0 & 0 \\ \cos\theta & -\sin\theta & 0 \\ 0 & 0 & \cos\theta \\ 0 & 0 & -\sin\theta \end{bmatrix} \tag{42}$$

Remark 1. The test and trial functions have three components, but the domain over which the weak eigen-formulation is defined is two-dimensional and excludes any singularity. Therefore the application of the p-version of the finite element method (FEM) for solving Eq. (41) is very efficient.

Remark 2. The bilinear forms N_R and N_{R*} are non-symmetric with respect to $\hat{u}$ and $\hat{v}$ thus they are not self-adjoint. As a consequence the 'minimum principle' does not hold, and any approximation of the eigenvalues obtained using a finite dimension subspace of $[H^1(\Omega_R)]^3$ cannot be considered as an upper bound of the exact ones, and the monotonic behavior of the error is lost as well. Convergence is assured under a general proof provided in Ref. [16], however.

Next consider the discretization of the weak formulation given by Eq. (40) using the p-version FEM over a finite dimensional subspace of $[H^1(\Omega_R)]^3$. Assuming that the domain Ω_R consist of three different materials as shown in Figure 25, let us divide it into three finite elements as shown. Let us consider a typical element bounded by θ_1 and θ_2 (element 1 in Figure 25). A standard element is considered in the ξ, η plane such that $-1 < \xi < 1$, $-1 < \eta < 1$ over which the polynomial basis and trial functions are defined. These standard elements are mapped into the real elements by proper mapping functions (for details, see Ref. [15] chapters 5 and 6). The functions $\hat{u}$ and $\hat{v}$ are expressed in terms of the basis functions $\Psi_i(\xi,\eta)$ in the standard plane:

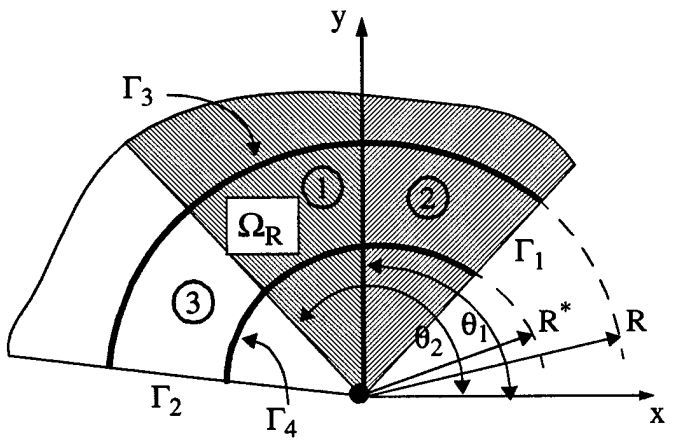

FIGURE 25. Discretization of the domain Ω_R.

$$\hat{u} = \begin{bmatrix} \psi_1 \ldots \psi_N & 0 \ldots 0 & 0 \ldots 0 \\ 0 \ldots 0 & \psi_1 \ldots \psi_N & 0 \ldots 0 \\ 0 \ldots 0 & 0 \ldots 0 & \psi_1 \ldots \psi_N \end{bmatrix} \begin{bmatrix} c_1 \\ \ldots \\ c_{3N} \end{bmatrix} = [\Psi]\{C\} \tag{43}$$

where C_i are the amplitudes of the basis functions and ψ_i are the products of the integral of the Legendre polynomials in ξ and η. Since $\underset{\sim}{\hat{u}}$ and $\underset{\sim}{\hat{v}}$ lie in the same space, we define similarly $\underset{\sim}{\hat{v}} = [\Psi]\{B\}$.

The unconstrained stiffness matrix corresponding to the bilinear form B in Eq. (41) is given by:

$$[K] = \int_{R^*}^{R}\int_{\theta_1}^{\theta_2}\left\{\left([A_r]\partial_r + [A_\theta]\frac{\partial_\theta}{r}\right)[\Psi]\right\}^T [E]\left\{\left([A_r]\partial_r + [A_\theta]\frac{\partial_\theta}{r}\right)[\Psi]\right\} r dr d\theta \tag{44}$$

Next we define the matrices:

$$[\partial P] = \begin{bmatrix} -P_1'\sin\theta & \dots & -P_N'\sin\theta & 0 & \dots & 0 & 0 & \dots & 0 \\ 0 & \dots & 0 & P_1'\cos\theta & \dots & P_N'\cos\theta & 0 & \dots & 0 \\ 0 & \dots & 0 & 0 & \dots & 0 & 0 & \dots & 0 \\ P_1'\cos\theta & \dots & P_N'\cos\theta & -P_1'\sin\theta & \dots & -P_N'\sin\theta & 0 & \dots & 0 \\ 0 & \dots & 0 & 0 & \dots & 0 & P_1'\cos\theta & \dots & P_N'\cos\theta \\ 0 & \dots & 0 & 0 & \dots & 0 & -P_1'\sin\theta & \dots & -P_N'\sin\theta \end{bmatrix}$$

$$[\tilde{P}] = \begin{bmatrix} P_1\cos\theta & \dots & P_N\cos\theta & 0 & \dots & 0 & 0 & \dots & 0 \\ 0 & \dots & 0 & P_1\sin\theta & \dots & P_N\sin\theta & 0 & \dots & 0 \\ 0 & \dots & 0 & 0 & \dots & 0 & 0 & \dots & 0 \\ P_1\sin\theta & \dots & P_N\sin\theta & P_1\cos\theta & \dots & P_N\cos\theta & 0 & \dots & 0 \\ 0 & \dots & 0 & 0 & \dots & 0 & P_1\sin\theta & \dots & P_N\sin\theta \\ 0 & \dots & 0 & 0 & \dots & 0 & P_1\cos\theta & \dots & P_N\cos\theta \end{bmatrix}$$

where $P_i(\xi)$ for $i>3$ are the integrals of the Legendre polynomials, and $P_1(\xi)=(1-\xi)/2$, $P_2(\xi)=(1+\xi)/2$. Therefore, the bilinear form N can be written as:

$$N_R(\underset{\sim}{\hat{u}}, \underset{\sim}{\hat{v}}) = [B]^T\left(\int_{-1}^{1}[\tilde{P}]^T[E][\partial P]\ |_{\eta=-1} d\xi\right)[C] = [B]^T[N_R][C] \tag{45}$$

The entries in $[N_R]$ are computed using Gauss quadrature. Similarly, the expression for the bilinear form M is evaluated as follows:

$$M_R(\underset{\sim}{\hat{u}}, \underset{\sim}{\hat{v}}) = [B]^T\left(\frac{\theta_2-\theta_1}{2}\int_{-1}^{1}[\tilde{P}]^T[E][\tilde{P}]\ |_{\eta=-1} d\xi\right)[C] = [B]^T[M_R][C] \tag{46}$$

The matrices $[N_{R*}]$ and $[M_{R*}]$ have the same values as those of $[N_R]$ and $[M_R]$, but of opposite sign. This is because the shape functions on boundaries Γ_3 and Γ_4 are the same (except for a sign change), and so is the mapping to the standard element. Denoting the set of amplitudes of the basis functions

associated with the boundary Γ_3 by $[C_R]$, and those associated with the boundary Γ_4 by $[C_{R*}]$, the eigenpairs can be obtained by solving the following generalized eigenvalue problem:

$$[K][C] - [N_R][C_R] + [N_{R*}][C_{R*}] = \lambda([M_R][C_R] - [M_{R*}][C_{R*}]) \tag{47}$$

Augmenting the coefficients of the basis functions associated with Γ_3 with those associated with Γ_4 and denoting them by the vector $[C_{RR*}]$, Eq. (47) becomes:

$$[K][C] - [N_{RR*}][C_{RR*}] = \lambda[M_{RR*}][C_{RR*}] \tag{48}$$

The vector that represents the total number of nodal variables in Ω_R is divided into two vectors, one containing the variables $[C_{RR*}]$ and the other the rest of the variables: $[C]^T = \{[C_{RR*}]^T, [C_{in}]^T\}$. By partitioning the stiffness matrix $[K]$, Eq. (48) can be written as:

$$\begin{bmatrix} [K] - [N_{RR*}] & [K_{RR*-in}] \\ [K_{in-RR*}] & [K_{in}] \end{bmatrix} \begin{bmatrix} C_{RR*} \\ C_{in} \end{bmatrix} = \lambda \begin{bmatrix} [M_{RR*}] & [0] \\ [0] & [0] \end{bmatrix} \begin{bmatrix} C_{RR*} \\ C_{in} \end{bmatrix} \tag{49}$$

The relation in Eq. (49) is used to eliminate $[C_{in}]$ by static condensation, thus obtaining the reduced eigenvalue problem:

$$[K_S][C_{RR*}] = \lambda[M_{RR*}][C_{RR*}] \tag{50}$$

where

$$[K_S] = [K] - [N_{RR*}] - [K_{RR*-in}][K_{in}]^{-1}[K_{in-RR*}]$$

In Eq. (50) $[K_S]$ is a full matrix. However the order of the matrices is relatively small, so the solution of the eigenvalue problem (using Cholesky factorization to compute $[K_{in}]^{-1}$) is not expensive. Note that the derivation was performed for a single element. For multiple elements along Γ_3 and Γ_4 the formulation is identical and the matrices $[K]$, $[N_R]$ and $[M_R]$ are obtained by an assembly procedure.

4.5 Task 5: Generalized stress intensity factors for edge singularities in elasticity problems

As in the case of the generalized flux intensity factors, the algorithm for the computation of the GSIFs is based on a L^2 projection of the finite element solution into the space of functions characterized by the asymptotic expansion in terms of the eigenpairs. The algorithm can be summarized as follows: Consider a section perpendicular to a singular edge of an elasticity problem as shown in Figure 26.

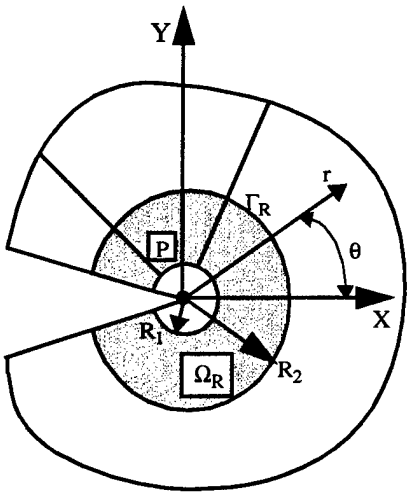

FIGURE 26. Typical cross-section of an edge singularity through point P.

The displacement field corresponding to the exact solution can be expanded around the singular edge at point P in terms of the eigenpairs and the generalized stress intensity factors:

$$\vec{u}(r,\theta) = \begin{Bmatrix} u_x(r,\theta) \\ u_y(r,\theta) \\ u_z(r,\theta) \end{Bmatrix} = \sum_{i=1}^{N} A_i r^{\lambda_i} \vec{f}_i(\theta) \tag{51}$$

where A_i are the GSIFs, λ_i are the eigenvalues and $\{f(\theta)\}=\{f_x(\theta), f_y(\theta), f_z(\theta)\}$ are the corresponding eigenfunctions. Let $\{u_{FE}(r,\theta)\}$ be the finite element solution of the displacement field around the singular edge. Then the L_2 projection of $\{u_{FE}\}$ into the domain Ω_R is characterized by the following:

$$\int_{\Omega_R} (\vec{u} - \vec{u}_{FE})\vec{v}\,dA = 0, \qquad for\ all\ \vec{v} \in S \tag{52}$$

where S is the space of eigenfunctions, and $\{v(r,\theta)\}$, is given by:

$$\vec{v}(r,\theta) = \sum_{i=1}^{N} B_i r^{\lambda_i} \vec{f}_i(\theta)$$

Substituting $\{u\}$ and $\{v\}$ into Eq. (52) and rearranging we have:

$$\lfloor B \rfloor \int_{\Omega_R} (\{\phi_x\}\lfloor \phi_x \rfloor + \{\phi_y\}\lfloor \phi_y \rfloor + \{\phi_z\}\lfloor \phi_z \rfloor) dA \{A\} = \lfloor B \rfloor \int_{\Omega_R} (\{\phi_x\} u_{FE|x} + \{\phi_y\} u_{FE|y} + \{\phi_z\} u_{FE|z}) dA \tag{53}$$

where:

$$\{\phi_x\} = r^{\lambda_i}\{f_x\}, \qquad \{\phi_y\} = r^{\lambda_i}\{f_y\}, \qquad \{\phi_z\} = r^{\lambda_i}\{f_z\} \tag{54}$$

Eliminating B_i from Eq. (53) and noting that $dA=rdrd\theta$, the following system is obtained:

$$\int_{R_1}^{R_2}\int_{\theta_1}^{\theta_2} (\{\phi_x\}\lfloor \phi_x \rfloor + \{\phi_y\}\lfloor \phi_y \rfloor + \{\phi_z\}\lfloor \phi_z \rfloor) r dr d\theta \{A\} = \int_{R_1}^{R_2}\int_{\theta_1}^{\theta_2} (\{\phi_x\} u_{FE|x} + \{\phi_y\} u_{FE|y} + \{\phi_z\} u_{FE|z}) r dr d\theta \tag{55}$$

From the definition of $\{\phi\}$ in Eq. (54) and integrating in the radial direction, the system of equation reduces to:

$$K_{ij}A_j = R_j$$

$$K_{ij} = \frac{R_2^{(\lambda_i+\lambda_j+2)} - R_1^{(\lambda_i+\lambda_j+2)}}{2+\lambda_i+\lambda_j} \int_{\theta_1}^{\theta_2} [f_{xi}(\theta)f_{xj}(\theta) + f_{yi}(\theta)f_{yj}(\theta) + f_{zi}(\theta)f_{zj}(\theta)]d\theta \tag{56}$$

$$R_j = \int_{R_1}^{R_2}\int_{\theta_1}^{\theta_2} r^{(\lambda_j+1)}(f_{xj}u_{FE|x} + f_{yj}u_{FE|y} + f_{zj}u_{FE|z})drd\theta$$

Solving the system of equations represented by Eq. (56) over the domain Ω_R gives the values of A_i (the GSIFs). Note that only a line integral is required to compute K_{ij} and an area integral to compute R_j. The displacement vector from the finite element solution $\{u_{FE}\}$ has to be evaluated relative to the local coordinate system located at the extraction point P.

The procedure implemented in Stress Check for the computation of the generalized stress intensity factors is the same as described for the heat transfer problem. First the elasticity problem is solved for the given topology, material properties and boundary conditions. After the finite element solution is available, the post-processing operation requires only to click with the mouse cursor along the singular edge. The program then determines a cutting plane normal to the singular edge at the pick point and computes the eigenvalues and corresponding eigenvectors as explained in the previous section. With the eigenpairs and the displacement field obtained from the finite element solution the program constructs the system given by Eq. (56), the solution of which provides the GSIFs as illustrated in the next section.

Stress Intensity Factors. Utilizing most of the functions and procedures developed for the computation of GFIFs/GSIFs, an algorithm was implemented to compute the stress intensity factors for cracks in isotropic materials using the contour integral method (CIM). The mode 1 and 2 stress intensity factor are computed from the finite element solution at any position along the crack front using the CIM as described in Ref. [15], page 227. The procedure is outlined in the following.

For plane stress and plane strain, the stress intensity factors in mode I and mode II are given by:

$$K_I = \sqrt{2\pi}A_1^{(1)}, \qquad K_{II} = \sqrt{2\pi}A_1^{(2)} \tag{57}$$

where $A_1^{(m)}$, $m = 1, 2$, is the first term in the asymptotic expansion of the solution in the neighborhood of the crack tip. Let (x,y) represent a local Cartesian coordinate system located at any point along the crack front in such a way that the local z-axis is tangent to the crack front at that point, and the x-axis is in the direction of the crack face. Let Γ be a circle of radius ρ centered at the point along the crack front, and assume that ρ is sufficiently close to the crack (Figure 27). It has been shown that A_1 can be computed from a line integral as:

$$A_1^{(m)} \approx \int_{\Gamma} \left(W_m T_{FE} - u_{FE} T^{(W_m)} \right) ds \qquad (58)$$

where W_m is an extraction function, T_{FE} is the traction vector along Γ computed from the finite element solution u_{FE}, and $T^{(Wm)}$ is the traction vector along Γ due to the extraction function. The traction and displacement vectors must be computed in relation to the local coordinate system attached to the crack front.

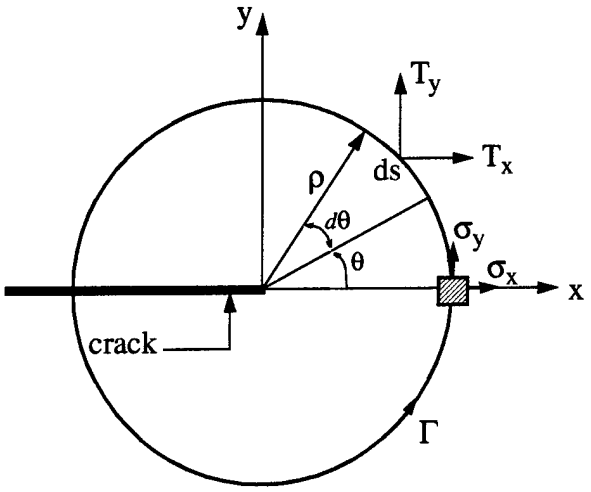

FIGURE 27. Contour around crack front.

The terms in Eq. (58) are computed from the finite element solution of the cracked body along the contour Γ as follows:

$$T_{FE} = \begin{bmatrix} T_x(x,y) \\ T_y(x,y) \end{bmatrix}_{FE} = \begin{bmatrix} \sigma_x \cos\theta + \tau_{xy} \sin\theta \\ \tau_{yx} \cos\theta + \sigma_y \sin\theta \end{bmatrix}_{FE}, \qquad u_{FE} = \begin{bmatrix} u_x(x,y) \\ u_y(x,y) \end{bmatrix}_{FE} \qquad (59)$$

The terms in Eq. (58) due to the extraction functions are given by:

$$W_m = \frac{\rho^{-\frac{1}{2}}}{D^{(m)}} \{\Psi^{(m)}(\theta)\}, \qquad T^{(W_m)} = -\frac{G\rho^{-\frac{3}{2}}}{D^{(m)}} \{\Upsilon^{(m)}(\theta)\} \qquad (60)$$

where G is the shear modulus, and $D^{(1)} = \pi(2\kappa - 1)$, $D^{(2)} = \pi(2\kappa + 3)$, where κ depends on the Poisson's ratio (ν). For plane strain $\kappa = 3 - 4\nu$, and for plane stress $\kappa = (3 - \nu)/(1 + \nu)$. Also, the vector functions that depend on the variable θ are given by:

$$\{\Psi^{(1)}(\theta)\} = \begin{bmatrix} \left(\kappa - \frac{1}{2}\right)\cos\frac{\theta}{2} - \frac{1}{2}\cos\frac{3\theta}{2} \\ \left(\kappa + \frac{1}{2}\right)\sin\frac{\theta}{2} - \frac{1}{2}\sin\frac{3\theta}{2} \end{bmatrix}, \qquad \{\Psi^{(2)}(\theta)\} = \begin{bmatrix} \left(\kappa + \frac{3}{2}\right)\sin\frac{\theta}{2} + \frac{1}{2}\sin\frac{3\theta}{2} \\ -\left(\kappa - \frac{3}{2}\right)\cos\frac{\theta}{2} - \frac{1}{2}\cos\frac{3\theta}{2} \end{bmatrix} \qquad (61)$$

$$\left\{\Upsilon^{(1)}(\theta)\right\} = \begin{bmatrix} \left(\frac{3}{2}\cos\frac{\theta}{2} + \frac{1}{2}\cos\frac{5\theta}{2}\right)\cos\theta + \left(\frac{1}{2}\sin\frac{5\theta}{2} - \frac{1}{2}\sin\frac{\theta}{2}\right)\sin\theta \\ \left(\frac{1}{2}\sin\frac{5\theta}{2} - \frac{1}{2}\sin\frac{\theta}{2}\right)\cos\theta + \left(\frac{5}{2}\cos\frac{\theta}{2} - \frac{1}{2}\cos\frac{5\theta}{2}\right)\sin\theta \end{bmatrix}$$

$$\left\{\Upsilon^{(2)}(\theta)\right\} = \begin{bmatrix} \left(-\frac{7}{2}\sin\frac{\theta}{2} - \frac{1}{2}\sin\frac{5\theta}{2}\right)\cos\theta + \left(\frac{1}{2}\cos\frac{5\theta}{2} + \frac{3}{2}\cos\frac{\theta}{2}\right)\sin\theta \\ \left(\frac{1}{2}\sin\frac{5\theta}{2} + \frac{3}{2}\cos\frac{\theta}{2}\right)\cos\theta + \left(-\frac{1}{2}\sin\frac{\theta}{2} + \frac{1}{2}\sin\frac{5\theta}{2}\right)\sin\theta \end{bmatrix} \quad (62)$$

In general, a three-dimensional problem is neither a plane stress nor a plane strain problem. Therefore the question is how to determine the value of κ for the extraction function in Eq. (61). The procedure to determine which value of κ to use is based on computing the stress components σ_x, σ_y, σ_z at a point in front of the crack (see Figure 27). Next define γ as the ratio:

$$\gamma = \frac{\sigma_z}{\sigma_x + \sigma_y}$$

If γ is close to Poisson's ratio (ν), then the condition approaches that of plane strain. If is close to zero, then is plane stress. The approach implemented in Stress Check was to compute the value of γ at a point along the integration path ($r = \rho$, $\theta = 0$), and apply the following rule to determine κ:

$$\kappa = \begin{cases} 3 - 4\nu & \text{if } (\gamma > 0.85\nu) \\ \frac{3-\nu}{1+\nu} & \text{if } (\gamma < 0.85\nu) \end{cases}$$

The advantages of this implementation are improved computational speed and the ability to include curved crack fronts. The improvements in performance are realized because the eigenvalues and corresponding eigenvectors need not be computed prior to computing the stress intensity factors. An example of the implementation is presented in the next section.

4.6 Task 6: Model problems - Eigenpairs and generalized stress intensity factors

The procedures described in the previous sections for the computation of the eigenpairs and the corresponding generalized stress intensity factors for edge singularities for elasticity problems in 3D, are illustrated in the following.

Elasticity problem 1: Isotropic reentrant corner. The first example of the implementation of the algorithm for the computation of the eigenpairs and generalized stress intensity factors for edge sin-

gularities, consider the traction-free isotropic L-shaped domain shown in Figure 28 loaded along the boundaries by the Mode 1 and Mode 2 stress components as given in Ref. [15]. The load is applied to the faces labeled 1, through 4 in Figure 28. The two free faces perpendicular to the singular edge were constrained from motion in the z-direction.

The finite element mesh created in Stress Check consisting of 18 solid elements with two layers of geometrically graded elements towards the reentrant corner is also shown in the figure. The elements were graded with a common factor of 0.15. The problem was solved for polynomial order ranging

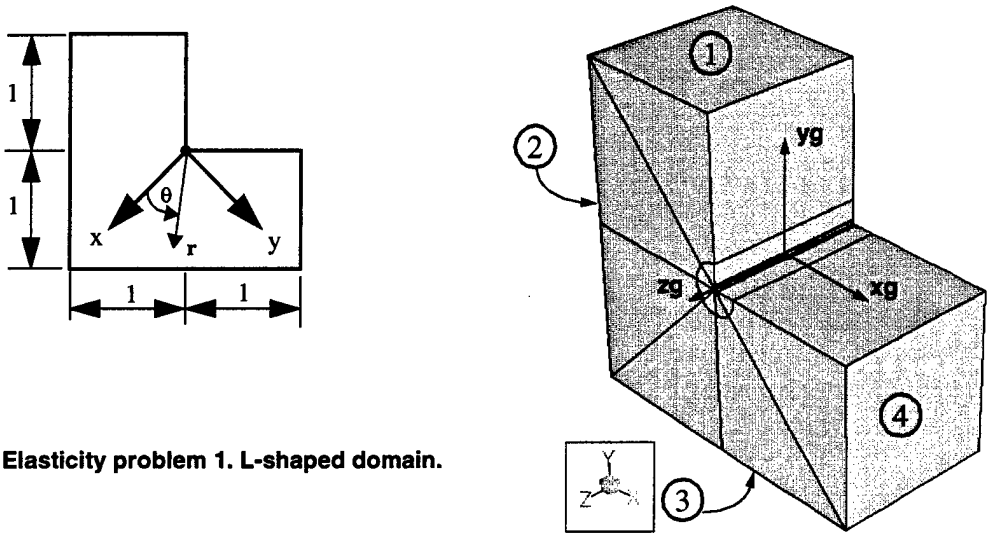

FIGURE 28. Elasticity problem 1. L-shaped domain.

from p=1 to 8. The estimated relative error in energy norm for the sequence of eight solutions is shown in Figure 29. For p=8 (5338 DOF) the global error of the finite element solution is less than 1%.

ErrorEstimate
L-SHAPED DOMAIN
(0) Solution = SOL, runs #1 to #8

Run #	DOF	Total Potential Energy	Convergence Rate	% Error
1	85	-4.299854922149e-001	0.00	24.66
2	307	-4.548143062914e-001	0.87	8.11
3	553	-4.571877574981e-001	1.32	3.73
4	988	-4.576467179110e-001	1.10	1.97
5	1630	-4.577446575364e-001	0.80	1.32
6	2533	-4.577780333023e-001	0.61	1.01
7	3751	-4.577941449008e-001	0.54	0.82
8	5338	-4.578038073468e-001	0.54	0.67
Estimated Limit		-4.578246109968524e-001		

FIGURE 29. Estimated relative error in energy norm for elasticity problem 1.

The exact values of the first three eigenvalues and the corresponding GFIFs are λ_1=0.544483, A_1=1.0, λ_2=2/3, A_2=0.0 and λ_3=0.908529, A_3=1.0, respectively. The eigenvalues computed in Stress Check are shown in Figure 30, together with the three components of the first and third eigenvectors. Note that all the eigenvalues are real.

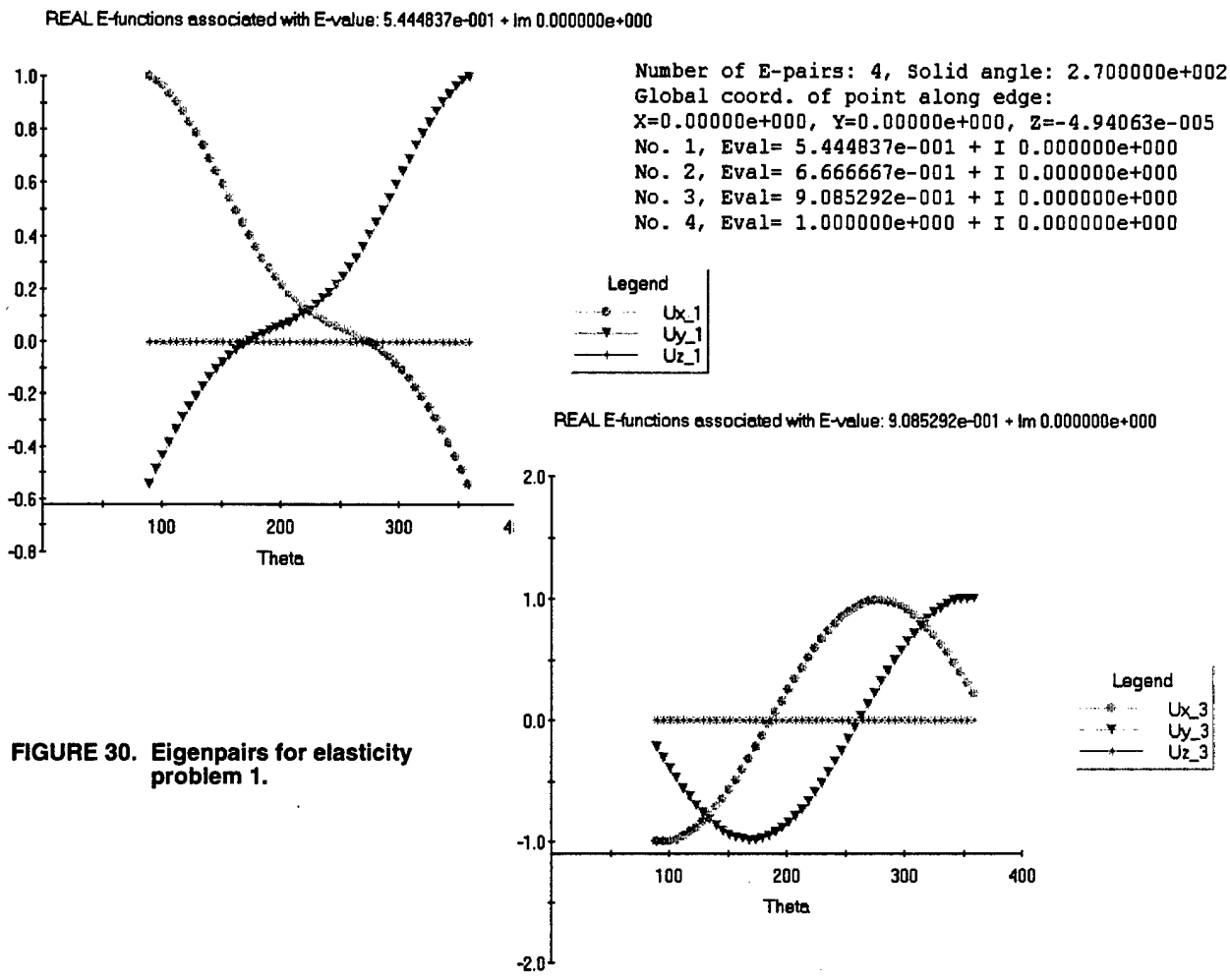

FIGURE 30. Eigenpairs for elasticity problem 1.

The values of the GSIFs computed by the numerical procedure described in the previous section are shown in the Figure 31. The tabular data shows the GSIFs computed from each finite element solution. The graph shows the values of A1 and A3 as a function of the number of degrees of freedom (DOF). The stress intensity factors are practically coincident with the exact values.

GSIFs
L-SHAPED DOMAIN
(0) Solution = SOL, runs 1 to 8 (nodes=22-22,angle=270.0),
Generalized Stress Intensity Factors, Int. Radius = 0.5

Run	DOF	Radius	A1	A2	A3	A4
1	85	5.000000e-001	-7.107936e-001	1.446139e-014	-9.391302e-001	8.031775e-001
2	307	5.000000e-001	-9.382039e-001	1.445316e-006	-9.890786e-001	8.060001e-001
3	553	5.000000e-001	-9.836161e-001	3.560110e-008	-9.983398e-001	8.104599e-001
4	988	5.000000e-001	-9.926223e-001	3.474569e-011	-1.000214e+000	8.112030e-001
5	1630	5.000000e-001	-9.936874e-001	4.783306e-010	-1.000123e+000	8.114920e-001
6	2533	5.000000e-001	-9.946648e-001	4.768257e-010	-9.999739e-001	8.113539e-001
7	3751	5.000000e-001	-9.955081e-001	-1.794964e-008	-9.999516e-001	8.113397e-001
8	5338	5.000000e-001	-9.961335e-001	-9.754908e-010	-9.999505e-001	8.113303e-001

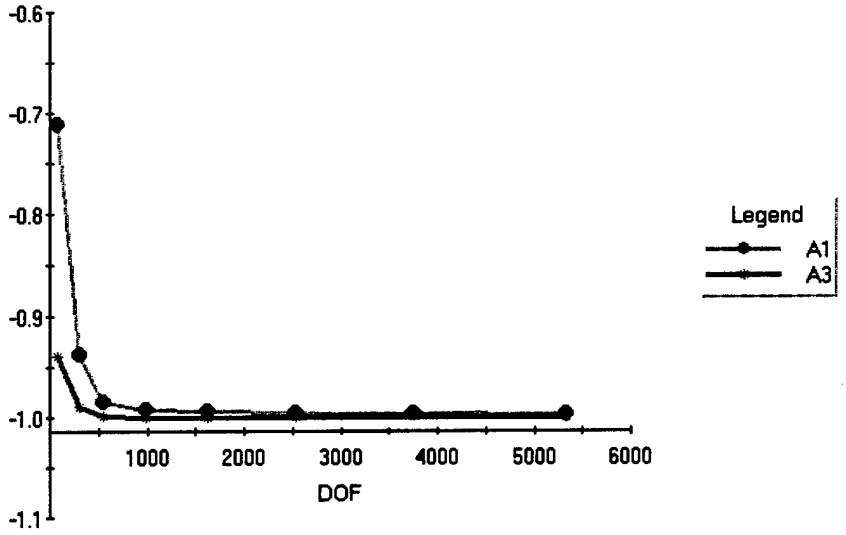

FIGURE 31. Generalized Stress Intensity Factors for elasticity problem 1.

Elasticity problem 2: Crack in isotropic material. Consider the case of a through-thickness crack in a thick isotropic plate under tension loading as shown in Figure 32. After the finite element solution is

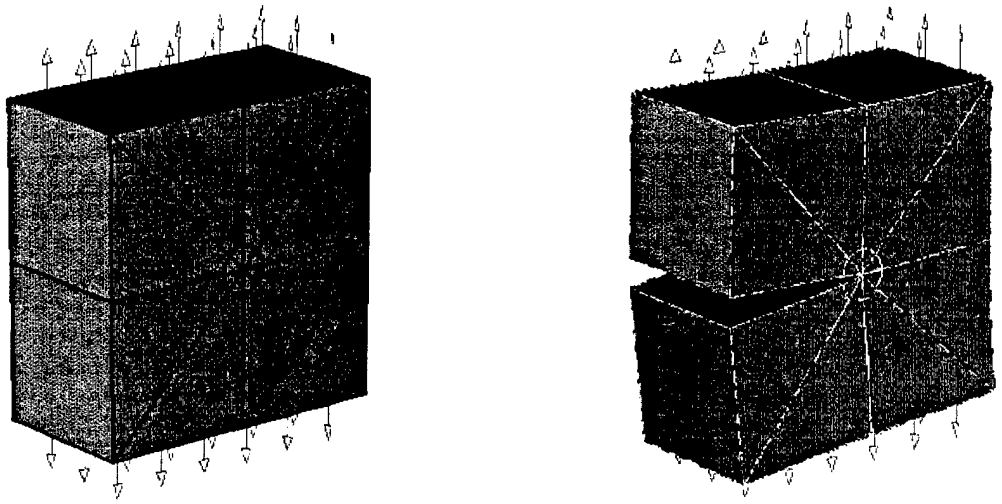

FIGURE 32. Through-thickness crack in thick plate. Undeformed and deformed configurations.

obtained, the procedure for the computation of the stress intensity factors requires the user simply to point and click with the mouse cursor to the desired location along the crack front.

The procedure implemented in Stress Check determines a cutting plane normal to the tangent to the crack edge at the pick point and extract the global components of the stresses and displacements along a circular path contained in the cutting plane. These stresses and displacements are projected into the cutting plane and integrated with the extraction function to compute the contour integral described in the previous section.

Figure 33 shows the results of the stress intensity factors (SIFs) obtained from a set of finite element solutions for polynomial orders ranging from p=1 to 6 at three locations along the crack front. Z=0.5 represents the center of the plate and Z=0.0 is one of the free faces. Note the variation of the SIFs along the crack front, with the largest value of K1 at the center of the plate. The estimated limits for the SIFs are also included which indicate the strong convergence characteristics of the implemented extraction procedure.

Elasticity problem 3: Inclusion problem. Consider a composite body consisting of two dissimilar isotropic, homogeneous and elastic wedges, perfectly bonded along the interfaces. The body is loaded on the circular boundary by the stress field corresponding to the exact solution of the asymptotic expansion about the singular point as given in Ref. [17]. The normal displacement is set to zero in the

Contour Integral Method: Angle=360, Radius=2.50e-01

Edge location: X=8.05e-17, Y=1.21e-17, Z=5.00e-01

Run #	DOF	K1	K2
1	108	2.344084e+000	8.085629e-002
2	369	4.301251e+000	3.570169e-002
3	678	4.861055e+000	3.683432e-002
4	1185	5.160177e+000	3.276876e-002
5	1914	5.268396e+000	3.567037e-002
6	2913	5.300811e+000	3.498816e-002

Estimated Limits
Limit value for K1 ... 5.319954e+000 (diff: 0.36%)
Limit value for K2 ... 3.497732e-002 (diff: 0.03%)

Edge location: X=8.05e-17, Y=1.21e-17, Z=2.51e-01

Run #	DOF	K1	K2
1	108	2.352391e+000	7.861335e-002
2	369	4.200244e+000	3.580445e-002
3	678	4.802555e+000	3.711076e-002
4	1185	5.153232e+000	3.338650e-002
5	1914	5.198848e+000	3.617087e-002
6	2913	5.189015e+000	3.574476e-002

Estimated Limits
Limit value for K1 ... 5.146324e+000 (diff: 0.83%)
Limit value for K2 ... 3.558739e-002 (diff: 0.44%)

Edge location: X=8.05e-17, Y=1.21e-17, Z=2.64e-02

Run #	DOF	K1	K2
1	108	2.359888e+000	7.658902e-002
2	369	3.935169e+000	3.609123e-002
3	678	4.649050e+000	3.783665e-002
4	1185	4.899167e+000	3.462604e-002
5	1914	4.893078e+000	3.787856e-002
6	2913	4.862767e+000	3.679010e-002

Estimated Limits
Limit value for K1 ... 4.856227e+000 (diff: 0.13%)
Limit value for K2 ... 3.682425e-002 (diff: 0.09%)

FIGURE 33. Stress intensity factors for elasticity problem 2.

two lateral faces. Figure 34 shows the description of the problem and the finite element mesh consisting of 10 solid elements. The first three eigenvalues characterizing the stress singularity along the edge are: $\lambda_1 = 0.5124722$, $\lambda_2 = 0.6001175$ and $\lambda_3 = 0.7309757$.

A sequence of finite element solutions was obtained for polynomial orders ranging from 1 to 8. The estimated relative error in energy norm is shown in Figure 35. The first four eigenvalues computed in Stress Check are shown in Figure 36, together with the corresponding generalized stress intensity factors (A_i, $i = 1$ to 4). Note that all the eigenvalues are practically identical to the analytical values, and the excellent convergence characteristics of the GSIFs with increasing number of degrees of freedom.

Finally, the three components of the first three eigenvectors are shown in Figure 37.

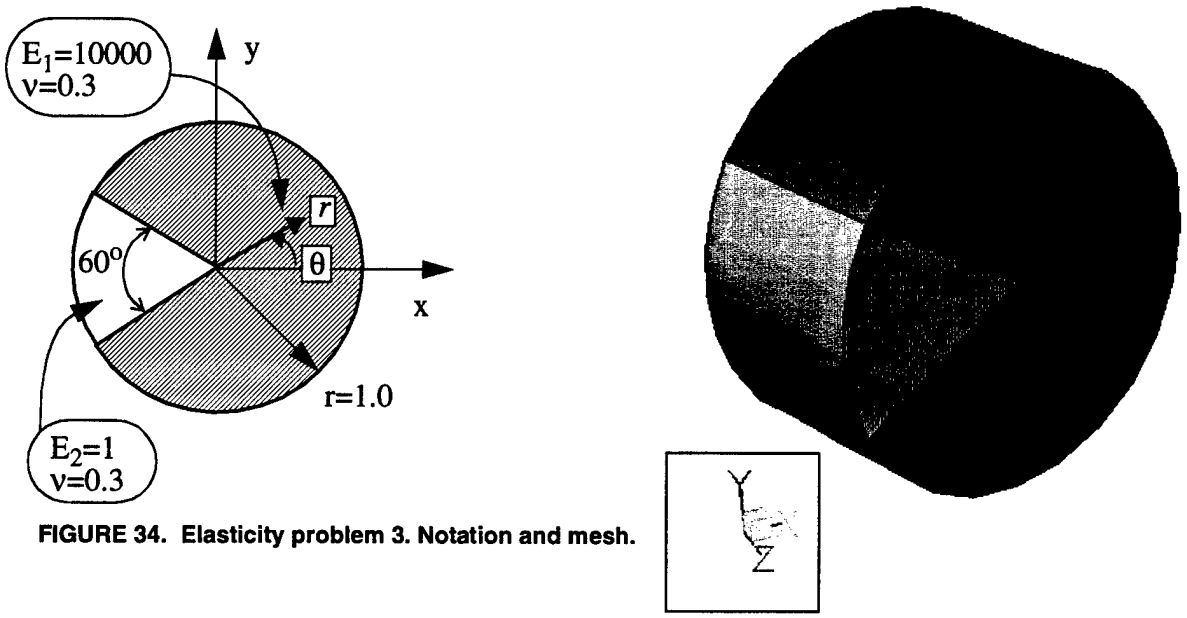

FIGURE 34. Elasticity problem 3. Notation and mesh.

Error
Inclusion problem
(1) Solution = SOL, runs #1 to #8

Run #	DOF	Total Potential Energy	Convergence Rate	% Error
1	41	-5.453568540785e-004	0.00	31.96
2	154	-5.980512136567e-004	0.72	12.40
3	287	-6.041965203489e-004	0.86	7.24
4	520	-6.057759815888e-004	0.58	5.14
5	868	-6.063591919594e-004	0.44	4.11
6	1361	-6.066690259315e-004	0.40	3.43
7	2029	-6.068609125881e-004	0.39	2.93
8	2902	-6.069886028295e-004	0.39	2.55
Estimated Limit		-6.073828017459567e-004		

FIGURE 35. Estimated relative error in energy norm for elasticity problem 3.

Elasticity problem 4: Angles-ply anisotropic laminate. Consider the singularities associated with a composite laminate with ply properties typical of a high-modulus graphite epoxy material. The material coefficients in the principal direction of the fibers are:

$$E_L=20\text{x}10^6 \text{ psi}, E_T=2.1\text{x}10^6 \text{ psi}, G_{LT}=G_{TT}=0.85\text{x}10^6 \text{ psi}, \nu_{LT}=\nu_{TT}=0.21$$

```
Number of E-pairs: 4, Solid angle: 3.600e+002
Global coord. along edge: X=0.0, Y=0.0, Z=7.45e-03
No. 1, Eval= 5.124722e-001 + I 0.000000e+000
No. 2, Eval= 6.001175e-001 + I 0.000000e+000
No. 3, Eval= 7.309757e-001 + I 0.000000e+000
No. 4, Eval= 1.000000e+000 + I 0.000000e+000
```

GSIF
Inclusion problem
(2) Solution = SOL, runs 1 to 8 (nodes=7-7,angle=360.0),
Generalized Stress Intensity Factors, Int. Radius = 0.2

Run	DOF	Radius	A1	A2	A3	A4
1	41	2.000e-001	8.566e-005	-1.135e-016	3.971e-004	2.663e-004
2	154	2.000e-001	1.286e-004	-1.684e-007	3.952e-004	1.704e-004
3	287	2.000e-001	1.423e-004	-8.186e-009	4.023e-004	1.694e-004
4	520	2.000e-001	1.466e-004	-8.658e-012	4.046e-004	1.724e-004
5	868	2.000e-001	1.490e-004	-4.625e-012	4.055e-004	1.728e-004
6	1361	2.000e-001	1.505e-004	-4.364e-012	4.059e-004	1.733e-004
7	2029	2.000e-001	1.515e-004	4.630e-012	4.062e-004	1.736e-004
8	2902	2.000e-001	1.522e-004	4.145e-012	4.063e-004	1.738e-004

Est.Limit A1=1.551560e-004 (1.91%)

FIGURE 36. Eigenvalues and GSIFs for elasticity problem 3.

where L and T refer to the fiber and transverse directions, respectively. There are three plies in the laminate and they are oriented at + or – 45 degrees about the global y-axis (Figure 38). Of interest are the eigenvalues associated with the free edge singularity between two plies, and those associated with a delamination (edge crack) between two plies. In the case of the free-edge singularities the eigenvalues reported in Ref. [18] are:

$$\lambda_1 = 0.974424,\ \lambda_{2,3} = 1.88147 \pm i\,0.234005,\ \lambda_{4,5} = 2.511526 \pm i\,0.792817$$

For the delamination (edge crack), the reported values are:

$$\lambda_{1,2} = 0.50 \pm i\,0.0343,\ \lambda_3 = 0.50$$

For the computation of eigenvalues in Stress Check it is necessary to perform at least one solution. In this case the mesh shown in Figure 38 consisting of 6 solid elements was solved for p=1 only. The eigenvalues were then extracted at the free edge singularity and at the crack singularities indicated in Figure 38. The results are shown in Figure 39. As can be seen they match perfectly the values reported in Ref. [18].

Elasticity problem 5: Composite patch. Consider the a composite patch bonded to a metallic structure as shown in Figure 40. Assuming that the thickness of the adhesive is negligible, the composite patch is in full contact with the metal. Therefore we want to investigate the edge singularity along the

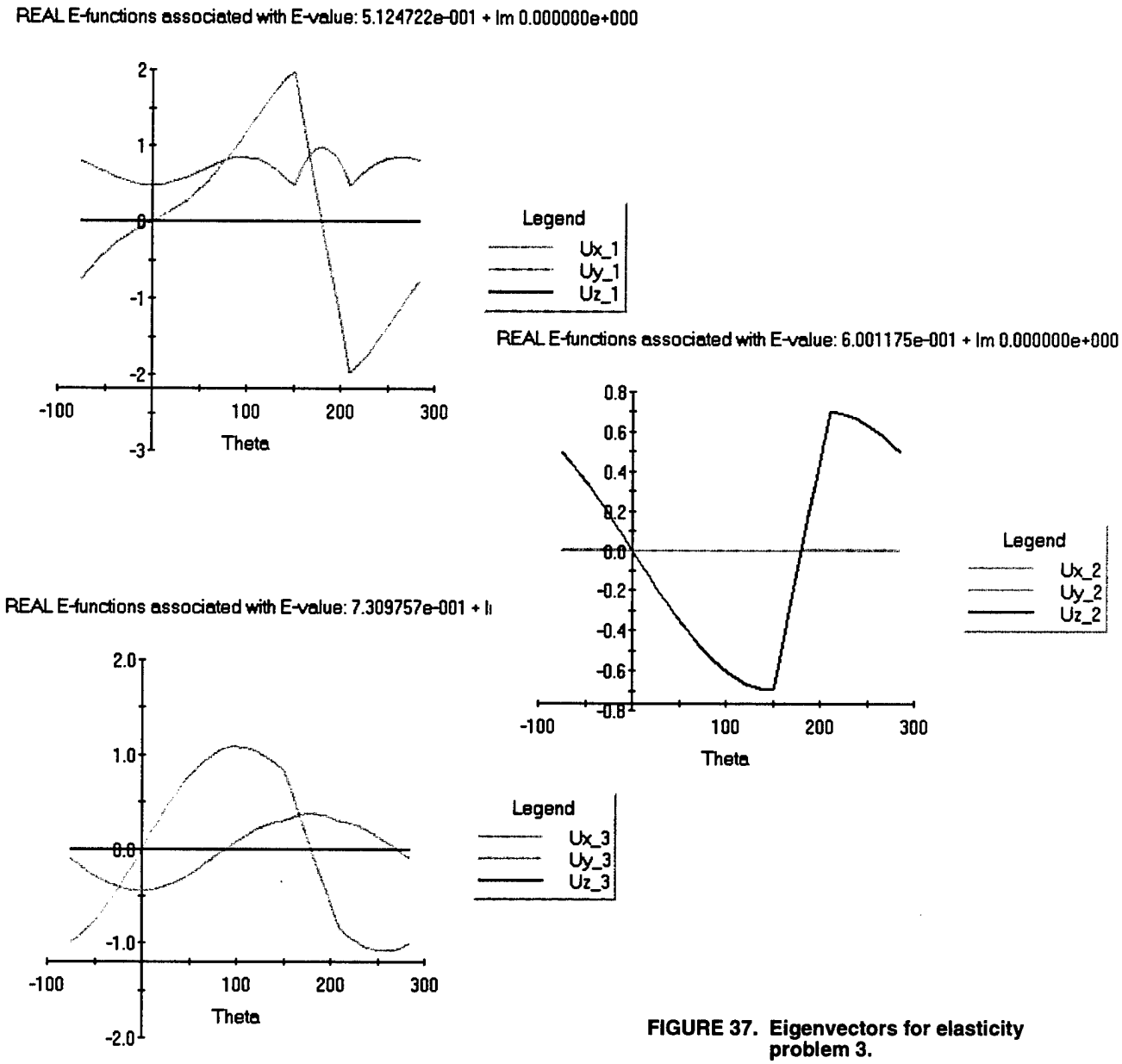

FIGURE 37. Eigenvectors for elasticity problem 3.

composite patch as a function of the termination angle α. The material coefficients in the principal direction of the fibers are:

$$E_L=20\text{x}10^6 \text{ psi}, E_T=2.1\text{x}10^6 \text{ psi}, G_{LT}=G_{TT}=0.85\text{x}10^6 \text{ psi}, \nu_{LT}=\nu_{TT}=0.21$$

with the fibers rotated an angle β about the y-axis. For the aluminum plate the following properties are considered: $E=10.5\text{x}10^6$ psi and $\nu=0.3$. We will investigate the eigenpairs obtained with a ply orientation of $\beta=45^o$ while changing the termination angle from α from 20^o to 90^o. The finite element

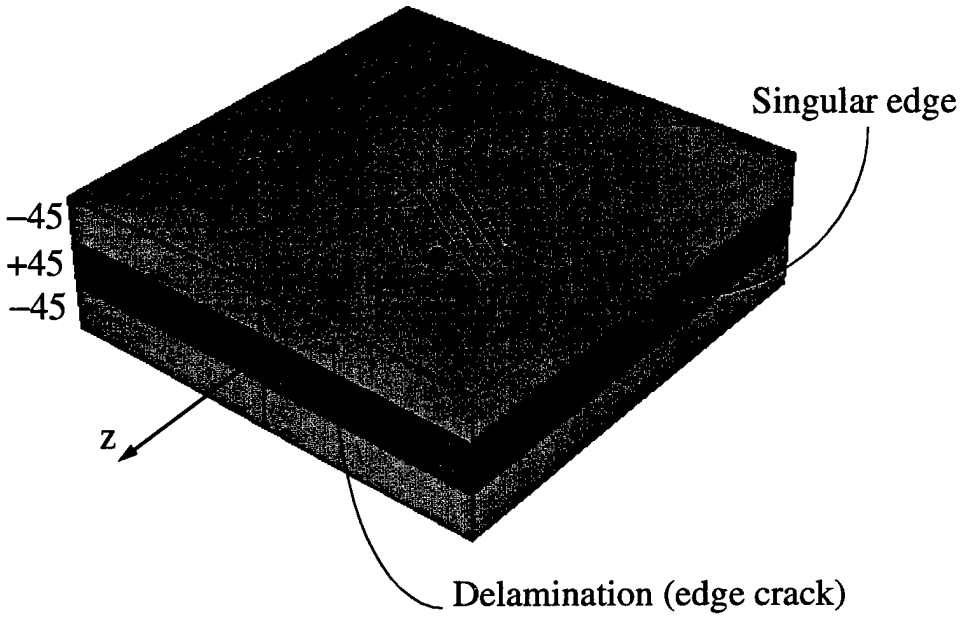

FIGURE 38. Elasticity problem 4. Notation and Mesh.

Edge Singularity

```
Number of E-pairs: 8, Solid angle: 180
Global coord. of point along edge:
    X=1.0, Y=0.2, Z=0.518353

No. 1, Eval= 9.744238e-001 + I 0.000000e+000
No. 2, Eval= 1.000000e+000 + I 0.000000e+000
No. 3, Eval= 1.000000e+000 + I 0.000000e+000
No. 4, Eval= 1.881466e+000 + I 2.340048e-001
No. 5, Eval= 1.881466e+000 + I-2.340048e-001
No. 6, Eval= 1.999999e+000 + I 0.000000e+000
No. 7, Eval= 2.511439e+000 + I 7.929259e-001
No. 8, Eval= 2.511439e+000 + I-7.929259e-001
```

Delamination

```
Number of E-pairs: 4, Solid angle: 360
Global coord. of point along edge:
   X=0.5, Y=0.1, Z=0.468659

No. 1, Eval= 5.000003e-001 + I 3.434452e-002
No. 2, Eval= 5.000003e-001 + I-3.434452e-002
No. 3, Eval= 5.000011e-001 + I 0.000000e+000
No. 4, Eval= 1.000000e+000 + I 0.000000e+000
```

FIGURE 39. Eigenvalues for elasticity problem 4.

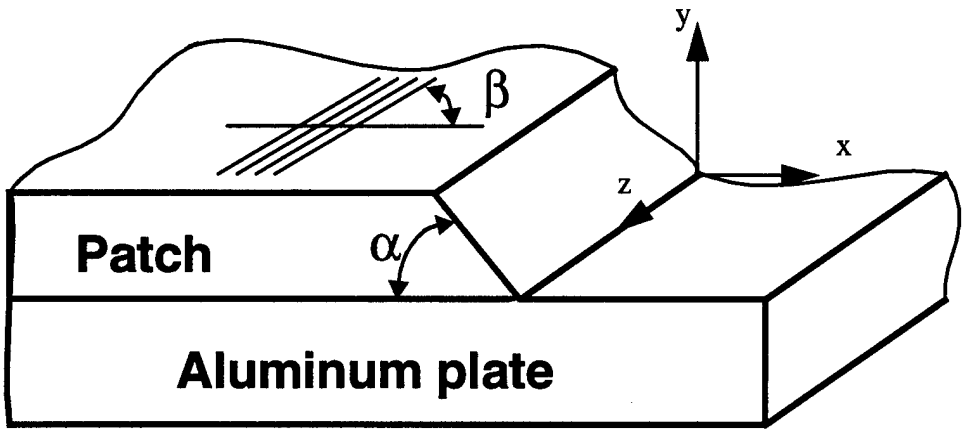

FIGURE 40. Elasticity problem 5. Composite patch over aluminum plate.

mesh consisting of three solid elements used for the numerical analysis is shown in Figure 41. Since

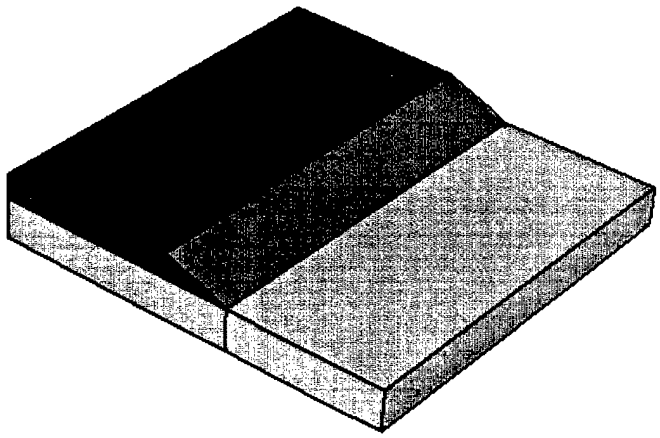

FIGURE 41. Finite element mesh fo elasticity problem 5.

the objective of the analysis is the computation of eigenpairs, it is sufficient to perform a finite element analysis at p=1. The results of the analysis using the procedures implemented in Stress Check are shown in Figure 42. Note that the first and second eigenvalues become smaller as the termination angle increases and their magnitudes are minimum (λ_1=0.66418, λ_2=0.750854) for $\alpha = 90^o$, which corresponds to a solid angle of 270°. If the patch would have been made of aluminum and the termination angle $\alpha = 90^o$, the first two eigenvalues would be: λ_1=0.544837, λ_2=0.666667, which is a 'stronger' edge singularity. These results are in agreement with those presented in Ref. [18]. Finally, Figure 43 shows the three components of the eigenvector associated with λ_1=0.66418 for $\alpha = 90^o$.

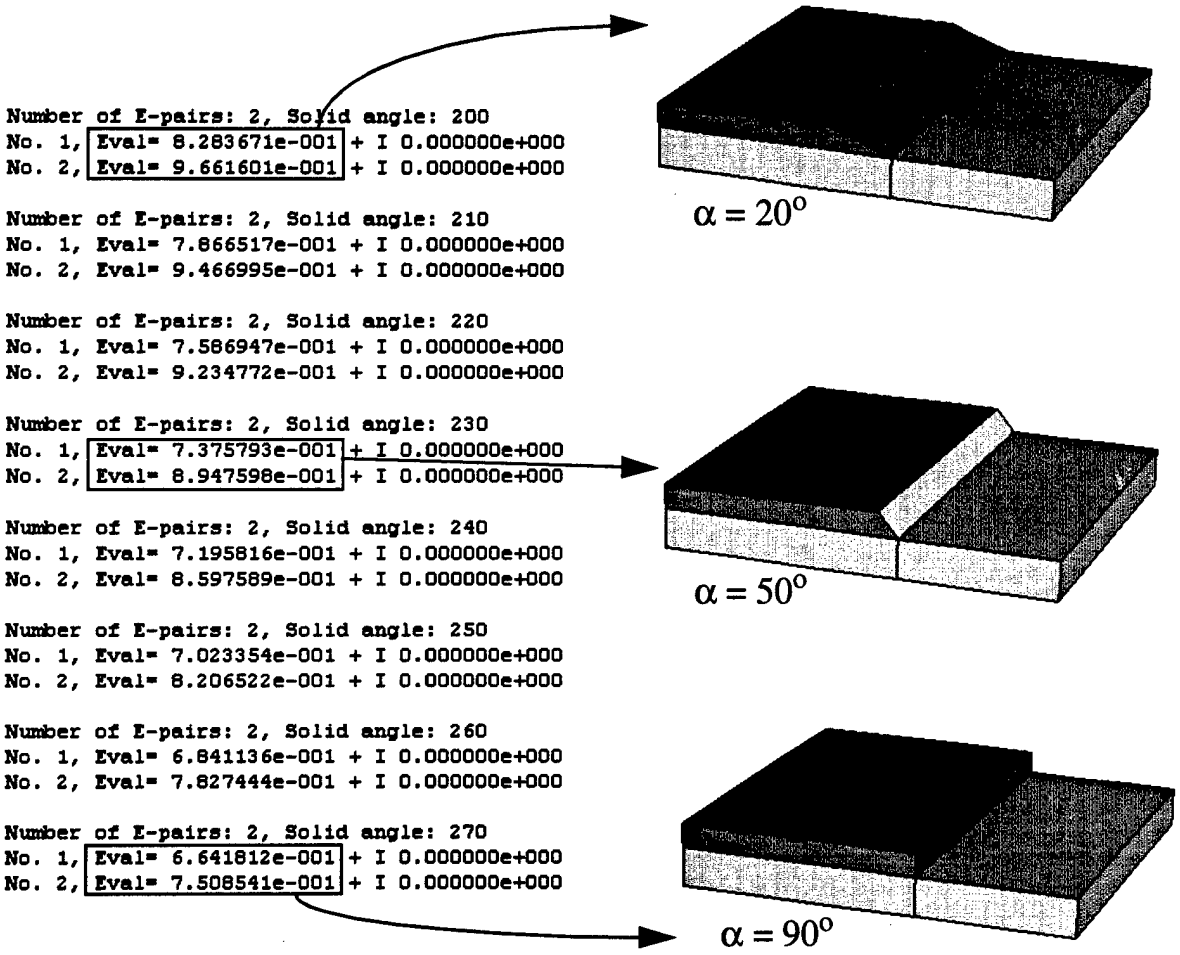

FIGURE 42. Eigenvalues for elasticity problem 5.

4.7 Task 7: Average stress/strain

A set of failure criteria for composite-laminated bonded structures based on stress averaging and material nonlinear analysis were identified as a necessary complement to the set of tools available for analysis. These criteria include:

- *Criteria for failure in the composite adherents (laminate)*: Two failure modes, in-plane failure and out-of-plane failure, are considered separately for the composite adherents. For in-plane failure, maximum stress, maximum strain, Tsai-Wu, Tasi-Hill and Hashin criteria are widely used in the industry. For the out-of-plane failure, a quadratic criterion for interlaminar normal and shear stresses is considered. Because of the stress singularity and high stress gradient near the edge of the laminate or near the edge of a bonded joint, the use of the average stress is necessary as follows:

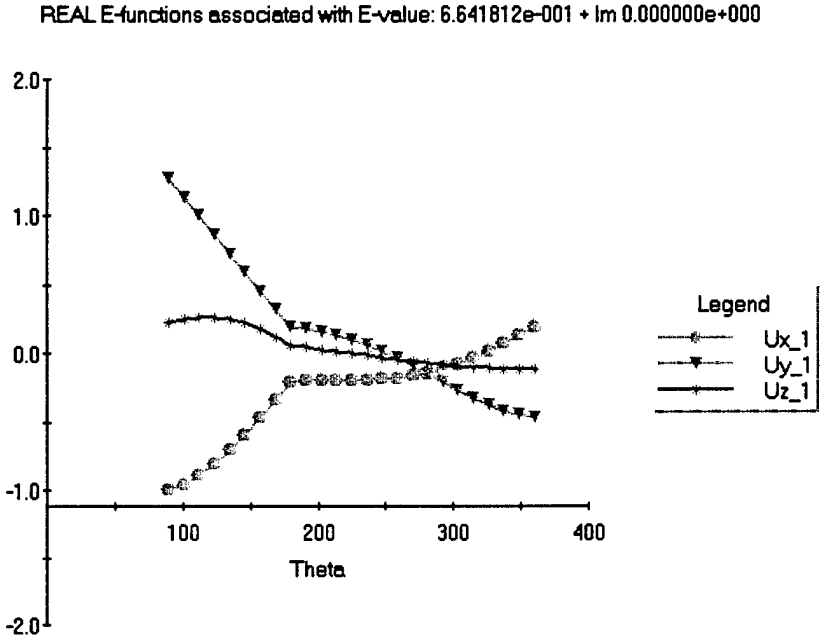

FIGURE 43. Eigenfunctions associated with λ_1=0.66418 for $\alpha = 90^o$. Elasticity problem 5.

$$\left(\frac{\tilde{\sigma}_z}{\sigma_0}\right)^2 + \left(\frac{\tilde{\tau}_{xz}}{\tau_0}\right)^2 \geq 1 \tag{63}$$

where

$$\tilde{\sigma}_z = \frac{1}{a_0}\int_0^{a_0} \sigma_z ds, \qquad \tilde{\tau}_{xz} = \frac{1}{a_0}\int_0^{a_0} \tau_{xz} ds \tag{64}$$

are the average interlaminar normal and shear stresses in the composite, a_0 is a characteristic length (of the order of the lamina thickness), σ_0 is the flatwise tensile strength of the composite and τ_0 is the interlaminar shear strength of the composite. A similar relation can be obtained for three dimensions, where the line integral is replaced by an area integral.

- *Criterion for failure at the adhesive/adherent interface*: Failure along the interface is similar to the interlaminar or out-of-plane failure of the laminate.
- *Criterion for failure in the adhesive layer*: Two major approaches have been applied to determine failure in the adhesive layer: Stress/strain based criteria and fracture or energy based criteria. Based on the data available and based on the anticipated users of the analysis tool, a stress/strain based criterion is recommended. Similar to the interlaminar stresses, very steep stress/strain gradients in

the adhesive layer can be expected at the end of the bonded joint. To relieve the effects of this stress concentration, an average strain criterion is therefore recommended. This criterion can be expressed as:

$$\left(\frac{\bar{\varepsilon}_z}{\varepsilon_0}\right)^2 + \left(\frac{\bar{\gamma}_{xz}}{\gamma_0}\right)^2 \geq 1 \tag{65}$$

where the shear and peel strain terms are averaged over a characteristic length a_0 of the order of the adhesive thickness, and are computed from a material nonlinear analysis of the bonded joint. The adhesive failure strains, ε_0 and γ_0 include the plasticity component and are highly dependent on the material model used in the analysis.

A capability was implemented in Stress Check to compute average stress/strain along element edges, element faces, element volumes and arbitrary curves. The average is understood in the integral sense, and when appropriate, the user controls the number of points used for the numerical integration. If the average is computed along an element edge, face or volume, then the integration is performed using Gauss quadrature, and the number of integration points is selected internally by the program. If the average is performed along an arbitrary path which runs inside one or more elements, then the integration is performed using the trapezoidal rule and the user controls the number of integration points.

For example, if the average stress σ_z is requested along an element edge of length a_0, the program performs the numerical integration indicated in Eq. (64). The arc length a_0 is determined automatically based on the screen selection. If the selected object is an element face, the integral is performed over the area of the face. If the selected object is an element, then a volume integral is performed. The length, area or volume of the selected object is also reported with the corresponding average quantity. The procedure to compute the average is illustrated with an example.

Example: Consider a typical composite bonded joint under axial loading shown in Figure 44. After the linear solution is obtained, the user selects Results > Points and completes the extraction form for the desired average quantity as shown in Figure 45. In this example, the average of σ_y (labeled Sy in the form) is computed along the indicated element edge for a sequence of finite element solutions ranging from p-level=1 to 8. The result shown includes the average for each run with the convergence information and the length of the selected edge.

The quantities for which the average can be computed include the displacement components in the global system, all directional strain and stress components, principal strains and stresses. Additionally, the average can be computed for quantities extracted in a local coordinate system and any other function that can be described using the formula option in Stress Check. This allows formulating an expression of "margin of safety" based on average quantities for any failure mode in the adhesive, adherent or adhesive/adherent interface. For example, an expression for the "margin of safety" (*MS*) for the interlaminar out-of-plane failure of composite adherents can be written as:

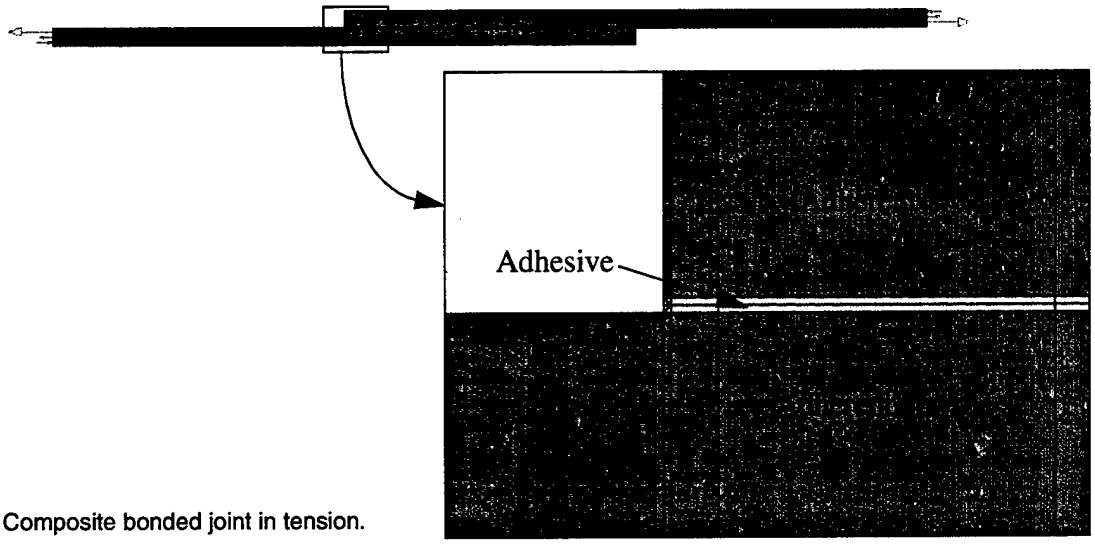

FIGURE 44. Composite bonded joint in tension.

$$MS = \left(\frac{\bar{\sigma}_z}{\sigma_0}\right)^2 + \left(\frac{\bar{\tau}_{xz}}{\tau_0}\right)^2 - 1 \tag{66}$$

In this case, the average of the normal and shear stresses are computed first before the expression of *MS* is evaluated.

4.8 Task 8: Limit load analysis

The evaluation of a composite bonded joint requires a material nonlinear analysis for the design load followed by the determination of the failure loads based on some predefined criteria. The evaluation of failure load by an automatic procedure, that can be utilized from the handbook framework of Stress Check, required the development and implementation of a special nonlinear solution procedure consisting of two steps:

- *Design load*: First the design load is applied to the bonded joint and, after a material nonlinear analysis is performed, the margins of safety are computed for the different modes of failure identified for the joint as described in the previous section. For each mode of failure a different expression for the margin of safety is required, which may be based on average quantities as described above.
- *Failure load*: After the design load analysis, it is necessary to determine the failure load based on the margins of safety. The evaluation of failure load by an automatic procedure from the handbook framework of Stress Check required developing a special nonlinear solution procedure which performs automatic nonlinear runs with load increments specified by the user and checks at the end of

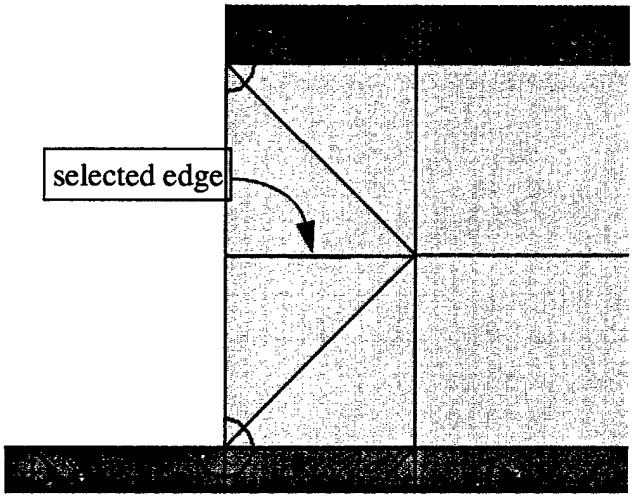

Integral Average Extraction

(0) Solution = SOL, runs #1 to #8
Total length of integration path = 4.500000e-003

Run #	DOF	Sy
1	147	4.286346e+003
2	415	1.310178e+004
3	711	1.168556e+004
4	1127	1.263005e+004
5	1663	1.284542e+004
6	2319	1.283276e+004
7	3095	1.277126e+004
8	3991	1.271559e+004

Est.Limit=1.263160e+004 (0.66%)

Average values for increasing p-levels

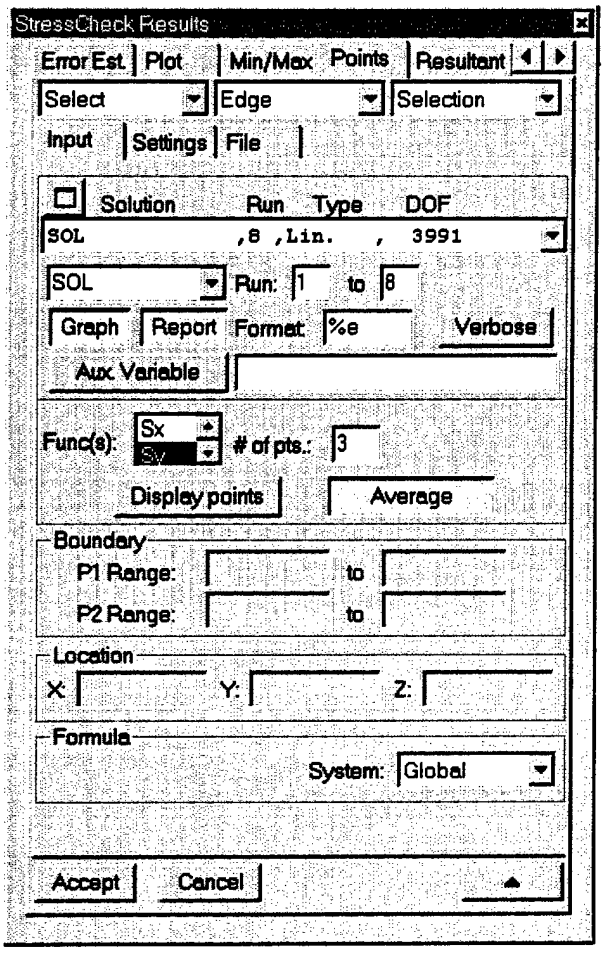

FIGURE 45. Extraction of the average σ_y along an element edge.

each load step to determine whether any of the failure criteria have been exceeded ($MS \leq 0$). Once the first failure mode is reached, it is possible to stop the analysis or continue to increment the load until all margins are exceeded.

The implementation of the automatic procedure was developed using the material nonlinear capability of Stress Check based on the deformation theory of plasticity and the von Mises yield criterion. Only the adhesive material have elastic-plastic properties which can be defined as elastic-ideally-plastic, bilinear, Ramberg-Osgood or by five parameters that characterize the stress-strain curve.

Example: Consider the bonded lap joint shown in Figure 46. Only one quarter of the joint is considered for the 2D plane-strain analysis as shown in the figure. The first few layers of the laminate are included explicitly and the rest are lumped into a sublaminate. The following material properties are specified for the composite layers and the adhesive:

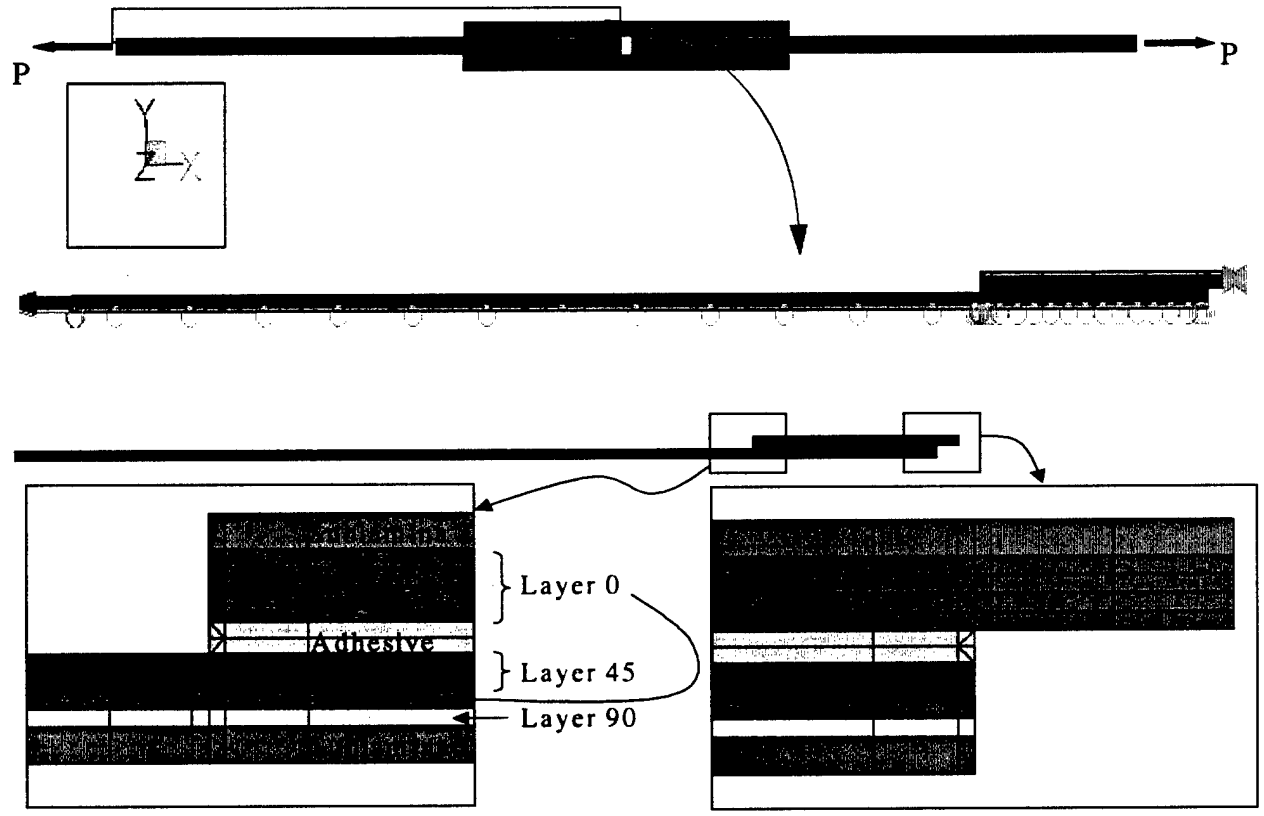

FIGURE 46. Bonded lap joint.

Composite: E_L=23.5x10^6 psi, E_T=1.3x10^6 psi, G_{LT}=0.55x10^6 psi, G_{TT}=0.44x10^6 psi, ν_{LT}=0.3, ν_{TT}=0.46

Adhesive: E=251,900 psi, ν=0.34, σ_Y=11,600 psi (elastic-plastic).

A design load is applied to the bonded joint (P=2,000 lb), and a material nonlinear analysis is performed to determine whether any of the following margin criteria are exceeded at the locations indicated in Figure 47:

$$MS_1 = 1 - \frac{\varepsilon_{eq}}{\varepsilon_0}, \qquad MS_2 = 1 - \left\{ \left(\frac{\bar{\sigma}_y}{\sigma_0}\right)^2 + \left(\frac{\bar{\tau}_{xy}}{\tau_0}\right)^2 \right\} \tag{67}$$

Note that a total of 10 margin criteria are considered for the composite joint, 5 on the left side and 5 on the right side. The failure types are delamination (Delam), interface failure (Interf) and adhesive failure (Adhes).

Criteria	Delam	Interf	Adhes
Extraction	Min/Max	Edge	Edge
Margin of Safety	MS_2	MS_2	MS_1
Average	NO	YES	YES
Locations	4	4	2

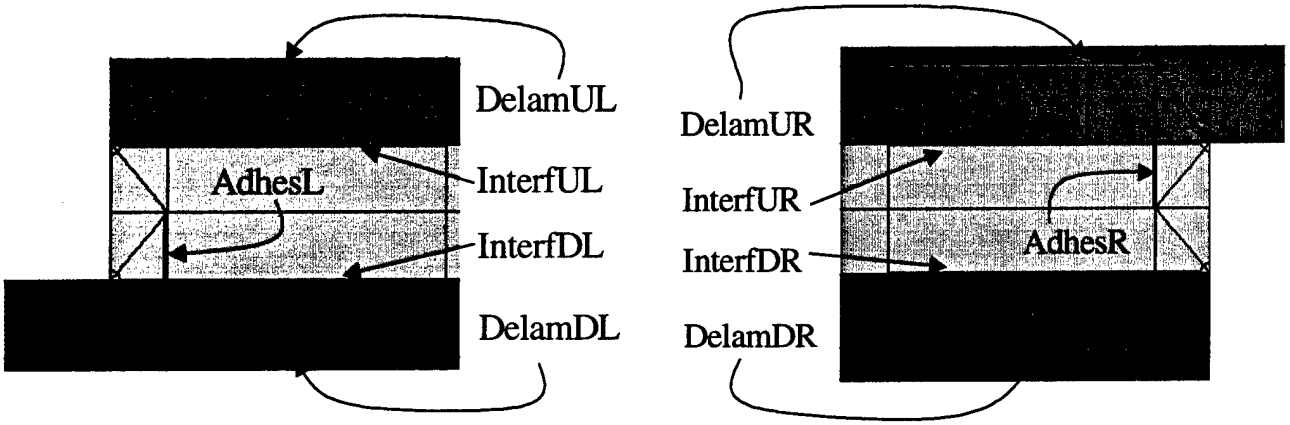

FIGURE 47. Extraction location and type for limit load analysis.

The load is increased (by 100 lb increments) and the nonlinear analysis continues until convergence is achieved. At the end of each converged solution all margin criteria are checked and if any margin is zero or negative ($MS \leq 0$), the magnitude of the load and the corresponding margin value is recorded. A solution record is also kept for further post-processing. Figure 48 shows the settings of the limit load interface in Stress Check.

After the sequence of linear solutions is available, one solution is selected to start the nonlinear analysis. The type of nonlinear run (material or general) is selected together with the convergence criteria (stress or energy), allowable tolerance (%) and the iteration limit for each load increment. Next, the load parameter information is completed, including the load increment and the upper bound for the load. It is possible to stop the analysis after the first margin is exceeded by checking the box labeled 'stop at 1st M.S. failure'. If left unchecked, the solution will proceed until all margin criteria are exceeded or the upper bound of the load is reached, whatever occurs first. Finally, all the relevant margin criteria defined for the problem are selected in the scroll window and the limit load analysis is initiated.

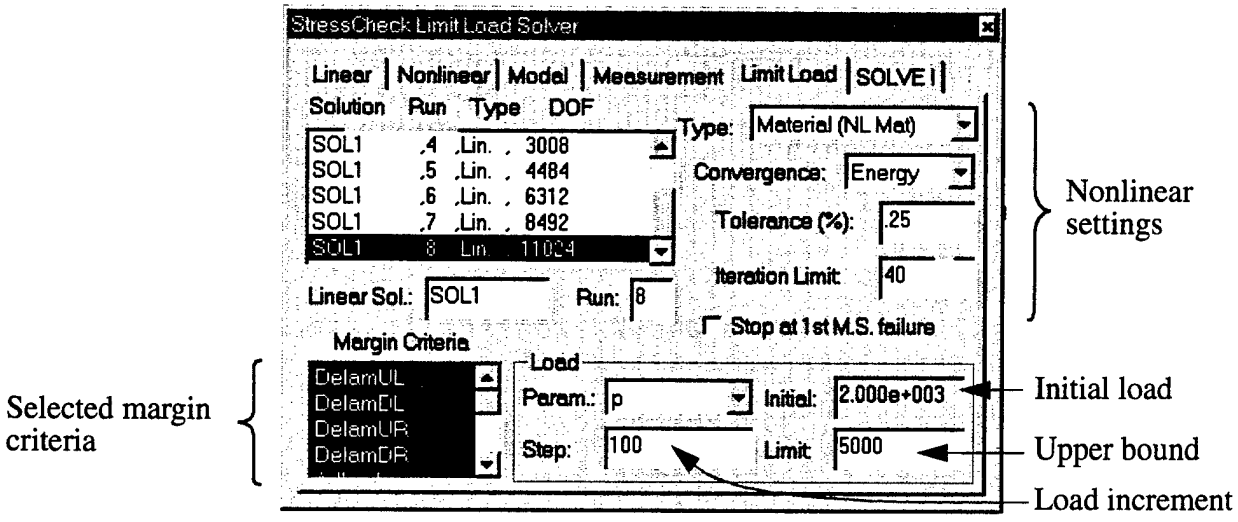

FIGURE 48. Limit load interface. Setting for example problem.

After the limit load analysis is completed, a report window provides a summary of the results as shown in Figure 49. Two margin criteria were exceeded: An interface failure occurred on the left side

```
                    Limit Load Summary
            Plate with central hole. NonLinear model
                      ID= SOL1, run #8
-------------------------------------------------------------------
 Criteria Number  Margin Criteria   Limit Load    Margin Value
-------------------------------------------------------------------
          1            DELAMUL      5.000000e+003   5.114385e-001
          2            DELAMDL      5.000000e+003   1.555231e-001
          3            DELAMUR      5.000000e+003   9.346218e-001
          4            DELAMDR      5.000000e+003   6.299574e-001
          5            ADHESL       4.000000e+003  -2.606208e-002
          6            ADHESR       5.000000e+003   8.395282e-001
          7            INTERFUR     5.000000e+003   7.228068e-001
          8            INTERFDR     5.000000e+003   6.769590e-001
          9            INTERFDL     2.400000e+003  -1.849117e-002
         10            INTERFUL     5.000000e+003   1.762295e-001
-------------------------------------------------------------------
2 out of 10 Margin criteria exceeded.
```

FIGURE 49. Results from the limit load analysis of the example problem.

of the joint just below the adhesive line (InterfDL) at a load of 2,400 lb, and an adhesive failure developed on the left side (AdhesL) at 4,000 lb.

Finally, Figure 50 shows the elastic-plastic equivalent (von Mises) stress distribution in the adhesive layer for P=2,400 lb, P=4,000 lb and P=5,000 lb.

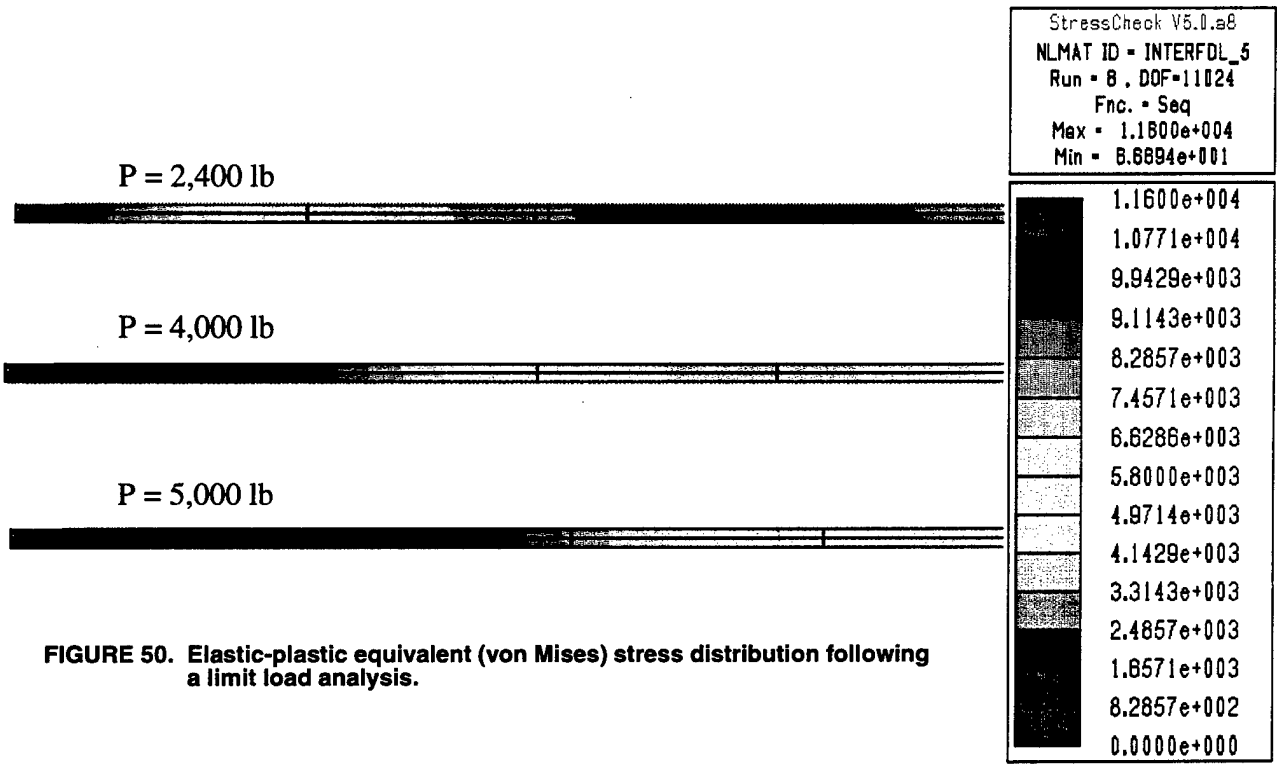

FIGURE 50. Elastic-plastic equivalent (von Mises) stress distribution following a limit load analysis.

4.9 Task 9: Sub-laminate property input

A capability was implemented to facilitate the input of orthotropic material properties for individual plies and for sub-laminate properties for 2D plane-strain and 3D analyses.

- *Individual plies*: When the ply-angles are not contained in the standard 2D working plane (the plane-strain XY plane), the material matrix needed for the 2D analysis are extracted from the 3D material matrix. The material coefficients are entered in the material directions, and then assigned to the elements together with the ply angle information. The program performs all necessary transformations to compute the equivalent 2D properties in the XY work plane. The appropriate 3D properties are be applied when the planar model is extruded into 3D as well.
- *Sub-laminates*: When a set of plies need to be combined in a single layer (sub-laminate), the properties of the sub-laminate are obtained by homogenization. Again, the 3D material coefficients in the material axes of the composite are entered together with the stacking sequence of the sub-laminate, and the program computes the equivalent 2D properties in the Stress Check XY work plane for the stack. The appropriate 3D properties are applied when the planar model is extruded into 3D as well.

The procedures implemented in Stress Check to account for these two activities include the following:

1 The material coefficients of a single orthotropic ply are entered in the direction of the material axes (Figure 51a). Nine engineering coefficients (E_{11}, E_{22}, E_{33}, G_{12}, G_{23}, G_{31}, ν_{12}, ν_{23}, ν_{13}) in the direction of the material axes and the ply thickness must be provided. The three coefficients of thermal expansion (α_{11}, α_{22}, α_{33}) and the mass density can also be entered, but they are not required unless there is thermal loading or a modal analysis is needed.

2 After the material properties for a single ply are entered, the ply group information must be provided. This includes the angular orientation of each ply in the group, in accordance with the following convention: A positive ply angle (θ) is measured as a counterclockwise rotation about the z-axis of a local coordinate system (xyz). The z-axis of the local is aligned with the material 3-axis as shown in Figure 51b.

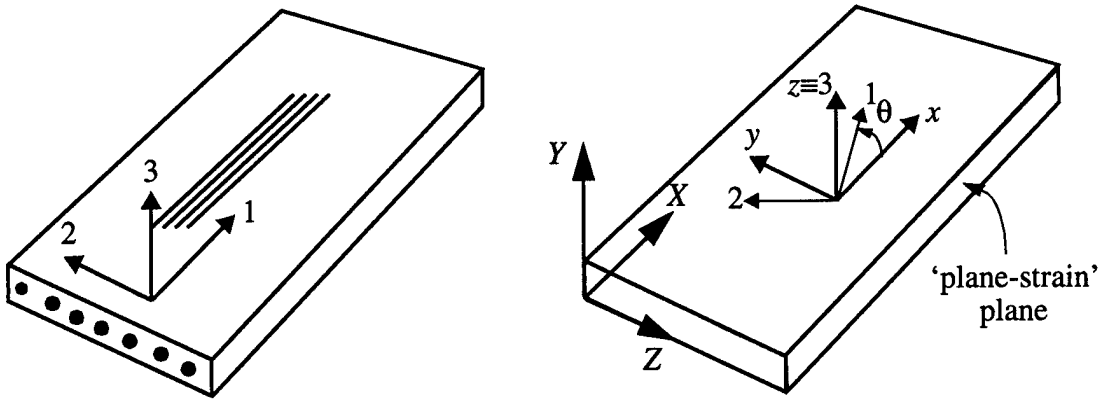

(a) Material axes

(b) Rotation of material axes

FIGURE 51. Material coordinate systems for orthotropic plies.

3 The ply groups are assembled into a stack by providing the total number of layers in the laminate, defining whether the stack is symmetric or not and entering the stacking sequence based on the ply group names. This procedure provides a great flexibility, since various ply groups of different material properties can be assembled together to represent a single sub-lamina.

4 Finally, the stack is assigned to the elements in the mesh identifying the local coordinate system, the z-axis of which is assumed to coincide with the material 3-axis and must be perpendicular to the plane of the ply (Figure 51b). The case of a single ply assigned to an element is treated as a particular case of a sublaminate with one orthotropic layer.

The two-dimensional material stiffness matrix needed for the plane-strain analysis is then extracted form the three-dimensional material matrix in global coordinates (XYZ). When a group of laminae is assigned to a single element, the three-dimensional effective properties are computed by homogenization, following the procedure described in Ref. [19] and discussed in detail below.

4.9.1 Formulation

The 3D stress-strain relations for an orthotropic material in the material coordinate system (Figure 51a) can be written as:

$$\{\bar{\sigma}\} = [C]\{\bar{\varepsilon}\} \tag{68}$$

where,

$$\{\bar{\sigma}\} = \begin{bmatrix} \sigma_{11} \\ \sigma_{22} \\ \sigma_{33} \\ \tau_{12} \\ \tau_{23} \\ \tau_{31} \end{bmatrix}, \qquad \{\bar{\varepsilon}\} = \begin{bmatrix} \varepsilon_{11} \\ \varepsilon_{22} \\ \varepsilon_{33} \\ \gamma_{12} \\ \gamma_{23} \\ \gamma_{31} \end{bmatrix}, \qquad [C] = \begin{bmatrix} C_{11} & C_{12} & C_{13} & 0 & 0 & 0 \\ & C_{22} & C_{23} & 0 & 0 & 0 \\ & & C_{33} & 0 & 0 & 0 \\ & \text{sym.} & & C_{66} & 0 & 0 \\ & & & & C_{44} & 0 \\ & & & & & C_{55} \end{bmatrix} \tag{69}$$

$[C]$ is the material stiffness matrix with nine independent constants. The relation between the C_{ij} and the engineering coefficients is given by (Ref. [20], page 41):

$$C_{11} = (1 - \nu_{23}\nu_{32})VE_{11}, \qquad C_{22} = (1 - \nu_{31}\nu_{13})VE_{22}, \qquad C_{33} = (1 - \nu_{12}\nu_{21})VE_{33}$$

$$C_{12} = (\nu_{21} + \nu_{23}\nu_{31})VE_{11}, \qquad C_{13} = (\nu_{13} + \nu_{23}\nu_{12})VE_{33}, \qquad C_{23} = (\nu_{32} + \nu_{12}\nu_{31})VE_{22}$$

$$C_{44} = G_{23}, \qquad C_{55} = G_{31}, \qquad C_{66} = G_{12}$$

$$V = (1 - \nu_{12}\nu_{21} - \nu_{23}\nu_{32} - \nu_{31}\nu_{13} - 2\nu_{12}\nu_{23}\nu_{31})^{-1}$$

$$\nu_{21} = \nu_{12}\frac{E_{22}}{E_{11}}, \qquad \nu_{32} = \nu_{23}\frac{E_{33}}{E_{22}}, \qquad \nu_{31} = \nu_{13}\frac{E_{33}}{E_{11}}$$

Next consider the situation shown in Figure 51b, in which a rotation θ about the z-axis (coincident with the material 3-axis) is performed for the kth layer in the laminate. The stress-strain relations in the xyz local system can be written as:

$$\{\sigma\}_{xyz} = [Q^{(k)}]\{\varepsilon\}_{xyz} \tag{70}$$

where,

$$\{\sigma\}_{xyz} = \begin{bmatrix} \sigma_x \\ \sigma_y \\ \sigma_z \\ \tau_{xy} \\ \tau_{yz} \\ \tau_{zx} \end{bmatrix}, \qquad \{\varepsilon\}_{xyz} = \begin{bmatrix} \varepsilon_x \\ \varepsilon_y \\ \varepsilon_z \\ \gamma_{xy} \\ \gamma_{yz} \\ \gamma_{zx} \end{bmatrix}, \qquad [Q^{(k)}] = \begin{bmatrix} Q_{11} & Q_{12} & Q_{13} & Q_{16} & 0 & 0 \\ & Q_{22} & Q_{23} & Q_{26} & 0 & 0 \\ & & Q_{33} & Q_{36} & 0 & 0 \\ & \text{sym.} & & Q_{66} & 0 & 0 \\ & & & & Q_{44} & Q_{45} \\ & & & & & Q_{55} \end{bmatrix}^{(k)} \tag{71}$$

The material matrix for the kth layer in the local system $[Q^{(k)}]$ is obtained by the following transformation (Ref. [20], page 31):

$$[Q^{(k)}] = [T]^T[C][T]$$

$$[T] = \begin{bmatrix} m^2 & n^2 & 0 & 0 & 0 & mn \\ n^2 & m^2 & 0 & 0 & 0 & -mn \\ 0 & 0 & 1 & 0 & 0 & 0 \\ 0 & 0 & 0 & m & -n & 0 \\ 0 & 0 & 0 & n & m & 0 \\ -2mn & 2mn & 0 & 0 & 0 & m^2 - n^2 \end{bmatrix}$$

where $[C]$ is given in Eq. (69), $m = \cos\theta$ and $n = \sin\theta$. Equations (70) and (71) represent the stress-strain relations for a lamina in a local coordinate system after a rotation θ about the z-axis.

Next we consider a laminate of constant thickness h composed of N-layers of thickness t_k ($h = \sum_{k=1}^{N} t_k$). Each lamina can have an arbitrary orientation (z-rotation) with respect to the local coordinate system (xyz). The properties of this laminate can be effectively represented by an homogeneous anisotropic solid. Consider the stress-strain relations for the homogeneous solid in the local system of the form:

$$\{\sigma\}_{xyz} = [\bar{Q}]\{\varepsilon\}_{xyz}$$

$$[\bar{Q}] = \begin{bmatrix} \bar{Q}_{11} & \bar{Q}_{12} & \bar{Q}_{13} & \bar{Q}_{16} & 0 & 0 \\ & \bar{Q}_{22} & \bar{Q}_{23} & \bar{Q}_{26} & 0 & 0 \\ & & \bar{Q}_{33} & \bar{Q}_{36} & 0 & 0 \\ & \text{sym.} & & \bar{Q}_{66} & 0 & 0 \\ & & & & \bar{Q}_{44} & \bar{Q}_{45} \\ & & & & & \bar{Q}_{55} \end{bmatrix} \tag{72}$$

where the effective elastic constants of the solid $\bar{Q}_{ij}$ are computed from the material matrices of the individual plies by the transformations (Ref. [19]):

$$\bar{Q}_{11} = \frac{1}{h}\left(\sum_{k=1}^{N} t_k Q_{11}^{(k)} + \sum_{k=2}^{N} (Q_{13}^{(k)} - \lambda_{13}) t_k (Q_{13}^{(1)} - Q_{13}^{(k)})/Q_{33}^{(k)}\right)$$

$$\bar{Q}_{12} = \frac{1}{h}\left(\sum_{k=1}^{N} t_k Q_{12}^{(k)} + \sum_{k=2}^{N} (Q_{13}^{(k)} - \lambda_{13}) t_k (Q_{23}^{(1)} - Q_{23}^{(k)})/Q_{33}^{(k)}\right)$$

$$\bar{Q}_{13} = \frac{1}{h}\left(\sum_{k=1}^{N} t_k Q_{13}^{(k)} + \sum_{k=2}^{N} (Q_{33}^{(k)} - \lambda_{33}) t_k (Q_{13}^{(1)} - Q_{13}^{(k)})/Q_{33}^{(k)}\right)$$

$$\bar{Q}_{22} = \frac{1}{h}\left(\sum_{k=1}^{N} t_k Q_{22}^{(k)} + \sum_{k=2}^{N} (Q_{23}^{(k)} - \lambda_{23}) t_k (Q_{23}^{(1)} - Q_{23}^{(k)})/Q_{33}^{(k)}\right)$$

$$\bar{Q}_{23} = \frac{1}{h}\left(\sum_{k=1}^{N} t_k Q_{23}^{(k)} + \sum_{k=2}^{N} (Q_{33}^{(k)} - \lambda_{33}) t_k (Q_{23}^{(1)} - Q_{23}^{(k)})/Q_{33}^{(k)}\right)$$

$$\bar{Q}_{16} = \frac{1}{h}\left(\sum_{k=1}^{N} t_k Q_{16}^{(k)} + \sum_{k=2}^{N} (Q_{13}^{(k)} - \lambda_{13}) t_k (Q_{36}^{(1)} - Q_{36}^{(k)})/Q_{33}^{(k)}\right)$$

$$\bar{Q}_{26} = \frac{1}{h}\left(\sum_{k=1}^{N} t_k Q_{26}^{(k)} + \sum_{k=2}^{N} (Q_{23}^{(k)} - \lambda_{23}) t_k (Q_{36}^{(1)} - Q_{36}^{(k)})/Q_{33}^{(k)}\right)$$

$$\bar{Q}_{36} = \frac{1}{h}\left(\sum_{k=1}^{N} t_k Q_{36}^{(k)} + \sum_{k=2}^{N} (Q_{33}^{(k)} - \lambda_{33}) t_k (Q_{36}^{(1)} - Q_{36}^{(k)})/Q_{33}^{(k)}\right)$$

$$\bar{Q}_{66} = \frac{1}{h}\left(\sum_{k=1}^{N} t_k Q_{66}^{(k)} + \sum_{k=2}^{N} (Q_{36}^{(k)} - \lambda_{36}) t_k (Q_{36}^{(1)} - Q_{36}^{(k)})/Q_{33}^{(k)}\right)$$

$$\bar{Q}_{33} = \frac{h}{\sum_{k=1}^{N} t_k / Q_{33}^{(k)}}$$

$$\bar{Q}_{44} = \left(\sum_{k=1}^{N} \frac{t_k Q_{44}^{(k)}}{h\Delta_k}\right)/\Delta$$

$$\bar{Q}_{45} = \left(\sum_{k=1}^{N} \frac{t_k Q_{45}^{(k)}}{h\Delta_k}\right)/\Delta$$

$$\bar{Q}_{55} = \left(\sum_{k=1}^{N} \frac{t_k Q_{55}^{(k)}}{h\Delta_k}\right)/\Delta$$

$$\lambda_{13} = \bar{Q}_{13} \qquad \lambda_{23} = \bar{Q}_{23}$$

$$\lambda_{33} = \bar{Q}_{33} \qquad \lambda_{36} = \bar{Q}_{36}$$

$$\Delta_k = Q_{44}^{(k)} Q_{55}^{(k)} - (Q_{45}^{(k)})^2$$

$$\Delta = \left(\sum_{k=1}^{N} \frac{t_k Q_{44}^{(k)}}{h\Delta_k}\right)\left(\sum_{k=1}^{N} \frac{t_k Q_{55}^{(k)}}{h\Delta_k}\right) - \left(\sum_{k=1}^{N} \frac{t_k Q_{45}^{(k)}}{h\Delta_k}\right)^2$$

(73)

Once the material matrix for the homogenized solid is computed in the local system (*xyz*), we need to determine the material matrix in the global system (*XYZ*) shown in Figure 51b, and then extract the material matrix associated with the 'plane-strain' plane (*XY*-plane).

In the global system, the three-dimensional stress-strain relations can be written in the following form:

$$\{\sigma\}_{XYZ} = [E_{3D}]\{\varepsilon\}_{XYZ} \tag{74}$$

where the global material matrix $[E_{3D}]$ of the homogenized solid is computed from the local matrix $[\bar{Q}]$ as follows:

$$[E_{3D}] = [T_0]^T[\bar{Q}][T_0] \tag{75}$$

The transformation matrix $[T_0]$ is given by:

$$[T_0] = \begin{bmatrix} l_1^2 & l_2^2 & l_3^2 & l_1l_2 & l_2l_3 & l_3l_1 \\ m_1^2 & m_2^2 & m_3^2 & m_1m_2 & m_2m_3 & m_3m_1 \\ n_1^2 & n_2^2 & n_3^{2n} & n_1n_2 & n_2n_3 & n_3n_1 \\ 2l_1m_1 & 2l_2m_2 & 2l_3m_3 & l_1m_2+l_2m_1 & l_2m_3+l_3m_2 & l_3m_1+l_1m_3 \\ 2m_1n_1 & 2m_2n_2 & 2m_3n_3 & m_1n_2+m_2n_1 & m_2n_3+m_3n_2 & m_3n_1+m_1n_3 \\ 2n_1l_1 & 2n_2l_2 & 2n_3l_3 & n_1l_2+n_2l_1 & n_2l_3+n_3l_2 & n_3l_1+n_1l_3 \end{bmatrix} \tag{76}$$

where l_i, m_i, n_i are the direction cosines that relate a point in the global (XYZ) coordinate system to a point in the local (xyz) coordinate systems:

$$\begin{Bmatrix} x \\ y \\ z \end{Bmatrix} = \begin{bmatrix} l_1 & l_2 & l_3 \\ m_1 & m_2 & m_3 \\ n_1 & n_2 & n_3 \end{bmatrix} \begin{Bmatrix} X \\ Y \\ Z \end{Bmatrix} \tag{77}$$

Since the transformation indicated by Eq. (75) is very general, the 3D global material matrix can be fully populated. Therefore, the material matrix in Eq. (75) can be written as (using a single index notation for the 21 independent coefficients):

$$[E_{3D}] = \begin{bmatrix} E_1 & E_2 & E_4 & E_7 & E_{11} & E_{16} \\ & E_3 & E_5 & E_8 & E_{12} & E_{17} \\ & & E_6 & E_9 & E_{13} & E_{16} \\ & \text{sym.} & & E_{10} & E_{14} & E_{19} \\ & & & & E_{15} & E_{20} \\ & & & & & E_{21} \end{bmatrix} \tag{78}$$

The 2D plane-strain material matrix is extracted for Eq. (78) by pulling out the rows and columns associated with the *XY*-plane of the global system:

$$\begin{bmatrix} \sigma_X \\ \sigma_Y \\ \tau_{XY} \end{bmatrix} = \begin{bmatrix} E_1 & E_2 & E_7 \\ & E_3 & E_8 \\ \text{sym} & & E_{10} \end{bmatrix} \begin{bmatrix} \varepsilon_X \\ \varepsilon_Y \\ \gamma_{XY} \end{bmatrix} \tag{79}$$

The material matrix in Eq. (79) is used for the computation of the stiffness matrices for 2D-elasticity under plane-strain conditions, and the material matrix in Eq. (78) is used for the computation of the stiffness matrices for 3D-elasticity for those elements with laminate property assignments.

4.9.2 Examples

Two examples are presented to illustrate the implementation. In the first example each layer of the laminate is explicitly included in the model, while in the second example some plies are replaced by a single element with homogenized properties. A comparison between the two is performed to assess the influence of the homogenization in the results.

Example 1: Consider a 16-ply $[4(0/90)]_S$ simply supported laminated composite strip under plane strain conditions subjected to a sinusoidal traction as shown in Figure 52. Each ply is of the same

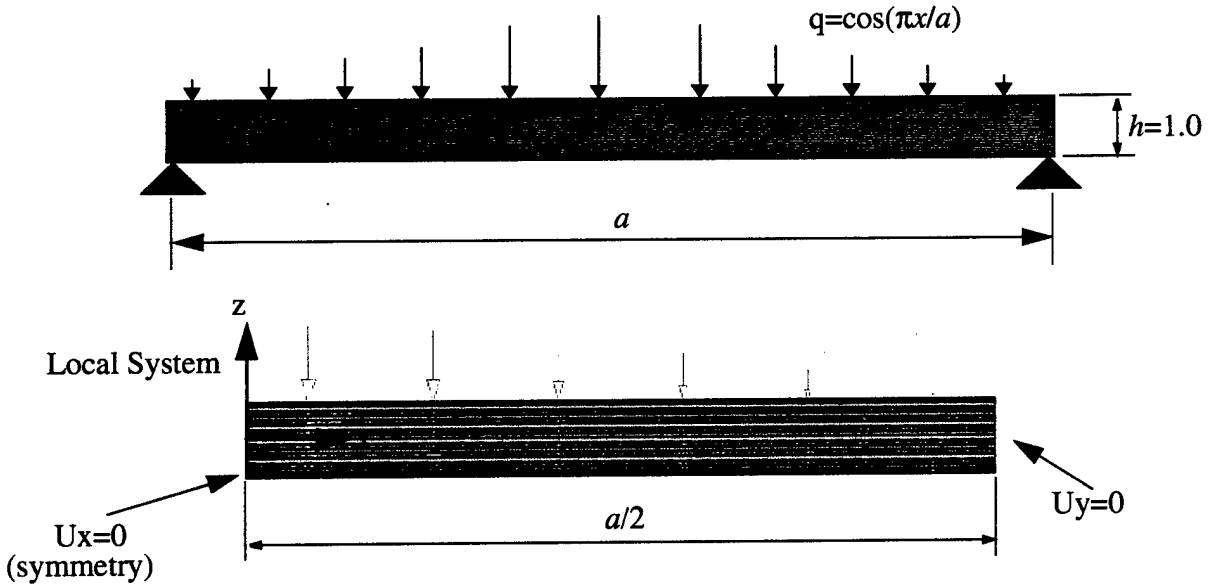

FIGURE 52. 16 ply $[4(0/90)]_S$ simply-supported laminated composite under sinusoidal load. Notation and mesh.

material and thickness (t=0.0625 mm) with the following properties:

$$E_L = 1.38\text{x}10^5 \text{ MPa}, E_T = 9.3\text{x}10^5 \text{ MPa}$$
$$G_{LT} = 4.6\text{x}10^5 \text{ MPa}, G_{TT} = 3.1\text{x}10^5 \text{ MPa}$$
$$\nu_{LT} = 0.3, \nu_{TT} = 0.5$$

Because of symmetry, only half of the beam was considered for the analysis. The mesh shown in Figure 52 consists of 16 quadrilateral elements, one for each ply. The material properties for a each ply are entered in the material definition form shown in Figure 53a. All nine engineering coefficients (E_{11}, E_{22}, E_{33}, G_{12}, G_{23}, G_{31}, ν_{12}, ν_{23}, ν_{13}) in the direction of the material axis and the ply thickness must be provided in this form. The three coefficients of thermal expansion (α_{11}, α_{22}, α_{33}) and the mass density are optional. After the material properties for a single ply are entered, the ply group information must be provided as shown in Figure 53b: The ply group name, the lamina material name and the ply layout angles. The stack form shown in Figure 53c is used to assemble the ply groups by providing the stack sequence name, the number of layers in the laminate, whether the stack is symmetric or not and the stacking sequence based on the ply group names. As shown in Figure 53, the

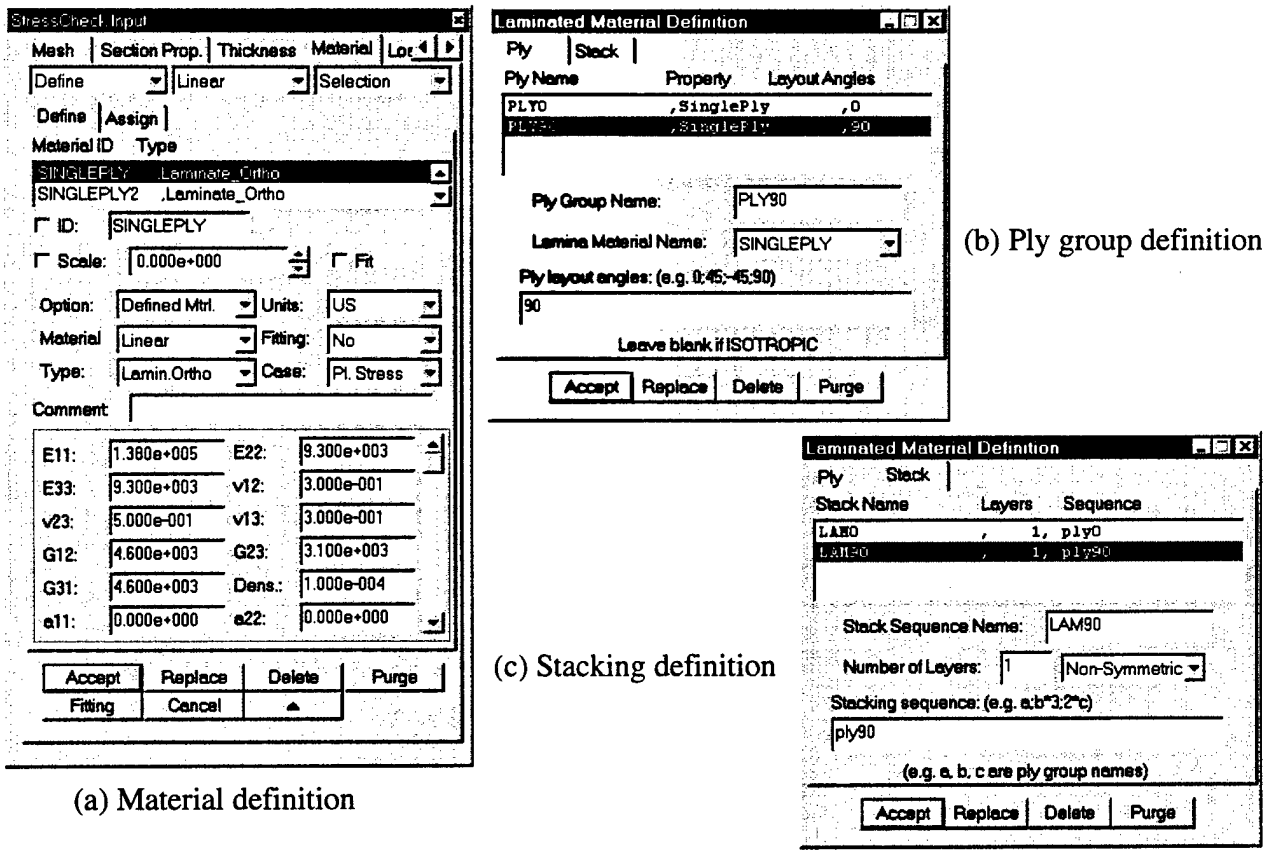

(a) Material definition

(b) Ply group definition

(c) Stacking definition

FIGURE 53. Input forms for laminate properties definition. Example 1

material property SINGLEPLY, defined in the material definition form, is used to define the ply group

PLY90 with a ply layout of 90 degrees with respect to the z-axis of a local system and the stack LAM90 is created with a single ply using the plygroup PLY90. The last step is to assign the material stacks to the elements and select the local coordinate system, the z-axis of which is assumed to be aligned with the material 3-axis. The material assignment form is shown in Figure 53. The orientation of the local coordinate system relative to the global system is used to determine the material matrix in the global system as explained in the previous section.

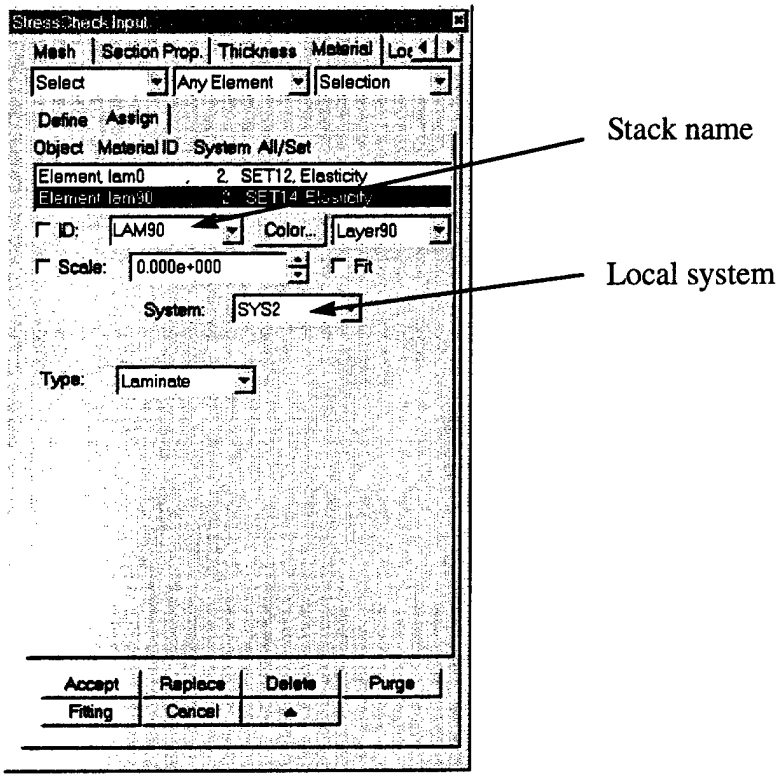

FIGURE 54. Input form for laminate properties assignment to elements.

A sequence of finite element solutions was obtained for polynomial orders ranging from 1 to 8 for a length to thickness ratio (a/h) of 20. The estimated relative error in energy norm and the deformed configuration for run #8 are shown in Figure 55. The largest vertical deflection of the laminated strip occurs along the symmetry line (Uy = -0.24125).

The distribution of the normal stress σ_x is shown in Figure 56 for run #8. The maximum value occurs at the lower surface along the symmetry line ($\sigma_x^{max} = 394$). These results will be compared with those of example 2.

Error Estimate
16-ply laminate [4(0/90)]s
(0) Solution = SOL, runs #1 to #8

Run #	DOF	Total Potential Energy	Convergence Rate	% Error
1	34	-3.677339739171e-001	0.00	93.70
2	100	-2.726732225119e+000	1.03	30.75
3	166	-3.004822685327e+000	3.69	4.73
4	264	-3.011498754148e+000	4.84	0.50
5	394	-3.011573787861e+000	6.25	0.04
6	556	-3.011574291076e+000	7.83	0.00
7	750	-3.011574292972e+000	2.92	0.00
8	976	-3.011574293285e+000	2.92	0.00

Estimated Limit -3.011574293369909e+000

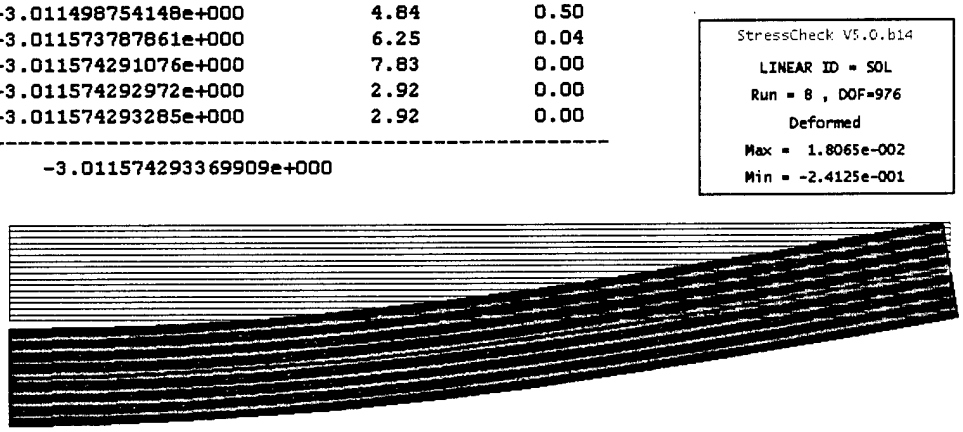

FIGURE 55. Estimated relative error in energy norm and deformed configuration for example 1.

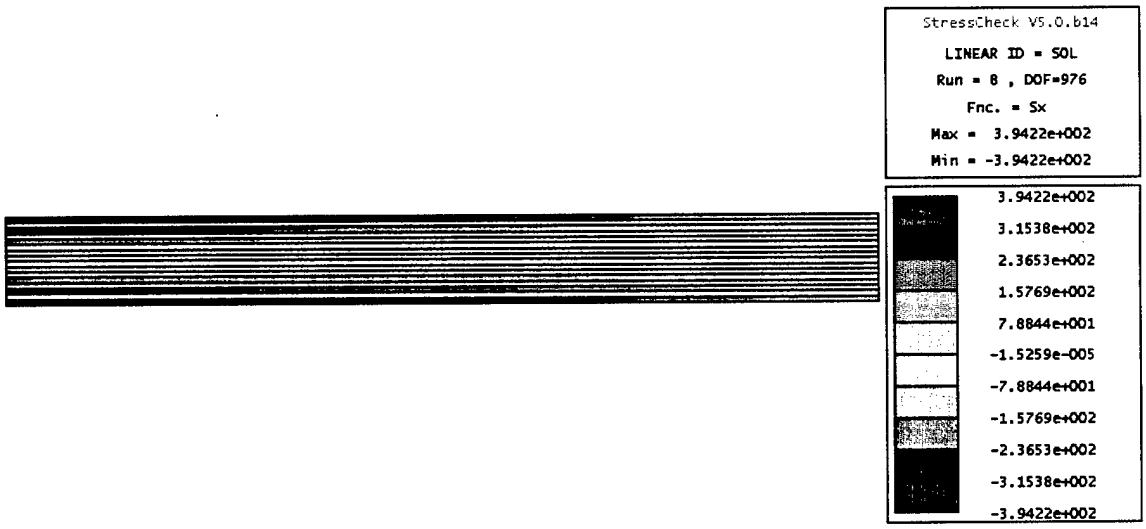

FIGURE 56. Normal stress distribution (Sx) for example 1.

Example 2: Consider the same 16-ply $[4(0/90)]_S$ simply supported laminated composite strip of example 1, but with the eight central layers replaced by a single element with equivalent properties. The finite element mesh is shown in Figure 57. The ply group definition and stacking sequence for the

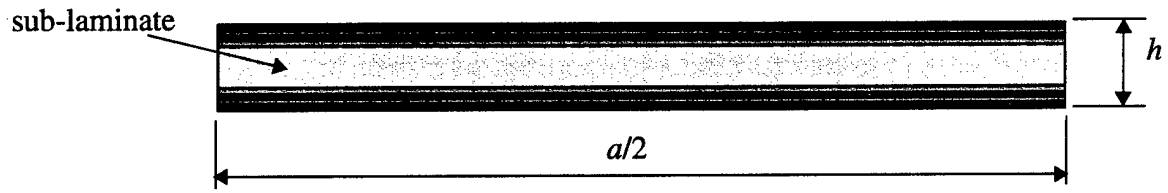

FIGURE 57. Mesh for a 16 ply $[4(0/90)]_S$ simply-supported laminated composite under sinusoidal load with the eight central layers replaced by a single element.

8 individual layers (4 above and 4 below the sub-laminate) are the same as shown in Figure 53 for example 1. The corresponding input records for the sub-laminate are shown in Figure 58. The central 8-plies $[2(0/90]_s$ can be described in more than one way in the input field of Figure 58a. For example,

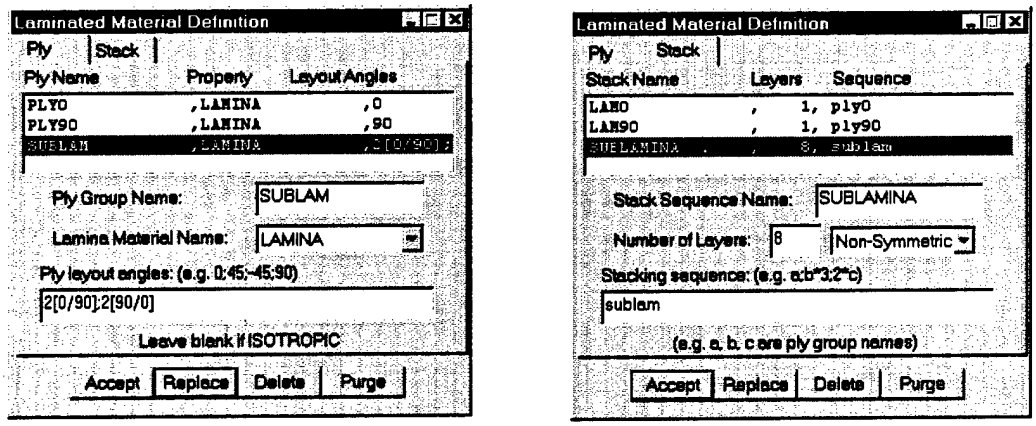

(a) Ply group definition

(b) Stacking definition

FIGURE 58. Input forms for sub-laminate properties definition. Example 2

0/90/0/90/90/0/90/0, or 2[0/90];2[90/0] as shown. Alternatively, define only half of the sub-laminate (4-plies) in the ply definition form (that is, 2[0/90]) and then use the Symmetric option in the stacking sequence.

A sequence of finite element solutions was obtained for polynomial orders ranging from 1 to 8 for a length to thickness ratio (a/h) of 20. The estimated relative error in energy norm and the deformed

configuration for run #8 are shown in Figure 59. Note that the values of the total potential energy for run #8 (-3.112472) and largest vertical deflection for run #8 (-2.4933) are very close to those of example 1 (-3.011574 and -2.4125, respectively).

Error Estimate
16-ply lminate [4(0/90)]s
(0) Solution = SOL, runs #1 to #8

Run #	DOF	Total Potential Energy	Convergence Rate	% Error
1	20	-3.754066833833e-001	0.00	93.78
2	58	-2.812359168830e+000	1.04	31.05
3	96	-3.105194949305e+000	3.69	4.84
4	152	-3.112378997471e+000	4.75	0.55
5	226	-3.112470791549e+000	6.07	0.05
6	318	-3.112471534377e+000	7.59	0.00
7	428	-3.112471538458e+000	6.07	0.00
8	556	-3.112471538567e+000	6.07	0.00

Estimated Limit -3.112471538571881e+000

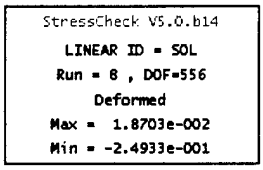

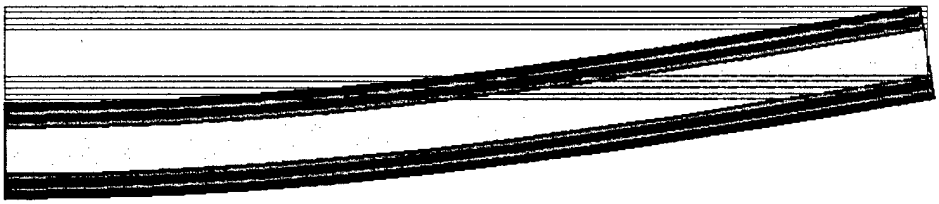

FIGURE 59. Estimated relative error in energy norm and deformed configuration for example 2.

The normal stress distribution σ_x for run #8 is shown in Figure 60. Note again that the maximum

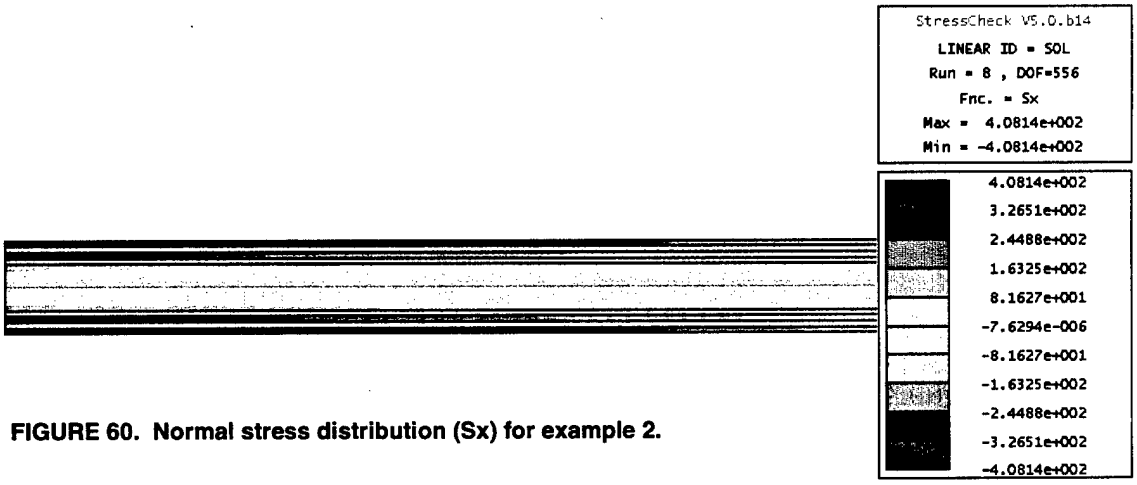

FIGURE 60. Normal stress distribution (Sx) for example 2.

stress occurs at the lower surface along the symmetry line ($\sigma_x^{max} = 408$) and it is very close to the value obtained for example 1 ($\sigma_x^{max} = 394$).

The analysis was repeated for several length-to-thickness ratios (*a/h*) and the results are summarized in Table 2. As can be seen, the results are very close, demonstrating the good approximating charac-

TABLE 2. Results for examples 1 and 2

a/h	Example	Potential Energy	U_y^{min}	σ_x^{max}
20	1	-3.01157	-0.2413	394
	2	-3.11247	-0.2493	408
40	1	-92.6603	-3.7077	1569
	2	-95.9683	-3.8401	1626
80	1	-2935.45	-58.714	6267
	2	-3041.95	-60.845	6495

teristics of the homogenization procedure implemented for the sub-laminate.

Both example problems were analyzed again, but this time in a fully three-dimensional setting using the extrusion option in Stress Check. Because the composite strip is a cross ply laminate, the results should be identical to those of plane-strain, provided that the normal displacements of the faces contained in the XY-plane are constrained.

In both cases a sequence of finite element solutions was obtained for polynomial orders ranging form 1 to 8. Figure 61 shows the estimated relative error in energy norm for both cases. Note that the potential energy values are the same as for the plane-strain cases (see Figures 55 and 59), but the number of degrees of freedom (DOF) have increased substantially for the 3D-solution.

GlobalError
16-ply laminate [4(0/90)]s
(0) Solution = SOL, runs #1 to #8

Run #	DOF	Total Potential Energy	Convergence Rate	% Error
1	68	-3.677339739127e-001	0.00	93.70
2	251	-2.726732224908e+000	0.85	30.75
3	434	-3.004822685147e+000	3.42	4.73
4	780	-3.011498767466e+000	3.83	0.50
5	1289	-3.011573787270e+000	5.11	0.04
6	2009	-3.011574290980e+000	2.25	0.01
7	2988	-3.011574293358e+000	0.00	0.01
8	4274	-3.011574292868e+000	0.01	0.01

Estimated Limit -3.011574230932173e+000

(a) Example 1

GlobalError
16-ply laminate [4(0/90)]s
(0) Solution = SOL, runs #1 to #8

Run #	DOF	Total Potential Energy	Convergence Rate	% Error
1	40	-3.754066833841e-001	0.00	93.78
2	146	-2.812359168826e+000	0.85	31.05
3	252	-3.105194949440e+000	3.41	4.84
4	451	-3.112378938211e+000	3.75	0.55
5	743	-3.112470791411e+000	4.96	0.05
6	1155	-3.112471534477e+000	2.27	0.02
7	1714	-3.112471538631e+000	0.00	0.02
8	2447	-3.112471538565e+000	0.00	0.02

Estimated Limit -3.112471446182672e+000

(b) Example 2

FIGURE 61. Estimated relative error in energy norm from the 3D analysis of examples 1 and 2.

Figure 62 shows the deformed configuration for run # 8 for both cases. Again the largest displacement is the same as in the case of plane-strain (compare with Figures 55 and 59).

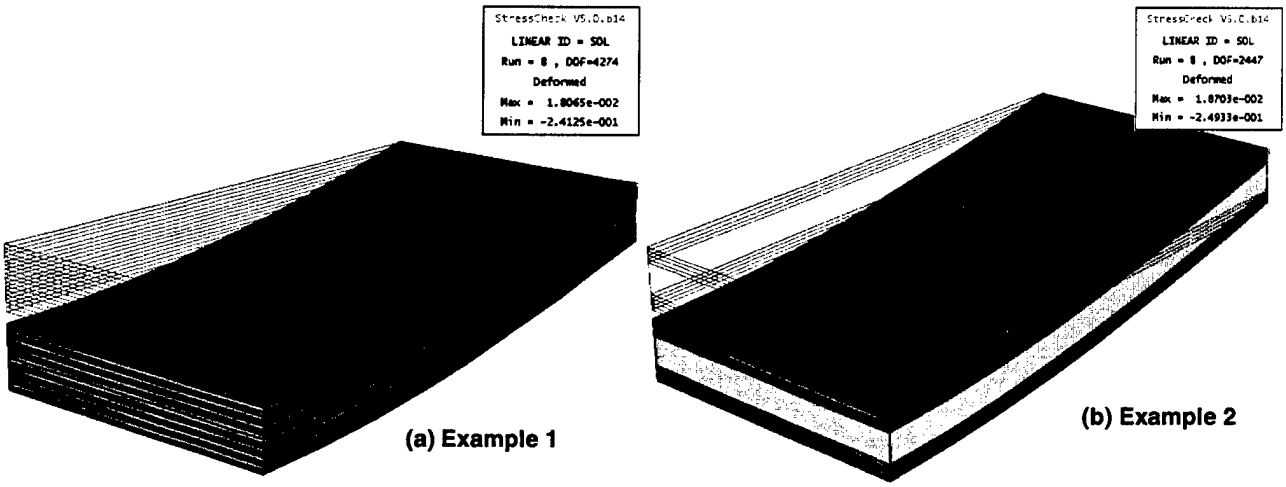

FIGURE 62. Deformed configuration from 3D analysis of examples 1 and 2.

Finally, Figure 63 shows the normal stress distribution σ_x for run #8 for both examples, which are identical to their plane-strain counterpart (compare with Figures 59 and 60).

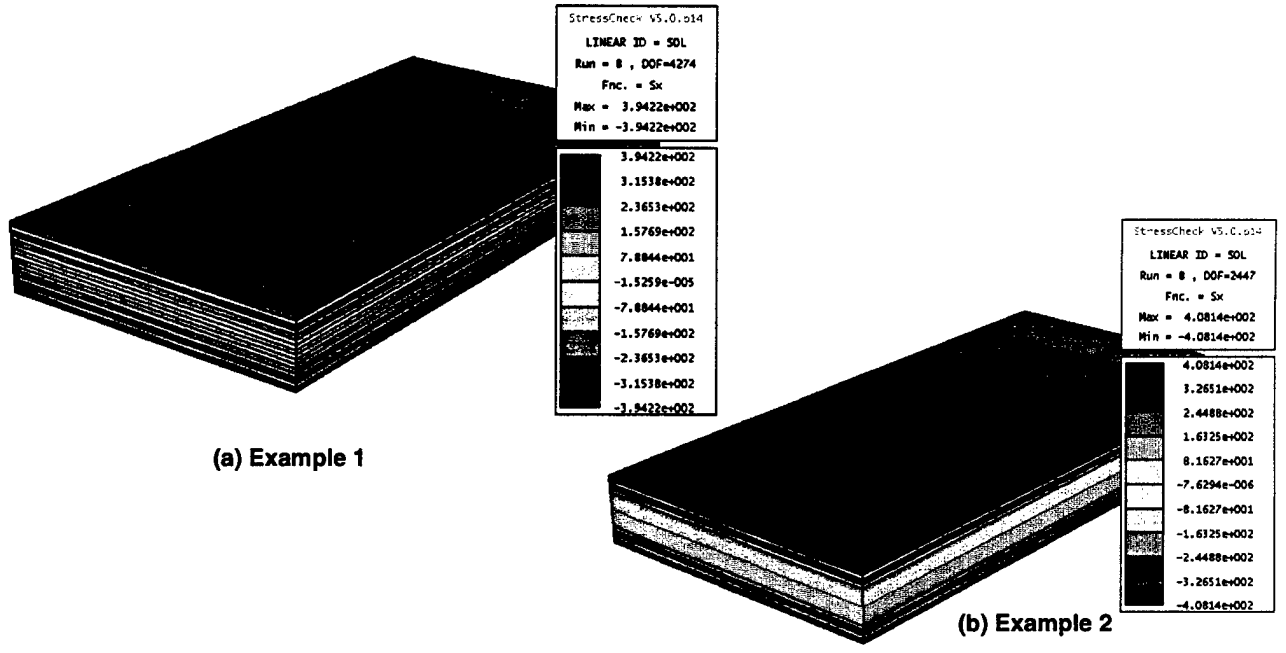

FIGURE 63. Normal stress distribution (Sx) from the 3D analysis of examples 1 and 2.

4.10 Task 10: Delivery of Stress Check software

One copy of Stress Check (Release 5.0) software executable on a Windows NT workstation and pertinent documentation will be delivered to Dr. Douglas J. Holzhauer, Mechanical Engineer, Air Force Rome Laboratory, RL/ERDS, Griffiss AFB, NY 13441-5700. Rome Laboratory shall have the same rights to Stress Check as a "paid-up" licensee.

All technical capabilities described in this report were incorporated in Release 5.0 of Stress Check which is currently undergoing beta testing. The official release date is December 1st 1999, at which time the software will be delivered to the Air Force.

5 Summary and conclusions

The technological developments implemented during the Phase II project are an essential prerequisite to proper interpretation of experimental data in much the same way as the ability to compute stress intensity factors in linear elastic fracture mechanics is an essential prerequisite to proper interpretation of experimentally obtained crack propagation data. The new capabilities, coupled with reference data obtained from simple experiments, will make it possible to evaluate design alternatives in the fields of electronic component design and composite materials technology. This capability, made available for professional use through the finite element analysis software (Stress Check), is expected to be of substantial interest to manufacturers of electronic components, aerospace companies, and their suppliers.

A change in the research objectives was needed because during the course of our investigation an improved and more generally applicable methodology for failure analysis of composite materials was conceived. The new technological capability provides improved numerical simulation tools for the design and analysis of laminated composite materials. The essential differences are that whereas the original task description envisioned failure analysis of composite materials entirely by means of linear models, utilizing the concept of generalized stress intensity factors, the new tasks advanced the development of computational support for failure criteria based on linear as well as nonlinear material properties.

The modification to the original goals of the Phase II project addressed the requirements of a working group of a government-industry consortium, called the Composite Affordability Initiative (CAI). This group was charged with the responsibility of identifying state-of-the-art numerical simulation technology that could be used in the design and analysis of composite joints with particular reference to the development of next generation fighter aircraft. The group conducted a detailed evaluation of the technology we have developed and concluded unanimously that Stress Check is the best available tool for analyzing and designing bonded composite joints. The evaluation also identified development tasks that needed to be completed in order to make Stress Check fully useful for the purposes of composite joint analysis. The new technological capabilities implemented as described in tasks 7 to 9 satisfies those additional requirements. They provide the numerical simulation tools that

can be used in the design and analysis of laminated composite joints, making advanced technology available for design engineers and analyst in the aerospace industry.

6 References

[1]Babuska, I. and Miller, A. The Post-processing Approach in Finite Element Method - Part 2: The Calculation of Stress Intensity Factors. *Int Jour. Num. Meth. Engrg.*, Vol. 20, pp. 1111-1129, (1984).

[2] Actis, Ricardo L. "Stress/Failure Analysis Software for Multi-Material Interfaces" Air Force Office of Scientific Research, Phase I Final Report, Project No. FQ8671-9501469 STTR/TS, December 1996.

[3] Yosibash, Z. and Szabo, B. A. Numerical Analysis of Singularities in Two-Dimensions. Part 1: Computation of Eigenpairs. *Int. Jour. Numer. Meth. Engrg.*, Vol. 38, pp. 2055-2082 (1995).

[4] Yosibash, Z. and Szabo, B. A. Numerical Analysis of Singularities in Two-Dimensions. Part 2: Computation of Generalized Flux/Stress Intensity Factors. *Int. Jour. Numer. Meth. Engrg.*, Vol. 39 (3), pp. 409-434 (1996).

[5] Yosibash, Z. Numerical Thermo-Elastic Analysis of Singularities in Two-Dimensions. *International Journal of Fracture*, Vol. 74, pp. 341-361 (1996).

[6] Yosibash, Z. *Numerical Analysis of Singularities and First Derivatives for Elliptic Boundary Value Problems in Two-Dimensions*. D. Sc. dissertation, Sever Institute of Technology, Washington University, St. Louis, Missouri, 1994.

[7] Oh, H. S. and Babuska, I. P-Version of the Finite Element Method for the Elliptic Boundary Value Problem with Interfaces. *Computer Meth. Appl. Mech. Engrg.*, Vol. 97 (2), pp. 211-231 (1992).

[8] Anderson, B., Falk, U., Babuska, I. and Von-Petersdorff, T. Reliable Stress and Fracture Mechanics Analysis of Complex Components Using a h-p Version of FEM. *Int. Jour. Numer. Meth. Engrg.*, Vol. 38, pp. 2135-2163 (1995).

[9] Babuska, I., Von-Petersdorff, T. and Anderson, B. Numerical Treatment of Vertex Singularities and Intensity Factors for Mixed Boundary Value Problems for the Laplace Equation in R^3. *SIAM. Jour. Numer. Analysis*, Vol. 31(5), pp. 1265-1288 (1994).

[10] Dauge, M. *Elliptic Boundary Value Problems in Corner Domains - Smoothness and Asymptotics of Solutions.* Lecture Notes in Mathematics 1341, Springer-Verlag, Heidelberg, 1988.

[11] Guo, B. and Oh, H.S. The Method of Auxiliary Mapping for the Finite Element Solutions of Elliptic Partial Differential Equations on Nonsmooth Domains in R^3. Preprint submitted for publication to *Mathematics of Computations* (1996).

[12] Ting, T.C.T., and Chou, S.C. Edge Singularities in Anisotropic Composites. *Int. Jour. Composites and Structures*, Vol. 17 (11), pp. 1057-1068 (1981).

[13] Wang, S.S. and Choi, S.C. Boundary Layer Effects in Composite Laminates: Part 1 - Free Edge Stress Singularities. *Trans. ASME, Jour. Appl. Mech.*, Vol 49, pp. 541-548 (1982).

[14] Yosibash, Z. Numerical Analysis of Edge Singularities in Three-Dimensional Elasticity. *Int. Jour. Numer. Meth. Engrg.*, Vol. 40, pp. 4611-4632 (1997).

[15] Szabo, B. A. and Babuska, I. *Finite Element Analysis.* John Wiley and Sons, Inc., 1991.

[16] Babuska, I. and Aziz, A.K. Survey Lectures on the Mathematical Foundations of the Finite Element Method. In A.K. Aziz, editor, *The Mathematical Foundations of the Finite Element Method with Applications to Partial Differential Equations*, pp. 3-343, Academic Press, New York, NY, USA, 1972.

[17] Chen, D. H. Analysis of Singular Stress Field Around the Inclusion Corner Tip. *Engineering Fracture Mechanics*, Vol. 49 (4), pp. 553-546 (1994).

[18] Yosibash, Z. Computing Edge Singularities in Elastic Anisotropic Three-Dimensional Domains. *Int. Jour. of Fracture.*, Vol. 86, pp. 221-245 (1997).

[19] Sun, C.T. and Li, S. Three-Dimensional Effective Elastic Constants for Thick Laminates. *Journal of Composite Materials*, Vol. 22, pp. 629-639 (1988).

[20] Tsai, S.W. "Mechanics of Composite Materials. Part II - Theoretical Aspects". Technical Report AFML-TR-66-149, Part II, Air Force Material Laboratory, Research and Technology Divivion, Wright-Patterson Air Force Base, November 1966.